AUBURN UNIVERSITY

SAMUEL GINN
COLLEGE OF ENGINEERING

Project Number: AL DOT-931-093

Automated Detection of Ground Deformation on Alabama Highways using Remote Sensing

by

Ali Khosravi, Ph.D., P.E.

Zahra Ghorbani

Najibullah Zulfeqar

Jack Montgomery, Ph.D., P.E.

Department of Civil and Environmental Engineering

Auburn University

for

Alabama Department of Transportation

Montgomery, Alabama

Highway Research Center

Harbert Engineering Center

Auburn University, Alabama 36849

March 2026

1. Report No.	2. Government Accession No.	3. Recipient Catalog No.
4. Title and Subtitle Automated Detection of Ground Deformation on Alabama Highways using Remote Sensing		5. Report Date February 2026 6. Performing Organization Code
7. Author(s) Ali Khosravi, Zahra Ghorbani, Najibullah Zulfeqar, Jack Montgomery		8. Performing Organization Report No. 931-093
9. Performing Organization Name and Address Highway Research Center Department of Civil Engineering 238 Harbert Engineering Center Auburn, AL 36849		10. Work Unit No. (TRAIS) 11. Contract or Grant No.
12. Sponsoring Agency Name and Address Alabama Department of Transportation 1409 Coliseum Blvd Montgomery, AL 36130		13. Type of Report and Period Covered 14. Sponsoring Agency Code
15. Supplementary Notes		

16. Abstract

Ground deformation poses a significant risk to Alabama's transportation infrastructure, particularly along highway corridors affected by landslides, embankment settlement, and hydrologically driven slope movement. This study develops and demonstrates an integrated satellite-based monitoring framework that combines multi-scale Interferometric Synthetic Aperture Radar (InSAR) processing, ground-based validation, environmental data integration, and machine learning–enhanced detection to support operational infrastructure monitoring across Alabama. Sentinel-1 C-band SAR data (2016–2025) were processed using complementary Small Baseline Subset (SBAS/NSBAS) and Persistent Scatterer (PS-InSAR) methodologies implemented through LiCSBAS and PyGMTSAR. The NSBAS workflow provided statewide deformation screening and regional situational awareness, while PS-InSAR enabled high-resolution monitoring of localized infrastructure assets and unstable slopes. Cross-comparison of methods demonstrated strong consistency in long-term deformation trends while highlighting the higher sensitivity of PS-InSAR for detecting localized acceleration and early-stage instability in vegetation-dominated environments.

A comprehensive validation framework was implemented using independent geodetic and field datasets, including continuous GNSS observations, ALDOT inclinometer measurements, corner reflector deployments, and environmental datasets such as precipitation and soil moisture. Results show that satellite-derived time series successfully captured both catastrophic and slow-moving deformation processes, including pre-failure acceleration at the US-231 landslide site and seasonal hydrologically driven creep at SR-219. GNSS comparisons confirmed that NSBAS products reliably represent regional deformation behavior, while PS-InSAR demonstrated strong agreement with localized field instrumentation. Corner reflector installations established the foundation for future absolute validation and precision monitoring as additional satellite acquisitions become available.

Building on validated deformation products, a web-based ALDOT GeoMonitor Portal was developed to integrate InSAR, GNSS, and environmental data within a unified decision-support environment. In addition, a deep learning–enhanced Early Detection and Alert System (EDAS) was developed using a decomposition-based modeling framework combining ARIMA and CNN–Attention–BiGRU architectures to detect anomalous displacement behavior and provide short-term predictive capability. Application at the Littleville corridor demonstrated the system's ability to identify deformation anomalies and quantify hydrologically driven acceleration patterns relevant to operational monitoring.

17. Key Words	18. Distribution Statement		
Remote Sensing, InSAR, PS-InSAR, NSBAS, LiCSBAS, PyGMTSAR, Ground Deformation, Landslide Monitoring, Highway Slopes	No restrictions		
19. Security Classification (of this report) Unclassified	20. Security Classification (of this page) Unclassified	21. No. of Pages 113	22. Price None.

Research Report

AUTOMATED DETECTION OF GROUND DEFORMATION ON ALABAMA HIGHWAYS USING REMOTE SENSING

Submitted to

The Alabama Department of Transportation

Prepared by

Ali Khosravi, Ph.D., P.E.

Zahra Ghorbani

Najibullah Zulfeqar

Jack Montgomery, Ph.D., P.E.

February 2026

DISCLAIMERS

The contents of this report reflect the views of the authors who are responsible for the facts and accuracy of the data presented herein. The contents do not necessarily reflect the official views or policies of the Alabama Department of Transportation, Auburn University, or the Highway Research Center. This report does not constitute a standard, specification, or regulation. Comments contained in this report related to specific testing equipment and materials should not be considered an endorsement of any commercial product or service; no such endorsement is intended or implied.

Ali Khosravi, Ph.D.

Research Supervisor

ACKNOWLEDGEMENTS

Material contained herein was obtained in connection with a research project, "Evaluation of Landslides along Alabama Highways," ALDOT Project 930-931, conducted by the Auburn University Highway Research Center. Funding for the project was provided by the Alabama Department of Transportation (ALDOT). The funding, cooperation, and assistance of many individuals from each of these organizations are gratefully acknowledged. The authors particularly acknowledge the contributions of the following individuals for serving on the project advisory committee and assisting with the data collection and processing:

Scott George	ALDOT, Materials and Tests Bureau, Montgomery
Kaye Chancellor Davis	ALDOT, Deputy State Materials and Tests Engineer, Montgomery
Christie, Eric	ALDOT, State Maintenance Engineer, Montgomery
Kidada Dixon	ALDOT, RAC Liaison, Montgomery
Kristy Harris	FHWA Liaison
William Brown	ALDOT, Materials and Tests Bureau, Montgomery
Stephanie Wynn	ALDOT, Materials and Tests Bureau, Montgomery
Zahra Ghorbani	Auburn University
Najibullah Zulfeqar	Auburn University
Yasser Maghsoudi	Professor at Exeter University (UK)
Faramarz Nilfouroushan	Professor at University of Gävle (HiG), Sweden

Table of Contents

List of Tables

List of Figures

Chapter 1 - Introduction

In Alabama, ground movements from landslides (Knights et al. 2020) and sinkholes (Montgomery et al. 2020) have led to significant damage and disruption to the state's highway network. Recent dramatic examples include the February 2020 landslide on US-231 (Montgomery et al. 2026), subsidence on I-65 near Warrior in February 2022, and a slope instability in the Littleville area along US Highway 43 in Colbert County (**Figure 1**). Each of these events has led to lane closures, traffic delays, and emergency repairs or investigations. While predicting these types of events is difficult, continuous and accurate monitoring of ground deformation along roads and highways is crucial for identifying risks before they develop into major failures. In current practice, ground deformation is commonly first reported by passing motorists or maintenance personnel. After these reports are received, investigations are completed involving geotechnical and/or geophysical surveys and instrumentation, such as inclinometers or survey monuments, may be installed to monitor movements. Traditional instrumentation can be accurate but provides measurements at only a single point and requires considerable resources and effort to install. This reactive approach to monitoring can be effective at smaller sites with a history of movement. Still, it cannot provide continuous measurements of deformation over an area and can only be applied to sites that have already been moved enough to show signs of distress. A proactive monitoring strategy that can detect ground deformation before damage occurs could increase safety and reduce repair costs and traffic disruptions associated with ground deformation.

Figure 1. (a) ALDOT drill crews installing subsurface moisture sensors along US-43 near Littleville (Colbert County) to investigate localized ground subsidence. (b) Slope instability area along Littleville Highway (Group 3), selected as the installation location for the second corner reflector.

Interferometric synthetic aperture radar (InSAR) is a promising proactive monitoring tool for ground deformation. InSAR is a satellite-based remote sensing technique (**Figure 2**) that can measure ground deformations at the millimeter scale regardless of weather conditions or time of day (Massonnet and Feigl, 1998). InSAR satellites also have a short revisit period and wide spatial coverage, allowing near-continuous monitoring of large regions. With the increase in the number of satellites and recent advancements in InSAR processing techniques, the accuracy of InSAR ground deformation measurements has continued to improve and is becoming a key technology for geohazard detection. Combining InSAR with machine learning techniques, such as deep learning, has further expanded the usefulness of these data.

While very effective and accurate at measuring small- to large-scale ground surface displacements, there are still barriers to fully utilizing this technique, especially in areas with high-density vegetation like Alabama. These challenges include: (1) a sensitivity to vegetation growth;

(2) an inability to distinguish between different sources of ground deformation (i.e., excavations, construction, landslides); and (3) InSAR-based ground deformation measurements are one-dimensional, captured only along the Line-Of-Sight (LOS) direction. These challenges have previously limited the applications of conventional InSAR technology to ground deformations along highways. However, this report demonstrates that many of these limitations can be overcome with new processing approaches and by integrating InSAR with other remote sensing data.

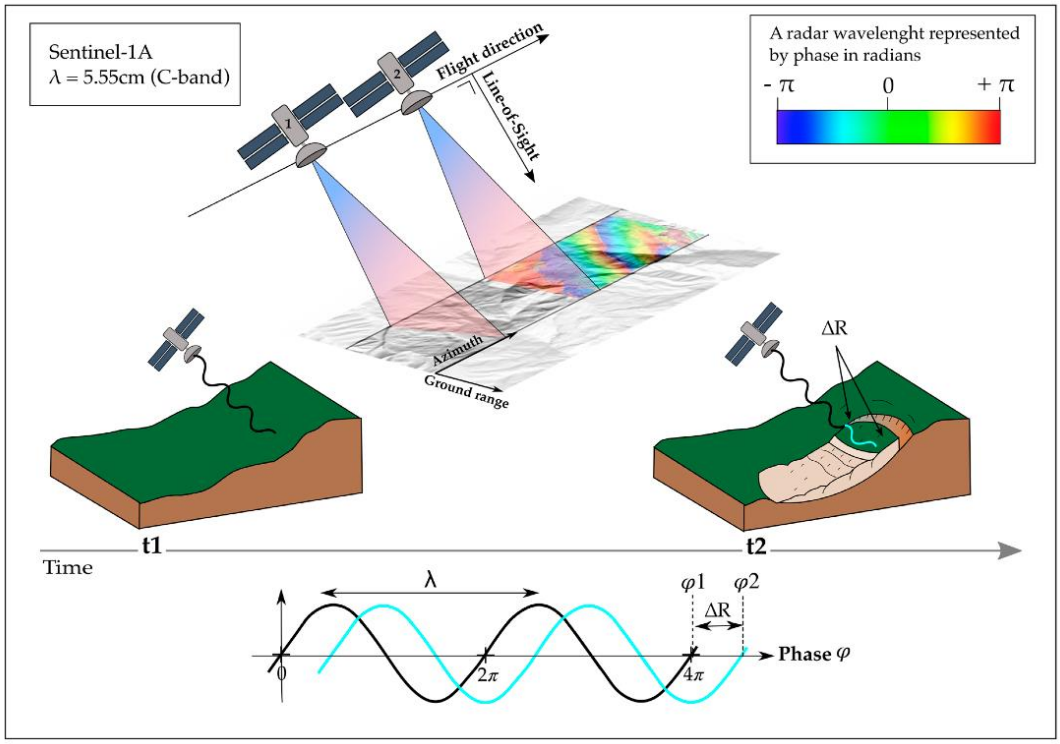

Figure 2. Geometry of a SAR image and principle of differential InSAR (DInSAR) during two successive passes (t1 and t2) of the satellite over the same area, in this case, respectively, before and after a landslide activation and generation of an interferogram; ΔR = difference of distance travelled by the phase φ; λ = wavelength of the sensor (Piroton et al., 2020).

1.1 Project Objectives

This research combines high spatial resolution InSAR measurements, optical remote sensing data, and deep learning algorithms to automatically detect and extract abnormal ground deformation (e.g., from landslides, subsidence, and sinkholes) along Alabama highways. Our approach is specifically designed for removing noise in InSAR time series of highly vegetated areas experiencing slow and small-scale deformations. The InSAR data is also integrated with other types of geotechnical, geospatial, and climate

data to better identify causes of deformations. The results of this research provide a new approach to continuously monitor deformations across large spatial regions and alert ALDOT personnel when abnormal deformations are detected. Implementation of this proactive monitoring approach is expected to increase the safety and reliability of Alabama's transportation system.

1.2 Scope of Work

The overall scope of work for this project is summarized in **Figure 3**. As shown, the project consists of five major tasks, described below.

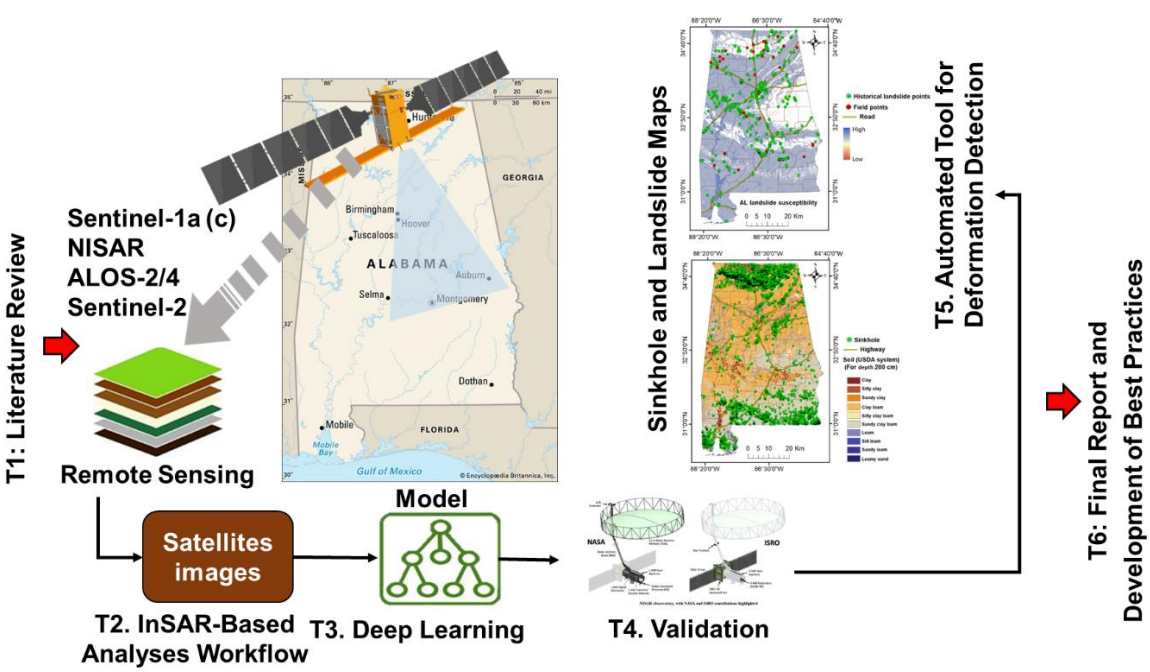

Figure 3. Overall project scope and major tasks.

Task 1 – Literature Review: Conducted a targeted review of remote sensing and deep learning methods for ground deformation detection and time-series anomaly analysis, with emphasis on landslides and sinkholes. The review evaluated key factors influencing performance, including vegetation cover, soil conditions, geomorphology, and infrastructure. Remote sensing approaches were assessed in comparison with traditional in-situ monitoring techniques based on the methods presented in this report.

Task 2 – InSAR-Based Deformation Analysis: Developed an InSAR workflow for statewide and corridor-scale deformation monitoring along Alabama highways. Sentinel-1 C-band SAR imagery (October 2016–present) was processed using both Small Baseline Subset (SBAS) and Persistent Scatterer Interferometric Synthetic Aperture Radar (PS-InSAR) approaches. SBAS time-series analysis was implemented using LiCSAR/LiCSBAS, while high-resolution PS-InSAR processing was performed using PyGMTSAR.

Deformation time series and velocity maps were generated at regional and site-specific scales, and cross-comparison between SBAS and PS-InSAR results was conducted to evaluate consistency, spatial sensitivity, and monitoring performance under varying terrain and vegetation conditions.

Task 3 – Deep Learning–Enhanced Detection: Applied deep learning methods to improve autonomous detection of millimeter-scale deformation in vegetated and low-coherence environments. Optical imagery (Sentinel-2 NDVI), InSAR time series, interferometric coherence, and predisposing factors were fused using convolutional and recurrent neural networks to enhance the detection of slow or subtle deformation.

Task 4 – Validation and Cross-Comparison: Validated deformation results using independent datasets, including existing inclinometer measurements, automated slope monitoring systems, and targeted GNSS surveys at selected sites.

Task 5 – Automated Screening and Early Detection System: Integrated InSAR, deep learning outputs, GIS layers, climate data, and ground-based measurements into a web-based automated system to identify and flag abnormal deformation along highway corridors and support inspection prioritization.

Chapter 2 - Literature Review

Advances in remote sensing and machine learning over the past two decades have significantly transformed how ground deformation processes such as landslides, subsidence, sinkholes, and embankment instability are detected and monitored. Traditional geotechnical instrumentation (e.g., inclinometers, extensometers, piezometers, and GPS surveys) continues to provide high-precision, site-specific measurements, but its limited spatial coverage, high installation cost, and dependence on field personnel make it impractical for statewide, continuous monitoring of distributed hazards. In contrast, remote sensing technologies, such as optical imagery, LiDAR, multispectral analysis, and InSAR, offer scalable, repeatable, and wide-area detection capabilities that can complement or even augment conventional instrumentation. Recent developments in neural networks, including CNNs, recurrent architectures (RNN/LSTM), transformers, and anomaly-detection models, have further expanded the potential of remote sensing datasets by enabling automated identification of subtle deformation patterns, precursory signals, and spatiotemporal anomalies that may precede failure. However, the performance of these techniques is highly dependent on environmental factors, such as soil type, moisture conditions, vegetation density, geomorphology, and the presence of infrastructure, which influence signal coherence and model reliability. This chapter provides a review of remote sensing–based deformation monitoring approaches and modern neural network algorithms, critically evaluating their strengths, limitations, and suitability for application across Alabama's diverse landscapes.

2.1 Geological Hazards in Alabama

2.1.1 Landslide

Landslides, defined as the downslope displacement of earth materials including rock masses, weathered debris, or soil deposits (Cruden, 1991), pose a significant threat to Alabama's highway infrastructure. These ground failures typically result from force imbalances where gravitational and driving forces exceed the inherent resistance of slope materials, often triggered by multiple interacting factors such as intense rainfall events, groundwater fluctuations, additional loading, or erosion processes (Cruden and Varnes 1996; Duncan et al. 2014). Although Alabama lacks the extreme relief of mountainous regions, landslides occur frequently in areas where steep slopes and saturated sediments converge. Beyond infrastructure impacts, landslides in the state also mobilize large volumes of sediment, degrading riverine ecosystems and aquatic habitats.

To characterize slope failures affecting transportation corridors, this study adopts the classification framework used in the ALDOT research report *Evaluation of Landslides along Alabama Highways*

(Montgomery et al., 2019). That statewide inventory applies the movement-based system of Varnes (1978), classifying failures as rotational slides, translational slides, falls, topples, surface erosion (creep), and flows. Maintaining consistency with this classification enables direct comparison between historical failure records and current monitoring results.

Analysis of the ALDOT landslide inventory indicates that shallow earth slides and translational movements in soil materials represent the dominant failure mechanisms along Alabama highways, with rotational slides occurring locally in specific geologic settings (Montgomery et al., 2019). Shallow surface erosion and slow-moving earthflows are also common, particularly in maintained highway embankments. Although these slower movements are rarely catastrophic, they can progressively damage infrastructure through pavement distortion, retaining wall displacement, and utility deformation (Cruden and Varnes, 1996; Alabama Emergency Management Agency, 2018). Overall, the documented failures are primarily soil-related rather than bedrock-dominated, reflecting the geologic and physiographic conditions characteristic of Alabama transportation corridors.

Beyond individual failure observations, statewide spatial analyses further clarify landslide susceptibility patterns. The Geologic Survey of Alabama developed a comprehensive GIS-based landslide susceptibility assessment that integrates topographic slope and relief, precipitation patterns, and seismic potential to identify areas prone to instability (Ebersole et al., 2011) **(Figure 4a)**. Analysis of the ALDOT landslide inventory shows clear spatial clustering of mapped landslides in steeper terrain **(Figure 4b)**.

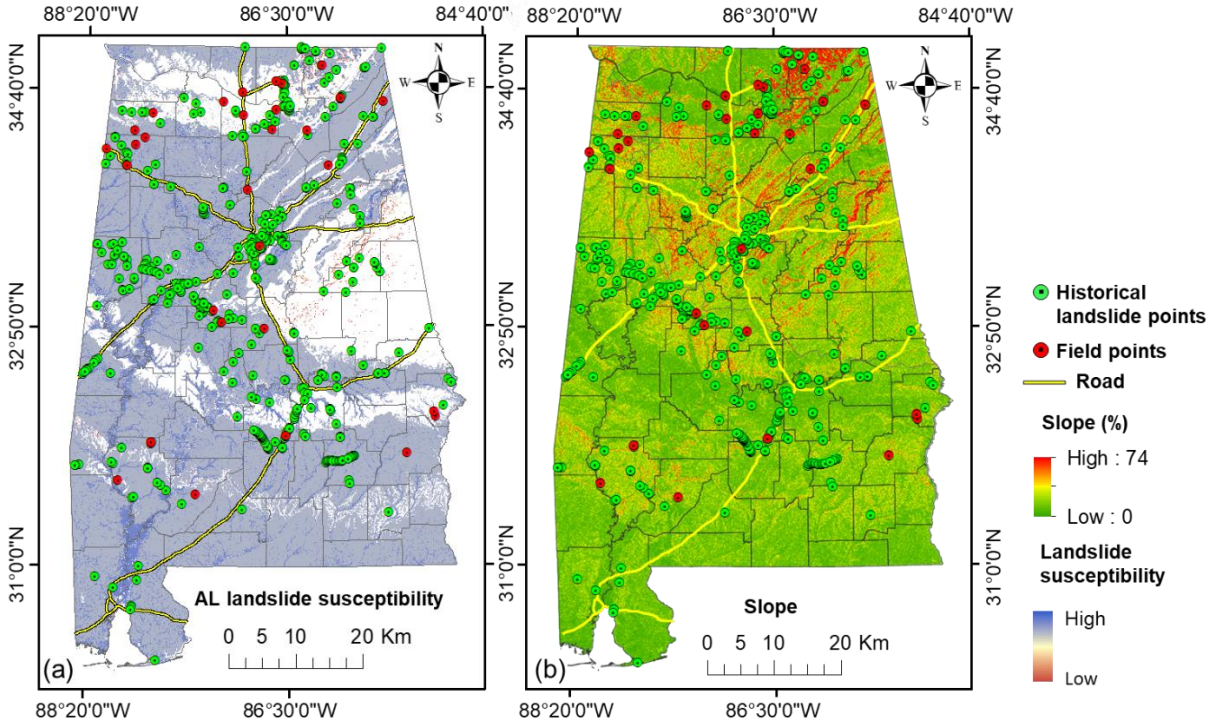

Figure 4. (a) Alabama landslide susceptibility Map (Ebersole et al. 2011) and (b) Slope map derived from NASADEM (30 m resolution), processed in Google Earth Engine, with historical landslide and field point locations.

Landslide occurrences along Alabama highways show strong associations with specific geologic groups, including the Tuscaloosa Group, Midway Group, and Selma Group Chalk, whereas failures are less frequent in limestone-dominated regions (Knights, 2018). Approximately 25% of analyzed landslides occur within 1,000 ft of converging geologic groups, suggesting that geologic contacts and boundary zones significantly influence slope performance (Knights, 2018). These boundaries represent mechanical and hydrologic contrasts that promote preferential failure development **(Figure 5)**.

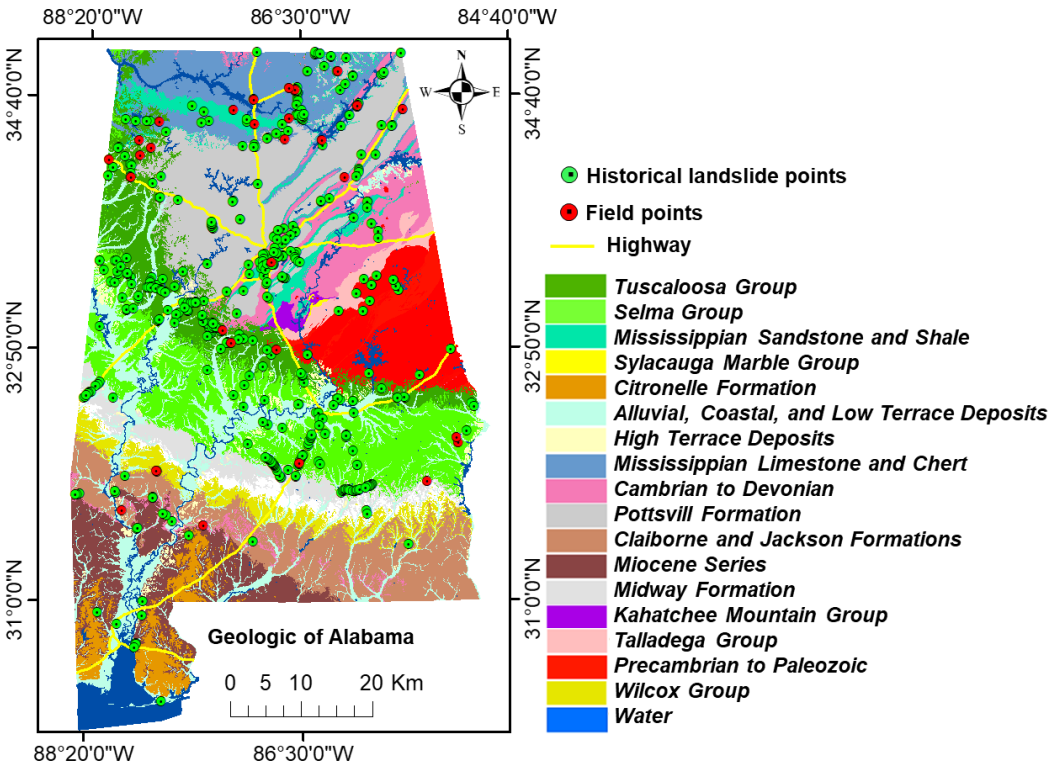

Figure 5. Landslide locations map along with the geological groups.

2.1.2 Sinkholes

Large portions of Alabama are underlain by carbonate bedrock formations, primarily limestone and dolostone, which are highly susceptible to karst processes and sinkhole development (Montgomery et al., 2020; ALDOT, 2021). These soluble lithologies undergo progressive chemical dissolution driven by groundwater circulation, leading to the formation of subsurface voids, conduits, and cavern systems (Montgomery et al., 2020; De Waele et al., 2009). Over time, the enlargement and coalescence of these features can result in surface depressions, gradual subsidence, or sudden catastrophic collapse (USGS, n.d.). Sinkhole susceptibility is particularly high in northern Alabama, where extensive carbonate sequences are overlain by variable thicknesses of unconsolidated soils and residuum (Montgomery et al., 2020; ALDOT, 2021). The dissolution process is further accelerated by the infiltration of slightly acidic precipitation and surface water, which exploits existing fractures, joints, and bedding planes, expanding them into interconnected subsurface drainage networks. When these voids grow large enough to exceed the structural capacity of the overburden, failure may occur in the form of cover-collapse sinkholes, cover-subsidence sinkholes, or broader ground subsidence events **(Figure 6)**. These karst-related hazards pose significant risks to transportation infrastructure and public safety. Notable examples include major remediation efforts along Interstate 20 near Heflin (2012) and Alabama State Route 21 in Talladega County (2013), where

sinkhole-related failures resulted in repair costs exceeding $10 million and caused prolonged traffic disruptions (Montgomery et al., 2020; Orange and Smith, 2014).

One of the most prominent natural features associated with karst activity in the state is the Golly Hole, Alabama's largest documented sinkhole, measuring approximately 300 ft wide, 325 ft long, and 120 ft deep (GSA 2024). While sinkhole formation is a natural geomorphic process in karst terrains, its occurrence and severity can be significantly exacerbated by human activities. Groundwater withdrawal, increased surface loading from construction, inadequate stormwater management, leaking utilities, and altered drainage patterns can all accelerate subsurface erosion and destabilization. Consequently, thorough geotechnical site characterization, hydrogeologic assessment, and long-term monitoring are critical for infrastructure planning and risk mitigation in karst-prone regions of Alabama.

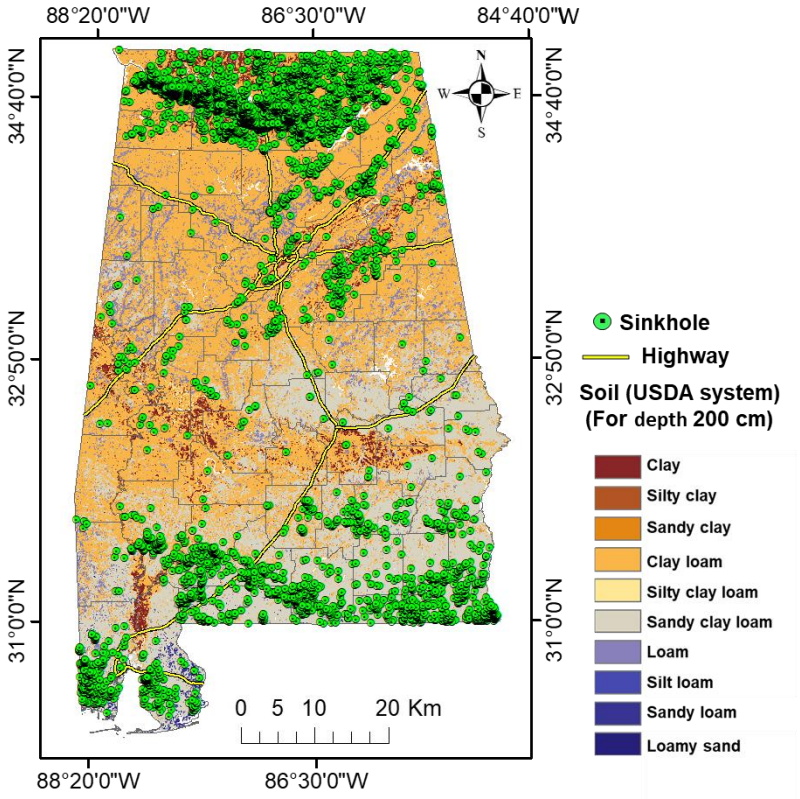

Figure 6. Alabama sinkholes and soil map. Sinkholes Points compiled by Sandy Ebersole and Anthony Tavis, October 2010.

2.2 Geodetic Monitoring for Land Deformation

Geodetic methods form the backbone of modern land-deformation monitoring because they measure ground movement directly within a well-defined coordinate system. Unlike geotechnical instruments, which are typically point-specific or geophysical methods that infer deformation indirectly from subsurface

properties, geodetic techniques quantify surface displacement in true geometric terms. This makes them indispensable for monitoring both localized instabilities (e.g., slope failures, embankment deformation) and broad regional trends such as subsidence, groundwater withdrawal impacts, or post-glacial rebound. A key strength of geodetic systems is their ability to detect subtle, cumulative displacements and map strain patterns over time. These capabilities stem from the integration of diverse technologies, each contributing complementary spatial or temporal strengths. Modern deformation monitoring networks often combine:

- **Robotic total stations**, which continuously track prism targets to measure precise angles and distances, provide high-resolution horizontal and vertical displacement at critical points.
- **Differential and geometric leveling**, the most accurate method for detecting vertical movement, widely used for monitoring settlement along levees, highways, and embankments.
- **GNSS/GPS receivers**, capable of continuous or campaign-based 3D positioning, allowing both long-term regional deformation studies and local slope-stability monitoring.
- **Radar interferometry (InSAR),** both spaceborne and terrestrial, offering spatially continuous measurements across large areas with millimeter-scale precision.
- **Aerial LiDAR and photogrammetric systems**, which generate high-resolution elevation models for mapping deformation patterns, fault scarps, landslide morphology, and surface subsidence.

Together, these methods form a multi-sensor geodetic framework that ensures resilience against the limitations of individual techniques. For example, line-of-sight restrictions may limit total station visibility; atmospheric delays can introduce noise in GNSS or InSAR signals; and LiDAR/photogrammetry performance may decline in dense vegetation. By designing networks with overlapping measurements, redundant control points, and closed-loop geometry, these limitations are mitigated through statistical adjustment and cross-validation.

Geodetic monitoring is structured around an interconnected network of reference stations, benchmarks, and observation points that enable surface deformation to be tracked across multiple spatial dimensions. In well-designed networks, combining angular measurements, distance observations, and height differences produces statistically robust estimates of movement while also enabling automatic detection of measurement inconsistencies (Beshr, 2015). Best-practice guidelines suggest that a monitoring network should detect displacement with a precision equal to one-third of the expected maximum deformation, achieving approximately 95% confidence over the monitoring period. In this integrated framework, each geodetic technique contributes unique advantages, high temporal frequency from GNSS, high spatial density from InSAR, high vertical precision from leveling, and high point precision from total stations, together offering a comprehensive, reliable approach to understanding land deformation processes

across complex terrain. The focus of this literature review will be on the InSAR technique, which is the core technology implemented.

2.2.1 InSAR for Land Deformation Monitoring

Although InSAR is fundamentally based on satellite remote sensing, it is widely regarded as a geodetic deformation-monitoring technique because it provides direct, quantitative measurements of surface displacement referenced to a stable coordinate framework. InSAR, therefore, occupies a unique position at the intersection of geodesy and remote sensing: it relies on orbital radar systems to acquire data, yet the deformation information extracted from radar phase belongs squarely to the geodetic domain. This dual identity often leads to ambiguity in classification, but for the purposes of land deformation monitoring, InSAR is most appropriately understood as a geodetic tool enabled by remote sensing technology.

As geodetic monitoring evolved beyond leveling, total station surveying, and GNSS networks, InSAR introduced a fundamentally different capability, the ability to detect millimeter-scale deformation continuously across wide areas without installing ground instruments. Synthetic Aperture Radar satellites transmit their own microwave energy and record the returning echoes, allowing them to operate independently of daylight and to acquire measurements through clouds, smoke, and most atmospheric conditions. This all-weather imaging capability made SAR an attractive observational platform, but its transformative geodetic potential emerged only when researchers discovered that the phase of radar signals could be used to measure extremely small changes in distance between the satellite and the ground (Massonnet and Feigl, 1998).

Interferometry exploits this property by comparing two SAR images acquired from nearly identical viewing geometries at different times. Because the radar phase is extremely sensitive to path length, even minute changes in elevation or surface position alter the phase recorded in the second acquisition. When these phase differences are analyzed, they reveal ground motion on the order of centimeters or even millimeters. Differential InSAR (DInSAR), which removes the topographic contribution using an external digital elevation model, isolates the deformation component with exceptional precision. This capability enabled InSAR to move deformation monitoring from a point-based to an area-based discipline, transforming the field by providing millions of measurement points simultaneously across regions spanning hundreds of square kilometers (Erol et al., 2004).

The emergence of InSAR was part of a broader transformation in remote sensing that began with the launch of Landsat in 1972 (Mantovani et al., 1996). Over several decades, improvements in spectral resolution, radiometric quality, and revisit frequency expanded the ability of passive optical sensors to monitor land surface changes, including vegetation loss, exposed scarps, and surface cracking after

landslides. However, optical systems depend on reflected sunlight and are constrained by cloud cover, rendering them ineffective in many conditions and limiting their value for continuous deformation monitoring. SAR systems resolved these limitations by shifting from passive observation to active illumination. Because radar energy interacts with the surface differently than reflected light, responding to roughness, dielectric properties, and moisture content, SAR provides a distinct physical measurement that complements optical observations. The addition of airborne SAR and ground-based radar systems further expanded the temporal and spatial flexibility of radar-based monitoring.

InSAR harnesses the strengths of SAR platforms while providing a fundamentally geodetic output. Modern SAR constellations, including Sentinel-1, ALOS-2, TerraSAR-X, Cosmo-SkyMed, and the recent NiSAR mission, offer frequent repeat intervals, stable orbits, and high-quality phase measurements that enhance the reliability of deformation mapping. These advances have established InSAR as one of the most powerful tools for identifying surface movements associated with landslides, embankment settlement, groundwater withdrawal, mining subsidence, volcanic inflation, post-glacial rebound, and tectonic strain accumulation (Massonnet and Feigl 1998; Crosetto et al. 2016; Drouin and Sigmundsson 2019). Unlike conventional geodetic surveys that provide discrete measurements, InSAR produces spatially continuous deformation fields that reveal movement gradients, accelerating zones, and deformation patterns invisible through any point-based approach.

The continuing development of InSAR cannot be separated from the evolution of SAR missions themselves. Early systems such as ERS-1 and ERS-2 provided the first stable datasets for interferometry (Massonnet and Feigl, 1998), while ENVISAT and RADARSAT expanded spatial coverage and imaging frequency. Subsequent high-resolution missions such as TerraSAR-X and Cosmo-SkyMed demonstrated the potential for detailed deformation mapping in urban and infrastructure environments. The launch of Sentinel-1 in 2014 marked a major technological shift, offering open data access, consistent long-term operation, short repeat cycles, and rigorous orbit control features that empowered widespread, operational InSAR applications across academic, government, and industry sectors (Torres et al., 2012). These improvements enabled the creation of nationwide deformation products, long-term monitoring programs, and automated processing pipelines that continue to shape the modern landscape of geodetic remote sensing.

SAR Mission Evolution: As mentioned earlier, the development of Interferometric Synthetic Aperture Radar (InSAR) is inseparable from the evolution of spaceborne SAR missions. Each satellite constellation has contributed specific advances in radar wavelength, orbital stability, spatial resolution, and revisit frequency factors that determine InSAR's precision and reliability for ground deformation monitoring.

Figure 7 presents a historical overview of major SAR missions, illustrating their operating agencies, frequency bands, and temporal progression (Paradella et al., 2021).

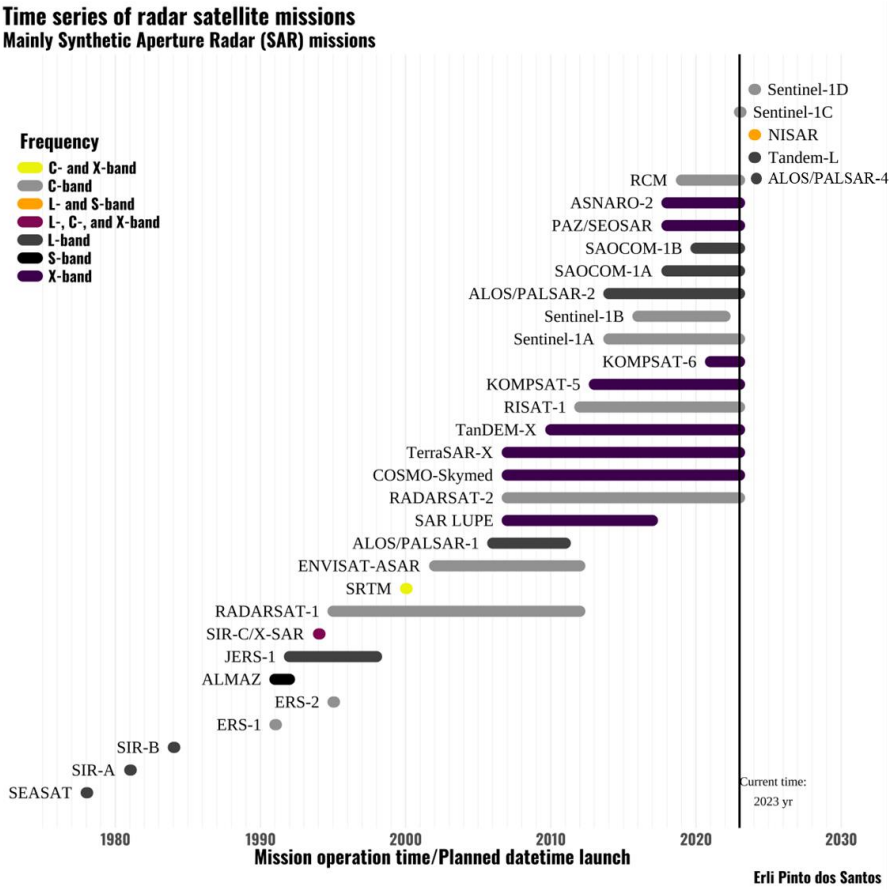

Figure 7. Synthetic-aperture radar missions (Paradella et al., 2021).

Sentinel-1 Mission (ESA): The European Space Agency's Sentinel-1 mission, part of the Copernicus Earth Observation Program, is a cornerstone for global InSAR-based deformation monitoring. The constellation includes two C-band satellites, Sentinel-1A (launched 2014) and Sentinel-1B (launched 2016), continuing the legacy of ERS-1/2 and ENVISAT. Sentinel-1's systematic acquisition strategy, short revisit time, and open-access data policy have enabled widespread operational use for land deformation and hazard monitoring. Although Sentinel-1B ceased operation in 2021, continuity is planned through Sentinel-1C and Sentinel-1D. Sentinel-1 supports multiple imaging modes optimized for different applications. The Interferometric Wide Swath (IW) mode, using TOPSAR beam steering, is the primary configuration for terrestrial deformation monitoring, providing a wide swath with reliable interferometric quality. Other modes, including Stripmap (SM), Extra-Wide (EW), and Wave (WV), support higher-resolution imaging or large-area maritime and polar observations (Ustin & Middleton, 2021).

COSMO-SkyMed (ASI): The COSMO-SkyMed constellation, developed by the Italian Space Agency, consists of four X-band SAR satellites launched between 2007 and 2014. The system provides high-resolution radar imagery for civilian and defense applications, including infrastructure monitoring, urban mapping, and deformation analysis. COSMO-SkyMed offers flexible acquisition modes that trade spatial resolution for coverage. Spotlight and StripMap modes enable detailed analysis of urban areas and transportation corridors, while ScanSAR modes support regional-scale monitoring. Its high temporal frequency, polarization diversity, and X-band sensitivity make COSMO-SkyMed well-suited for detailed InSAR deformation studies in built environments (Ustin & Middleton, 2021).

TerraSAR-X and TanDEM-X (DLR): TerraSAR-X, launched in 2008 by the German Aerospace Center (DLR), is a high-resolution X-band SAR mission designed for scientific and operational monitoring. Its companion satellite, TanDEM-X (launched 2010), flies in close formation, enabling bistatic and interferometric acquisitions that have advanced deformation monitoring and global topographic mapping. The TerraSAR-X/TanDEM-X constellation provides high coherence in urban and engineered environments, making it particularly valuable for Persistent Scatterer InSAR applications involving infrastructure such as bridges, dams, levees, and buildings. The mission also produced the TanDEM-X global digital elevation model, one of the most accurate global DEM datasets available (Ustin & Middleton, 2021).

PAZ Mission (Spain / Hisdesat): PAZ, launched in 2018, is Spain's first radar imaging satellite and operates an X-band SAR instrument for civilian and defense applications. The mission was designed to operate synergistically with TerraSAR-X and TanDEM-X, forming a virtual X-band constellation with improved revisit frequency and temporal coverage. PAZ supports high-resolution imaging suitable for urban mapping, infrastructure monitoring, and InSAR deformation analysis. Its compatibility with existing X-band systems enables consistent multi-mission datasets for Persistent and Distributed Scatterer InSAR studies (Ustin & Middleton, 2021).

ALOS PALSAR-2 Mission (JAXA): ALOS-2 PALSAR-2, launched in 2014 by JAXA, is an advanced L-band SAR mission building on the legacy of ALOS-1. Its longer wavelength provides superior coherence in vegetated and agricultural regions, where C-band and X-band systems often decorrelate. This capability makes PALSAR-2 particularly valuable for deformation monitoring in forested, subtropical, and rural environments. The mission has been widely used for subsidence, landslide, volcanic, and earthquake deformation studies (Suzuki et al., 2012).

NISAR Mission (NASA–ISRO): NISAR is a joint NASA–ISRO mission launched in July 2025, carrying dual-frequency L-band and S-band SAR instruments. It is the first satellite to routinely acquire two wavelengths simultaneously, enabling improved characterization of surface deformation, vegetation, and

land cover. The mission follows a systematic global acquisition strategy with high temporal frequency, making it a major future resource for InSAR-based deformation monitoring across diverse environments, including infrastructure corridors, agricultural regions, cryosphere, and tectonically active areas (NASA–ISRO, 2023).

ALOS-4 / PALSAR-3 Mission (JAXA): ALOS-4, launched in 2024, is the successor to ALOS-2 and carries the PALSAR-3 L-band SAR instrument. The mission features a substantially expanded swath width (up to ~200 km) while maintaining interferometric quality, enabling more efficient large-area deformation monitoring. With improved revisit frequency and strong coherence retention in vegetated terrain, ALOS-4 enhances JAXA's long-term L-band InSAR capability for hazard assessment, environmental monitoring, and infrastructure stability analysis (JAXA, 2024).

Available SAR band types: Unlike passive optical systems that depend on reflected solar radiation across visible and infrared wavelengths, Synthetic Aperture Radar (SAR) systems actively emit and receive microwave energy, allowing continuous data acquisition regardless of lighting conditions or cloud cover. Optical sensors record only the portion of the electromagnetic spectrum illuminated by the Sun, of which the human eye perceives just a narrow visible range, whereas SAR instruments operate across microwave frequencies from approximately 1 to 40 GHz. Each frequency band exhibits distinct scattering, penetration, and interaction behaviors with Earth's surface, making wavelength selection a fundamental design parameter in SAR remote sensing. The interaction between SAR microwaves and surface targets is governed primarily by the relationship between the radar wavelength and the characteristic dimensions of the objects being imaged (**Table 1**, **Figure 8**). Shorter wavelengths interact strongly with fine-scale features near the surface, whereas longer wavelengths penetrate deeper into vegetation, snow, and soil before scattering. This provides SAR with unique observational flexibility: by selecting specific bands and polarizations, sensors can be optimized for applications ranging from high-resolution infrastructure monitoring to deep vegetation penetration for biomass assessment (Fernández-Landa, n.d.).

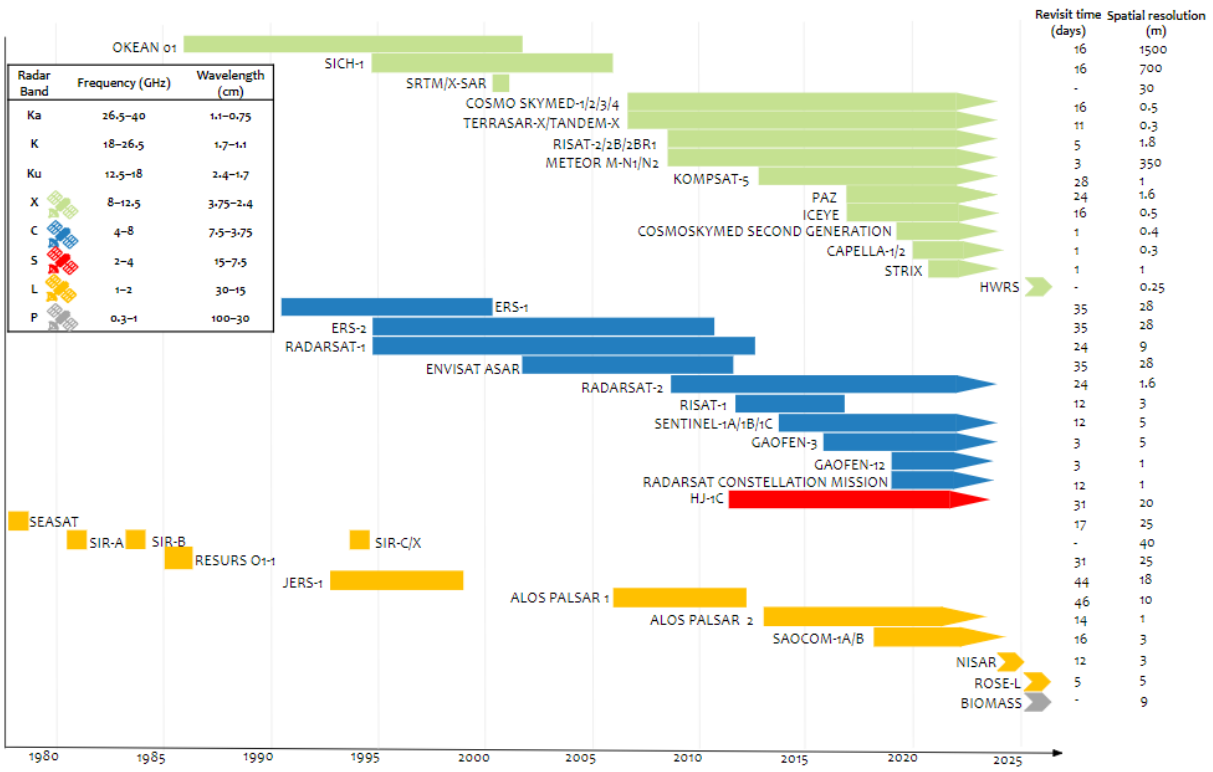

Figure 8. SAR band types (Fernández-Landa, n.d.).

Table 1: Available SAR band types (Fernández-Landa, n.d.).

Band	Frequency	Wavelength	Characteristics	Typical Application
Ka	27–40 GHz	1.1–0.8 cm	Not very useful for SAR	Airport surveillance
K	18–27 GHz	1.7–1.1 cm	Not very useful for SAR	Airport surveillance
Ku	12–18 GHz	2.4–1.7 cm	Not very useful for SAR	Airport surveillance
X	8–12 GHz	3.8–2.4 cm	High resolution, low penetration, not useful in vegetated areas	Urban and infrastructure monitoring, ice and snow, weather
C	4–8 GHz	7.5–3.8 cm	Medium resolution, medium penetration, higher coherence	Change detection, ice, urban and infrastructure monitoring, maritime navigation, glaciers
S	2–4 GHz	15–7.5 cm	Experimental SAR, high penetration	Agriculture monitoring, Marine radar

L	1–2 GHz	30–15 cm	Medium resolution SAR, high penetration	Geophysical monitoring, biomass and vegetation mapping, soil moisture
P	0.3–1 GHz	100–30 cm	Experimental SAR, susceptible to ionosphere, No sensors yet	Biomass, tropical forest mapping, mapping, soil moisture

Band-Dependent Penetration and Vegetation Interaction: The profound influence of wavelength on SAR penetration depth is clearly demonstrated in forestry and biomass-monitoring applications (**Figure 9**). Short-wavelength X-band energy interacts mainly with the upper canopy surface, producing detailed measurements of leaves and small branches but limited penetration into deeper vegetation layers. In contrast, L-band microwaves penetrate mid-canopy layers, enabling characterization of trunk and branch structure, while experimental P-band systems can reach the forest floor, interacting with major biomass components and soil substrates. This wavelength-dependent scattering hierarchy allows multi-band SAR systems to extract structural information across different layers of vegetated environments:

- **X-band:** captures fine-scale canopy texture and surface roughness.
- **L-band:** characterizes intermediate vegetation structure and larger biomass elements.
- **P-band:** penetrates to near-ground features, facilitating deep biomass estimation and soil mapping.

Such frequency-specific behavior is central to selecting appropriate SAR bands for applications ranging from forest structure analysis to soil moisture retrieval, land subsidence mapping, and geophysical hazard assessment (Fernández-Landa, n.d.).

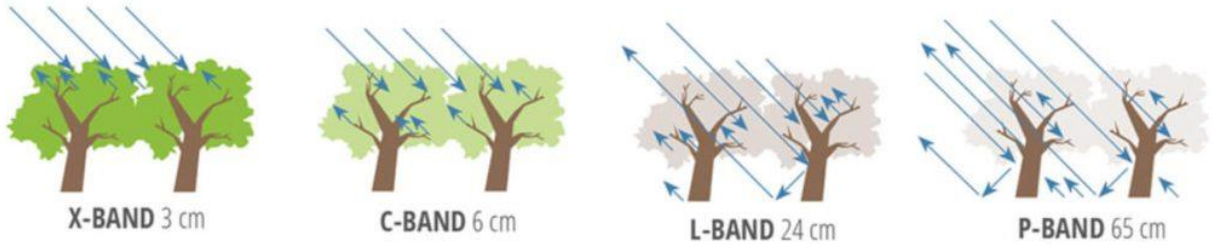

Figure 9. Different frequency bands (Fernández-Landa, n.d.).

C-Band (3.8–7.5 cm): C-band, used by missions such as Sentinel-1 and Radarsat-2, provides a balance between surface sensitivity and moderate vegetation penetration. Although its backscatter characteristics can be complex and somewhat less predictable due to interactions with roughness, moisture, and vegetation structure, C-band remains highly effective for detecting meter-scale features. Its versatility supports a wide

range of applications, including urban deformation monitoring, deforestation tracking, agricultural change detection, and general land-use analysis (Fernández-Landa, n.d.).

X-Band (2.4–3.8 cm): X-band sensors, including TerraSAR-X and COSMO-SkyMed, operate at high frequencies that capture exceptionally detailed surface information. Their short wavelengths interact primarily with canopy tops and surface elements, limiting penetration depth but enabling high-resolution observation of centimeter-scale features. This makes X-band particularly valuable for infrastructure monitoring, landslide scar detection, snow and ice mapping, and weather-related observation scenarios where fine spatial detail is essential.

P-Band (30–100 cm): At the long-wavelength end of the SAR spectrum, P-band achieves the greatest penetration into vegetation and, under suitable conditions, into soil. This capability allows detection of structural elements several meters below the canopy surface, making P-band highly relevant for geological surveys, deep biomass estimation, archaeological prospecting, and large-scale deforestation monitoring. Although no operational spaceborne P-band SAR missions exist yet due to ionospheric interference challenges, experimental systems have demonstrated their significant scientific potential.

L-Band (15–30 cm): L-band SAR provides an optimal compromise between spatial resolution and vegetation penetration, enabling characterization of subsurface and structural features that shorter wavelengths cannot resolve. Missions such as ALOS PALSAR and ALOS-2 have demonstrated the band's suitability for land deformation monitoring, soil moisture retrieval, biomass estimation, crop condition analysis, and ice-sheet motion mapping. Although its spatial resolution is generally coarser than C- or X-band systems (e.g., ALOS at 50 m × 50 m versus Sentinel-1 at 20 m × 5 m), L-band's coherence retention and deeper penetration make it exceptionally effective for interferometric applications, particularly in vegetated or decorrelation-prone environments (*https://detektia.com/en/sar-synthetic-aperture-radar/*).

2.2.1.1 InSAR Time-Series Analysis Techniques

While conventional InSAR relies on comparing two radar images to estimate ground displacement, the true analytical strength of the technique emerges when long archives of images, sometimes spanning months to decades, are processed as a time series. Time-series analysis overcomes the key limitations of single interferograms, including atmospheric noise, temporal decorrelation, orbital errors, and the difficulty of distinguishing true deformation from artifacts. Two methodological frameworks dominate modern InSAR time-series analysis, each suited to different land-cover types and deformation behaviors.

The first approach, Persistent Scatterer InSAR (PS-InSAR), was pioneered by Ferretti et al. (2001). PS-InSAR isolates point targets that maintain highly stable radar backscatter over long time periods. These persistent scatterers typically occur in urban settings (e.g., buildings, road surfaces, metallic structures), but

they may also include natural reflectors such as rock outcrops or cliff faces. By analyzing dozens to hundreds of radar acquisitions, the method suppresses atmospheric artifacts, extracts phase histories at millimeter precision, and produces dense displacement point clouds ideally suited for detecting gradual urban subsidence, structural deformation, and infrastructure instability. The second framework, Small Baseline Subset (SBAS), introduced by Berardino et al. (2002) and refined by Lanari et al. (2004), takes a fundamentally different approach. Instead of focusing on isolated, highly coherent point scatterers, SBAS retains coherence by selecting interferogram pairs with short spatial and temporal baselines, thereby maximizing phase stability across distributed natural surfaces. SBAS is particularly advantageous in vegetated, agricultural, and rural environments where PS-InSAR coherence deteriorates. Although spatial point densities are typically lower and precision somewhat reduced compared to PS-InSAR, SBAS excels for monitoring wide-area deformation, including landslides, groundwater-related subsidence, volcanic uplift, and seasonal surface oscillations. Together, these two techniques deliver complementary strengths, enabling comprehensive monitoring across heterogeneous landscapes. PS-InSAR dominates in the built environment, while SBAS enables reliable deformation mapping across natural terrain. Their combined use has supported applications ranging from rapid urban subsidence detection to centimeter-scale landslide monitoring, sinkhole precursors, mining deformation, and long-term hydrogeological processes (Wasowski and Bovenga 2014; Chaussard et al. 2014; Shi et al. 2019; Wang et al. 2011).

During the past two decades, the expansion of InSAR time-series capabilities has been driven by three concurrent technological advances. First, satellite missions now offer improved spatial resolution, higher radiometric sensitivity, and shorter revisit times. Second, new processing algorithms have substantially reduced atmospheric artifacts and orbital errors, enabling the extraction of subtle deformation signals. Third, cloud-computing infrastructures and automated workflows now support large-scale processing of thousands of scenes, making regional or national-scale monitoring feasible for the first time. However, despite these advances, operational adoption remained limited for many years due to high data costs and inconsistent acquisition strategies. Pre-2014 SAR missions exemplify this challenge. The COSMO-SkyMed constellation (Covello et al., 2010), although composed of four satellites and capable of rapid emergency response (Reale et al., 2011; Grandoni et al., 2014), was constrained by dual civilian-military priorities and commercial pricing, both of which restricted routine monitoring. These barriers were not unique to COSMO-SkyMed; they characterized nearly all SAR systems prior to 2014 and severely limited widespread scientific and operational InSAR use.

The launch of ESA's Sentinel-1 mission under the Copernicus program fundamentally changed the landscape. With Sentinel-1A (2014) and Sentinel-1B (2016), InSAR gained its first global, systematically acquired, open-access SAR archive. Four capabilities proved transformative: continuous six-day revisit

cycles through coordinated constellation planning; wide-area imaging via the TOPS (Terrain Observation with Progressive Scans SAR) mode; near-real-time product availability within hours of acquisition; and complete free and open access (Showstack, 2014). Combined with appropriate spatial resolution for deformation detection (Torres et al., 2012), these factors eliminated the primary barriers to sustained operational monitoring. Yet one decade after its launch, Sentinel-1's transformative potential remains only partially realized. Much of today's work still focuses on retrospective analyses of known unstable areas (Kalia et al., 2017; Vecchiotti et al., 2017), rather than on building continuous, proactive monitoring frameworks capable of identifying emerging deformation before failure occurs. This underutilization is particularly notable in hydrogeological and slow-moving deformation contexts, precisely the problems that benefit most from long-term, systematic observation.

The subsections that follow examine the technical principles of PS-InSAR and SBAS in greater detail, emphasizing their algorithmic foundations, relative strengths and weaknesses, and suitability for different geological and infrastructure monitoring applications

Persistent Scatterer Interferometry (PSI) Analysis: Persistent Scatterer Interferometry (PSI) was developed to overcome one of the most significant limitations of conventional InSAR: maintaining reliable phase measurements over long time periods in the presence of atmospheric disturbances, temporal decorrelation, and surface changes. The method is based on a key observation that certain surface features maintain remarkably stable radar backscatters across dozens to hundreds of SAR acquisitions. These long-lived radar reflectors, known as persistent scatterers (PS), allow deformation monitoring with millimeter-level precision even in complex environments. PSI identifies these stable scatterers by analyzing the temporal phase behavior of each pixel across a sequence of interferograms **(Figure 10**). A spatially and temporally optimal "master" image is selected, and all remaining acquisitions are referenced to it. Instead of attempting to measure deformation everywhere, PSI targets only those pixels whose phase histories exhibit exceptional stability, thereby producing deformation measurements of very high reliability where appropriate PS targets exist. Urban environments are particularly well-suited to PSI because buildings, metallic structures, transportation infrastructure, and rock outcrops provide abundant, stable reflectors (Khan et al., 2021). Measurement densities in dense cities can exceed 1,000 points per square kilometer (Crosetto et al., 2016; Karamvasis and Karathanassi, 2020). However, PSI performance degrades significantly in agricultural, forested, or moisture-variable landscapes, ironically, regions commonly affected by substantial subsidence due to groundwater withdrawal. In such environments, vegetation growth, seasonal canopy changes, plowing cycles, and fluctuating soil moisture lead to rapid decorrelation, reducing the number of suitable PS targets and limiting PSI applicability.

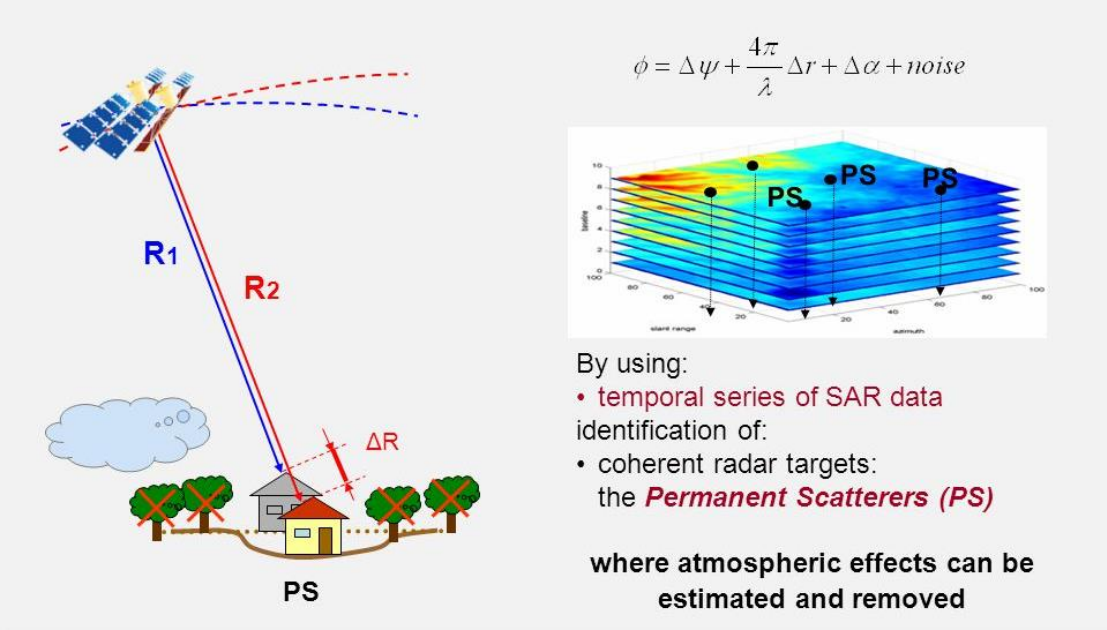

Figure 10. Temporal series of SAR data identification of coherent radar targets: the PS, where atmospheric effects can be estimated and removed (Billenberg, 2024).

To analyze persistent scatterers in this investigation, the Coherent Target Monitoring (CTM) algorithm was applied (Van der Kooij et al., 2005; Mei et al., 2008; EV-InSAR, 2004). CTM identifies stable measurement points using temporal coherence (TC), which quantifies pixel-wise phase stability over long time periods. A distinguishing advantage of CTM is its ability to incorporate both discrete point targets and distributed scatterers, expanding measurement coverage in heterogeneous terrain. PSI decomposes the differential interferometric phase (ϕ_{diff}) into its physical components (Equation 2):

$$\phi_{diff} = \phi_{def} + \phi_{atm} + \phi_{dem-error} + \phi_{noise} \quad (1)$$

where ϕ_{def} is the ground deformation signal, ϕ_{atm} is the atmospheric delay effects, $\phi_{dem-error}$ is the residual topographic phase, *and* ϕ_{noise} is system noise. Atmospheric correction begins by selecting a stable reference region with assumed uniform atmospheric behavior. Subtracting the mean phase of the reference area yields an atmosphere-corrected interferogram (ϕ_{aci}):

$$\phi_{aci} = \phi_{def} + \phi_{dem-error} + \phi_{noise} \quad (2)$$

Residual phase (ϕ_i) is then computed after removing modeled deformation and DEM-related components:

$$\phi_i = \phi_{aci} - \phi_{def} - \phi_{dem-error} \quad (3)$$

Temporal coherence (γ) of each pixel is calculated by combining phase information across *n* interferograms (Equation 5) (Van der Kooij et al. 2005; Mei et al. 2008; EV-InSAR 2004):

$$\gamma = \frac{\sqrt{\left[\sum_i \cos(\phi i)\right]^2 + \left[\sum_i \sin(\phi i)\right]^2}}{\mathrm{n}} \tag{4}$$

CTM iteratively searches for DEM error and linear deformation parameters that maximize temporal coherence. Atmospheric phase components are progressively refined by removing deformation and DEM error terms from the differential phase and smoothing the remaining atmospheric signal using only high-coherence pixels. This iterative refinement produces progressively improved interferograms for subsequent deformation estimation. PSI is particularly effective in urban environments, where engineered structures provide bright, stable reflectors and high signal-to-noise ratios (Khan et al., 2021). In areas lacking strong point scatterers, especially natural terrain with moderate to dense vegetation, spectral filtering methods can be used to extract Slowly Decorrelating Filtered Pixels (SDFP). These distributed targets exhibit coherent phase behavior only when analyzed as ensembles. While measurement density and precision are typically lower than classical PSI, the SDFP extension significantly broadens applicability into partially vegetated or mixed-use landscapes.

Small Baseline Subset (SBAS) Analysis: While PSI performs exceptionally well in urban environments dominated by stable artificial structures, many of the most critical deformation processes occur in landscapes where persistent scatterers are sparse or absent, such as agricultural valleys, forested hillslopes, desert fringes, and vegetated floodplains. The SBAS technique was developed specifically to overcome these limitations by adopting a fundamentally different strategy. Rather than seeking long-term stable point targets, SBAS exploits distributed scattering from natural surfaces by constructing interferogram networks with minimal temporal and spatial baselines. The essential insight behind this approach is that short revisit intervals and small orbital separations reduce temporal and geometric decorrelation, allowing coherence to be maintained even across surfaces that undergo seasonal or intermittent changes.

SBAS forms a network of interferograms that uses multiple master images rather than relying on a single master scene. Each acquisition may serve as both primary and secondary in different interferogram pairs, producing a redundant, interconnected measurement structure that maximizes temporal coverage. By restricting interferograms to short temporal baselines typically 12–24 days and small perpendicular baselines (often <150 meters), SBAS retains coherence over a large fraction of the scene. This strategy increases the number of usable pixels dramatically, enabling the method to incorporate Slowly Decorrelating Filtered Pixels (SDFP) natural surfaces that do not meet classical PSI stability thresholds but exhibit sufficient coherence when properly filtered. As a result, SBAS often provides broader spatial

coverage than PSI, particularly in rural or semi-vegetated regions. In favorable conditions, SBAS may measure deformation in 40–60% of pixels, compared to the sparsely distributed PS networks common in point-scatterer analyses (Tiwari et al., 2016; Smith et al., 2021). The approach relies heavily on spectral filtering to suppress decorrelation noise and identify pixels with consistent phase history. Deformation time series are then reconstructed by solving the interferogram network through constrained least-squares inversion, where temporal smoothness assumptions help compensate for gaps in the decorrelated or disconnected portions of the interferogram graph.

These advantages, however, come with inherent trade-offs. Because SBAS depends on distributed scatterers, its performance decreases sharply in areas characterized by rapid vegetation cycles, dense canopy cover, or highly reflective agricultural practices. Seasonal crop rotation, plowing, irrigation, and biomass fluctuations introduce significant temporal decorrelation, producing gaps in spatial coverage that are intrinsic to natural landscapes rather than limitations of the processing architecture. Even under optimized conditions, agricultural regions may exhibit persistent "blind spots" where deformation cannot be estimated reliably.

Over the past decade, the SBAS workflow has benefited enormously from advances in open-source processing frameworks. GMTSAR (Sandwell et al., 2011) provides an efficient, end-to-end SAR processor tightly integrated with Generic Mapping Tools (GMT). StaMPS (Hooper et al., 2007; Hooper, 2008), originally designed for PSI, has been extended to support SBAS through its SDFP module, offering robust atmospheric correction and phase unwrapping. MintPy (Yunjun et al., 2019) represents a modern Python-based framework capable of automated atmospheric filtering using ERA5 and ECMWF weather models, advanced network optimization, and cross-compatibility with processors such as ISCE, ARIA, HyP3, GMTSAR, and SNAP. LiCSBAS (Morishita et al., 2020), tightly coupled with the Sentinel-1 LiCSAR workflow, provides automated small-baseline processing with loop-closure correction and advanced noise filtering, a system discussed later in Section 4.2 as the primary tool used in this investigation. Additional tools such as pyGMTSAR (Pechnikov, 2023) extend GMTSAR functionality through Python interfaces, improved visualization, and Jupyter notebook integration. ISCE (Rosen et al., 2012), developed by NASA JPL and Stanford, offers comprehensive raw-data processing with full support for time-series workflows. Commercial systems such as ENVI SARscape, GAMMA Software (Werner et al., 2000; Wegmüller et al., 2016), and ESA's SNAP toolbox provide additional operational capabilities, though typically with higher computational or licensing barriers.

The choice of SBAS processor depends on data volume, computational resources, and application requirements. In this investigation, StaMPS was used for SDFP-based deformation analysis. The resulting spatial coverage reflects the inherent coherence characteristics of the landscape rather than limitations of

the processing strategy; in vegetated or agriculture-dominated regions of Alabama, decorrelation fundamentally restricts pixel-level continuity. Most importantly, PSI and SBAS should not be viewed as competing methods but as complementary components of a comprehensive InSAR monitoring strategy. PSI delivers high-precision, millimeter-level deformation time series at sparse but extremely reliable points ideal for built environments, infrastructure monitoring, and long-lived scatterers. SBAS offers moderate-precision, dense spatial coverage across natural terrain ideal for capturing regional subsidence, slow-moving landslides, and diffuse deformation patterns. Modern InSAR workflows, such as StaMPS (combined PS + SB) (Hooper, 2008), SqueeSAR (PS + DS) (Ferretti et al., 2011), and EZ-InSAR (ISCE + StaMPS + MintPy integration) (Hrysiewicz et al., 2023), increasingly merge both approaches, generating hybrid products that maximize measurement density while preserving the precision of stable reflectors. In Alabama, this complementarity is essential. Urban corridors, bridges, and engineered infrastructure are well-suited for PSI analysis, while forested slopes, agricultural basins, and vegetated river corridors require SBAS or additional support from optical remote sensing, LiDAR, or machine-learning–based coherence forecasting.

2.2.2 Optical Remote Sensing

Where InSAR quantifies millimeter-scale surface displacement through phase measurements, optical remote sensing captures vegetation loss, soil exposure, and surface disruption by measuring reflected solar radiation across the visible, near-infrared, and short-wave infrared spectrum. These fundamentally different sensing principles produce complementary strengths: InSAR excels at detecting *slow, progressive* deformation, whereas optical systems excel at identifying *sudden* changes in surface characteristics.

The most widely used optical approaches rely on multispectral indices that translate spectral reflectance into biophysical indicators of landscape change. The transition from healthy vegetation to exposed soil, a hallmark of fresh landslide scars, creates distinctive spectral signatures readily identified using multispectral indices (Scheip & Wegmann, 2021; Yang et al., 2019; Deijns et al., 2020; Wen & Teo, 2022). The Normalized Difference Vegetation Index (NDVI), derived from red and near-infrared reflectance, quantifies vegetation health and density (Rouse et al., 1974). The Normalized Difference Water Index (NDWI), combining near and short-wave infrared bands, identifies surface moisture and water content (Gao, 1996). Used together, these indices support regional screening for surface condition changes associated with slope instability and erosion.

Sentinel-2 provides an operational foundation for multispectral monitoring. The ESA constellation offers 13 spectral bands from visible to SWIR wavelengths, 10-meter resolution in key bands, and a 5-day revisit cycle suitable for detecting vegetation change along transportation corridors. NDVI uses Band 4 (665 nm) and Band 8 (842 nm), while NDWI uses Band 8 and Band 11 (1610 nm). In our pursuit of efficient

data processing and analysis, we have leveraged the capabilities of Google Earth Engine. This powerful cloud-based platform has enabled us to explore vegetation cover changes over time using the NDVI derived from Sentinel-2 imagery.

Figure 11 captures multi-year vegetation dynamics along the Littleville Highway (US 43) corridor in Alabama. For this, we implemented a systematic NDVI monitoring approach spanning 2020-2025. Summer NDVI composites were generated for each year, providing consistent seasonal snapshots that minimize cloud interference and capture peak vegetation conditions. The resulting temporal series reveals both the general stability of healthy vegetation (green areas, NDVI > 0.6) and localized disturbances where vegetation loss creates distinctive spectral signatures (yellow-orange areas, NDVI < 0.4). The detailed Google Earth Engine visualization **(Figure 11)** shows the Summer 2025 NDVI distribution across Alabama, with the NDVI scale ranging from -0.2 to 0.9, clearly delineating vegetated areas from bare soil, water bodies, and urbanized zones. This six-year time series provides valuable context for identifying surface changes that may correlate with ground deformation detected through InSAR analysis.

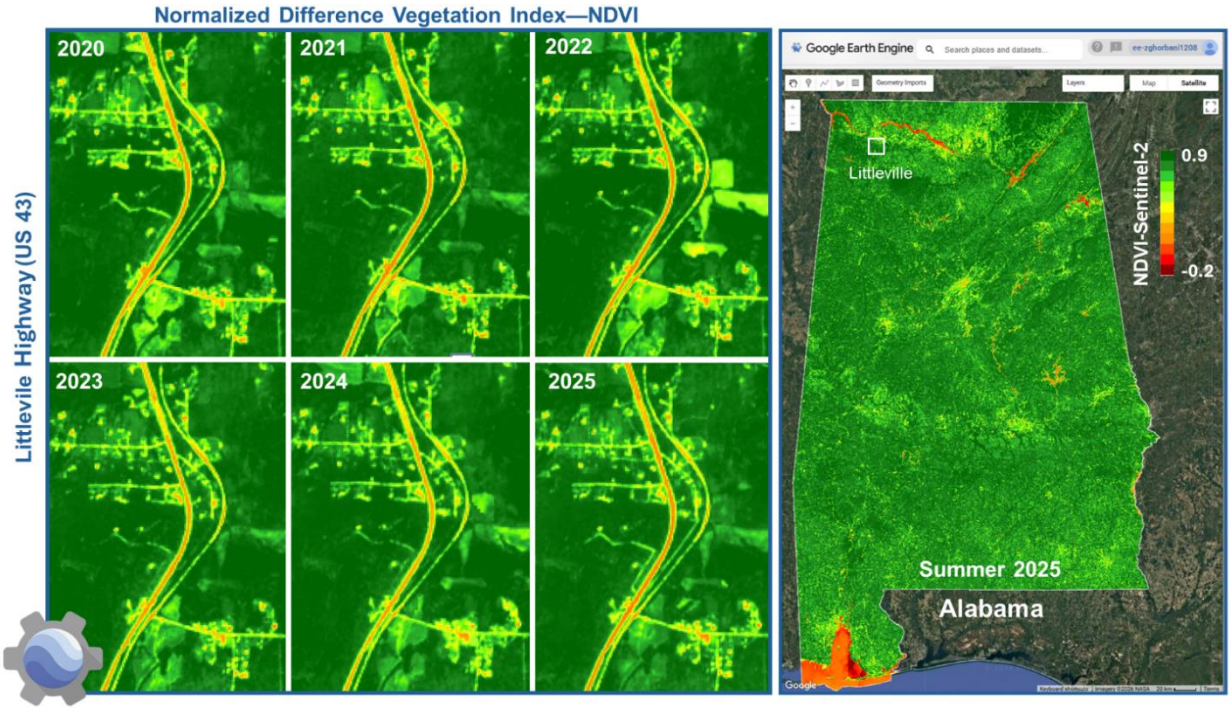

Figure 11. NDVI calculated from recent Sentinel-2 satellite imagery in Google Earth Engine from 2020 to 2025.

2.3 Deep Learning for Multi-Sensor Integration

Traditional InSAR processing pipelines, whether based on Persistent Scatterer Interferometry (PSI) or Small Baseline Subset (SBAS), follow deterministic algorithmic steps: phase unwrapping, atmospheric

correction, and time-series inversion. These physics-based frameworks perform reliably when temporal coherence remains high and atmospheric artifacts are moderate. However, under Alabama's environmental conditions, characterized by dense vegetation and high humidity, coherence degrades unpredictably. Atmospheric noise frequently exceeds the magnitude of subtle deformation signals (<10 mm/year), and deterministic algorithms struggle to distinguish true ground motion from decorrelation artifacts, unwrapping errors, or residual atmospheric disturbances. Deep learning introduces a fundamentally different paradigm. Instead of hand-crafting rules for distinguishing "real deformation" from noise, multi-layer neural networks learn discriminative patterns directly from data through hierarchical feature representations. When trained using areas with known deformation or stability GNSS reference stations, validated subsidence zones, or stable bedrock regions, deep learning models can learn complex nonlinear relationships between InSAR phase behavior, SAR amplitude/coherence characteristics, optical spectral signatures, terrain morphology, and actual ground deformation. Such relationships would be impractical to encode manually or through shallow machine learning methods such as Support Vector Machines (SVM), which depend heavily on feature engineering and cannot capture high-dimensional contextual patterns.

The key advantage of deep learning over traditional machine learning lies in its ability to perform automatic hierarchical feature extraction. Convolutional Neural Networks (CNNs), for example, learn spatial representations at successively higher levels of abstraction: early layers capture edges and fine textures; intermediate layers recognize geometric arrangements; and deeper layers encode complex objects or semantic relationships (Simonyan and Zisserman, 2014). This multi-scale representation is especially valuable for both SAR and optical imagery, where deformation-related patterns occur across a wide range of spatial scales from localized road embankment distress to regional slope instability associated with hydrological gradients. Deep learning has already transformed numerous domains in Earth observation that require systematic analysis of large, multi-spectral, or spatiotemporal datasets, including land cover classification, change detection, multi-sensor fusion, cloud removal, and automated feature extraction (Zhu et al., 2017). Unlike pixel-by-pixel classifiers or rule-based decision thresholds, deep networks leverage spatial context and temporal structure, acknowledging that deformation rarely appears as isolated anomalous pixels. Instead, deformation manifests as coherent spatial patterns reflecting geological structures, groundwater pathways, or infrastructure alignments.

Applications to Synthetic Aperture Radar (SAR) have expanded rapidly, including terrain classification (Parikh et al., 2020), automated target detection (Chen and Wang, 2014), environmental parameter retrieval such as sea-ice concentration (Wang et al., 2014), speckle noise suppression (Wang et al., 2017), and SAR–optical fusion for improved scene understanding (Hughes et al., 2018). Earlier SAR analyses relied heavily on handcrafted features or SVM-based classifiers (Zhao and Principe, 2001; Bryant

and Garber, 1999), which require substantial domain expertise and struggle to model the complex spatial and radiometric variability inherent in SAR imagery.

Modern deep learning approaches overcome these limitations through data-driven representation learning. CNNs trained directly on raw SAR amplitude imagery can autonomously learn discriminative features for classification or object detection (Chen and Wang, 2014). For despeckling, deep networks effectively separate coherent signal from multiplicative noise while preserving fine spatial details, addressing a key limitation of traditional filters that often blur edges and deform small features (Wang et al., 2017). Deep learning-based SAR–optical fusion methods similarly exploit complementary information from both modalities to enhance classification accuracy or detect subtle environmental changes (Hughes et al., 2018). Despite these advances, most deep learning applications to SAR focus on amplitude imagery, not interferometric phase, which presents unique mathematical challenges. Standard CNN architectures originally designed for natural images with linear intensity values do not inherently handle wrapped phase (with 2π discontinuities), nor do they account for circular statistics, coherence-based reliability measures, or the separation of atmospheric phase screens from true displacement signals (Anantrasirichai et al., 2018). These limitations underscore the need for specialized network architectures or feature transformations tailored to interferometric data.

2.3.1 Deep Learning Architectures

The application of deep learning to SAR imagery did not emerge in isolation but rather adapted architectures and training strategies developed initially for natural image analysis. Understanding this progression from early neural networks to modern convolutional architecture provides essential context for evaluating which approaches might succeed or fail when applied to InSAR deformation detection in Alabama's challenging environmental conditions. A fundamental principle constrains all machine learning applications: model performance cannot exceed the quality and representativeness of training data. Neural networks learn discriminative patterns by example; their ability to generalize new scenarios depends entirely on exposure to diverse, representative training cases during the learning phase. This constraint explains why two specific developments proved pivotal for deep learning's emergence as a practical technology.

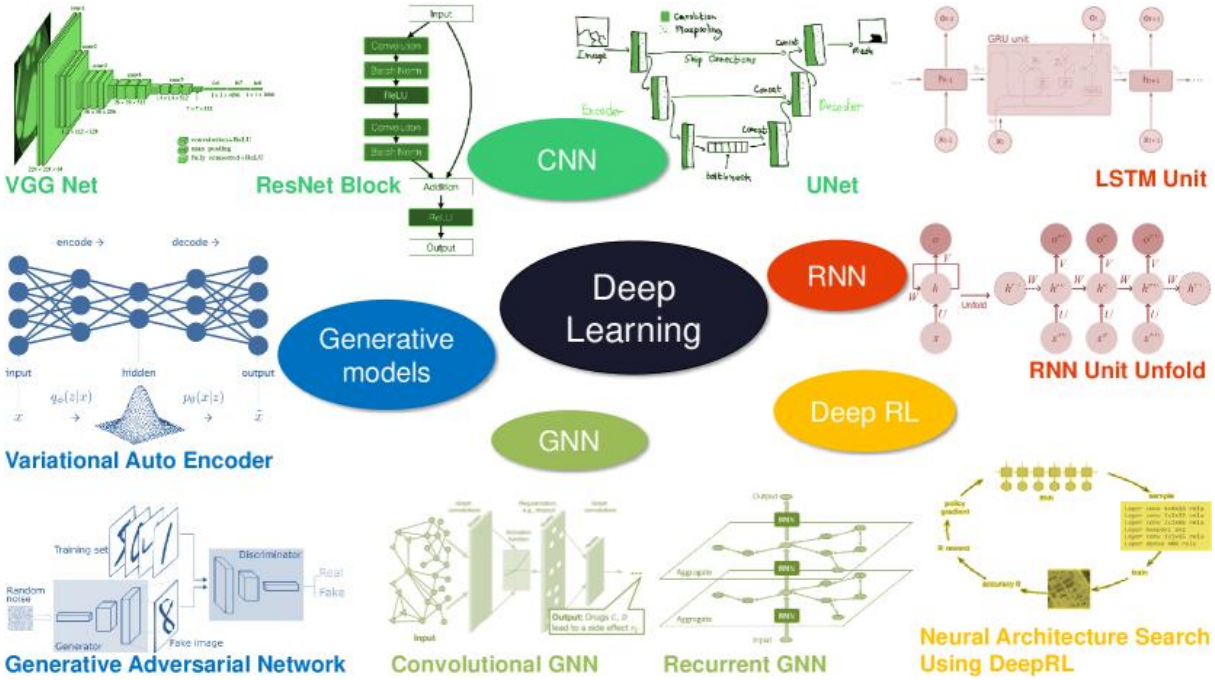

Figure 12. Overview of deep learning architectures showing core model types: variational autoencoders (VAE) and generative adversarial networks (GAN) for data generation; convolutional (CNN) and graph neural networks (GNN) for feature extraction; recurrent networks (RNN) for sequential processing; and deep reinforcement learning (DeepRL) for automated architecture optimization. Each diagram illustrates the distinctive computational flow and structural elements of its respective model type (Zhu et al., 2021).

Deep learning networks transform raw input data into hierarchical feature representations through successive nonlinear transformations. Each layer extracts increasingly abstract patterns: early layers detect simple edges and textures, intermediate layers recognize geometric arrangements and spatial structures, and deeper layers capture complex semantic relationships relevant to the task at hand. The autoencoder architecture illustrates these principles clearly. An encoder compresses input data into a compact latent representation, forcing the network to identify essential features while discarding irrelevant details. A decoder then reconstructs the original input from this compressed representation. Training minimizes reconstruction error, measured through metrics like mean squared error (Euclidean distance), forcing the network to learn efficient data encodings.

Modern optimization algorithms enable effective training of deep architectures. Stochastic Gradient Descent (SGD) iteratively adjusts network parameters to minimize loss functions, while adaptive methods like RMSProp and ADAM (Kingma & Ba, 2014) automatically adjust learning rates for each parameter, accelerating convergence and improving stability. These optimization techniques, combined with regularization strategies like dropout and batch normalization, enable training of networks with

millions of parameters on limited datasets without catastrophic overfitting. For InSAR applications, the key insight: networks can learn to compress complex multi-dimensional data (interferometric phase, coherence, amplitude, temporal patterns) into compact representations capturing deformation signatures while filtering atmospheric noise and decorrelation artifacts. However, effectiveness depends critically on the quality and representativeness of the training data, which is a challenge for Alabama applications where labeled deformation examples in heavily vegetated terrain remain scarce.

2.3.1.1 Convolutional Neural Networks (CNN)

CNNs emerged as the dominant architecture for spatial image analysis following AlexNet's breakthrough performance in the 2012 ImageNet challenge, achieving 15.3% error rate, dramatically outperforming previous approaches (Krizhevsky et al., 2012). This success demonstrated that deep convolutional architectures could learn discriminative features automatically from raw pixels rather than requiring hand-crafted feature engineering (Krizhevsky et al., 2012). Subsequent innovations improved performance and enabled deeper networks. VGGNet (2014) standardized on small 3×3 convolutional kernels stacked in deep sequences, reducing error to 6.8% while simplifying architecture design. ResNet introduced skip connections, allowing gradients to flow directly through many layers, addressing the vanishing gradient problem and enabling networks with 50-150+ layers. U-Net revolutionized image segmentation with its encoder-decoder architecture and skip connections, proving particularly effective with limited training data via aggressive data augmentation. DenseNet extended skip connections further by connecting each layer to all subsequent layers, improving feature reuse but requiring substantial memory resources.

These architectural developments have proven valuable for SAR image processing (Mazza et al., 2019; Lattari et al., 2019; Morgan, 2015). CNNs extract multi-scale spatial features from SAR amplitude and coherence images, recognizing patterns associated with terrain types, land cover classes, or deformation signatures. The encoder-decoder structure of U-Net proves particularly relevant for InSAR applications: the encoder extracts progressively abstract features from interferometric phase and coherence, while the decoder reconstructs pixel-wise predictions, potentially identifying which pixels represent real deformation versus atmospheric artifacts or decorrelation noise. However, the standard CNN architecture designed for natural images requires adaptation for InSAR data. Phase wrapping creates discontinuities that convolutional filters may misinterpret as edges. Temporal decorrelation can produce spatially correlated noise patterns that CNNs might learn as deformation signatures, unless carefully curated training data is used. Coherence varies spatially due to land cover rather than deformation, requiring networks to learn complex conditional relationships: high deformation in high-coherence areas indicates real movement, while apparent deformation in low-coherence areas likely represents noise. These domain-specific

challenges motivate InSAR-specific architectural modifications rather than the direct application of ImageNet-pretrained models.

2.3.1.2 Recurrent Neural Networks (RNN)

While CNNs excel at spatial feature extraction, InSAR time-series analysis requires processing temporal sequences of tens to hundreds of interferograms spanning months to years. Recurrent Neural Networks, introduced by Pearlmutter (1989), address this need through feedback connections that incorporate previous time-step information into current calculations. This recurrent structure enables processing variable-length sequences: text, speech signals, financial time series, or InSAR deformation measurements. Standard RNNs suffer from vanishing gradients when processing long sequences; gradients diminish exponentially through many time steps, preventing the learning of long-range dependencies. Long Short-Term Memory networks (Hochreiter & Schmidhuber, 1997) solve this through sophisticated memory cell structures with gating mechanisms that control information flow. LSTM cells selectively retain or forget information across many time steps, enabling robust learning of temporal patterns spanning hundreds of observations.

For InSAR deformation detection, temporal patterns distinguish real ground movement from atmospheric noise. Linear subsidence produces consistent phase change accumulation over time. Seasonal oscillations from groundwater or soil moisture follow annual cycles. Co-seismic offsets appear as sudden phase jumps. Atmospheric artifacts, conversely, exhibit spatially correlated but temporally random patterns. LSTMs can learn these discriminative temporal signatures, potentially improving deformation detection in low-coherence environments where individual interferograms provide ambiguous information (Ndikumana et al., 2018). However, LSTM architectures face challenges for InSAR applications. Training requires substantial computational resources, and each time step involves complex matrix operations through multiple gates. More critically, LSTMs struggle with very long sequences (>100-time steps) common in multi-year InSAR datasets, with gradient flow still degrading despite gating mechanisms. Recent alternatives, including temporal convolutional networks (TCNs) with dilated convolutions and transformer architectures with self-attention, may offer improved capability for modeling long-range temporal dependencies in InSAR time series. Unlike conventional recurrent architectures, these models can capture complex, non-linear temporal relationships and better preserve long-range dependencies, reducing the gradient degradation typically associated with recurrent networks(Bai et al., 2018; Vaswani et al., 2017).Such capabilities are particularly relevant for multi-year deformation monitoring, where subtle displacement trends must be distinguished from atmospheric fluctuations, seasonal variability, and decorrelation artifacts. However, regardless of architectural choice, the effectiveness of deep learning models remains fundamentally dependent on the quality, representativeness, and physical consistency of the training data.

2.4 Summary of Key Findings from the Literature Review

Recent advances in remote sensing, geodetic monitoring, and artificial intelligence have fundamentally transformed approaches to detecting and monitoring ground deformation hazards such as landslides, subsidence, and sinkholes. Traditional geotechnical instrumentation, including inclinometers, extensometers, and GNSS, remains essential for precise local measurements; however, these methods are limited by high cost, sparse spatial coverage, and operational constraints that prevent continuous statewide monitoring. As a result, modern hazard monitoring increasingly relies on satellite-based remote sensing methods that provide scalable, repeatable, and spatially continuous observations.

The literature highlights that Alabama's geologic and physiographic conditions create persistent vulnerability to ground instability. Landslides in the state are predominantly soil-related, commonly associated with shallow translational and rotational movements influenced by rainfall, groundwater fluctuations, and geologic contrasts. Statewide susceptibility studies reveal strong spatial correlations between landslide occurrence, topography, and specific geologic units. Similarly, extensive carbonate bedrock regions make Alabama susceptible to sinkhole formation driven by karst processes and groundwater-driven erosion. These hazards emphasize the need for large-area monitoring strategies capable of capturing both gradual deformation and sudden failures.

Geodetic monitoring frameworks provide the foundation for modern deformation analysis by measuring displacement within defined coordinate systems. Among geodetic techniques, Interferometric Synthetic Aperture Radar (InSAR) represents a major advancement, enabling millimeter-scale deformation detection over wide areas without ground instrumentation. Unlike optical imagery, SAR systems operate independently of weather and illumination, allowing continuous monitoring. The evolution of SAR missions, from early systems to modern open-access constellations such as Sentinel-1 and emerging L-band missions including ALOS-4 and NISAR, has greatly expanded the feasibility of operational deformation monitoring. Band selection plays a critical role, with shorter wavelengths offering higher resolution but limited vegetation penetration, while longer wavelengths provide improved coherence in vegetated environments. InSAR time-series analysis has emerged as the dominant framework for practical deformation monitoring. Two primary methodologies are widely adopted: Persistent Scatterer InSAR (PS-InSAR), which provides high-precision measurements at stable targets typically found in urban or infrastructure environments, and Small Baseline Subset (SBAS), which improves spatial coverage in natural or vegetated terrains by exploiting distributed scatterers. These approaches are complementary rather than competing, with hybrid implementations increasingly used to balance precision and spatial coverage. However, limitations remain, particularly in heavily vegetated areas where decorrelation, atmospheric noise, and seasonal variability reduce measurement reliability. Optical remote sensing

provides important complementary information by detecting surface condition changes, such as vegetation loss and soil exposure using indices like NDVI and NDWI. While optical data cannot directly measure displacement, it improves the interpretation of deformation processes and supports post-event analysis. Integration of SAR and optical data has been shown to enhance change detection and environmental characterization, but technical challenges such as geometric differences, radiometric inconsistencies, and registration complexity continue to limit widespread operational integration.

Recent advances in machine learning and deep learning offer promising solutions to many persistent limitations in traditional InSAR analysis. Neural networks, including convolutional neural networks (CNNs), recurrent neural networks (RNN/LSTM), transformers, and hybrid architectures, enable automated extraction of spatial and temporal deformation patterns from large multi-sensor datasets. Unlike deterministic processing pipelines, deep learning models can learn complex nonlinear relationships between radar phase behavior, coherence, optical characteristics, terrain morphology, and environmental conditions. This capability is particularly important in challenging environments where conventional InSAR processing suffers from decorrelation or atmospheric noise. However, previous studies also emphasize that model performance depends strongly on representative training data and physically meaningful validation.

Chapter 3 – InSAR-Based Deformation Analysis

Developing a reliable and operational InSAR workflow is critical for translating satellite-based deformation measurements into a practical monitoring tool for Alabama's transportation infrastructure. Although InSAR provides millimeter-scale sensitivity, its effectiveness depends strongly on workflow design, from data ingestion and interferogram generation to coherence assessment, atmospheric correction, time-series analysis, and automated detection, particularly in environmentally complex regions. Alabama presents significant challenges for InSAR due to dense vegetation, high humidity, and strong soil moisture variability, all of which reduce coherence and introduce atmospheric phase noise. Deformation processes of interest, such as landslides, subsurface erosion, and sinkhole development, are often subtle or non-linear, requiring robust time-series approaches capable of extracting signals from noisy data. To address these conditions, the workflow integrates two complementary InSAR methods: a network-based NSBAS approach using LiCSBAS to provide broad spatial coverage and a Persistent Scatterer (PS) approach with PyGMTSAR to obtain high-precision deformation estimates at coherent transportation assets. Together, these methods form a computationally efficient and automated system designed for consistent, long-term monitoring across Alabama's highway network.

3.1 Small baseline processing with LiCSBAS

For time-series analysis of LiCSAR interferograms, we employed LiCSBAS an open-source Python-based processor specifically designed for automated processing of LiCSAR products (Morishita et al., 2020). This selection addresses three critical operational requirements for Alabama highway monitoring:

- **Direct LiCSAR integration:** LiCSBAS processes pre-computed LiCSAR interferograms directly, eliminating the need to generate interferograms from Single Look Complex (SLC) data, removing computational barriers and specialized SAR processing expertise requirements that would limit transportation agency implementation.
- **Automated workflow:** The tool provides end-to-end processing from interferogram download through velocity estimation and time-series generation, with automated quality control, unwrapping error detection, and atmospheric correction enabling systematic monitoring without manual intervention for each processing cycle.
- **Computational efficiency:** Compared to alternatives like GMTSAR (requiring raw SLC processing), StaMPS (requiring MATLAB and complex parameter tuning), or commercial SARscape (licensing costs), LiCSBAS significantly reduces processing time and storage requirements while maintaining accuracy suitable for infrastructure monitoring applications.

Processing Methodology: LiCSBAS implements a modified Small Baseline Subset (NSBAS) approach adapted for systematic Sentinel-1 processing **(Figure 13)**.

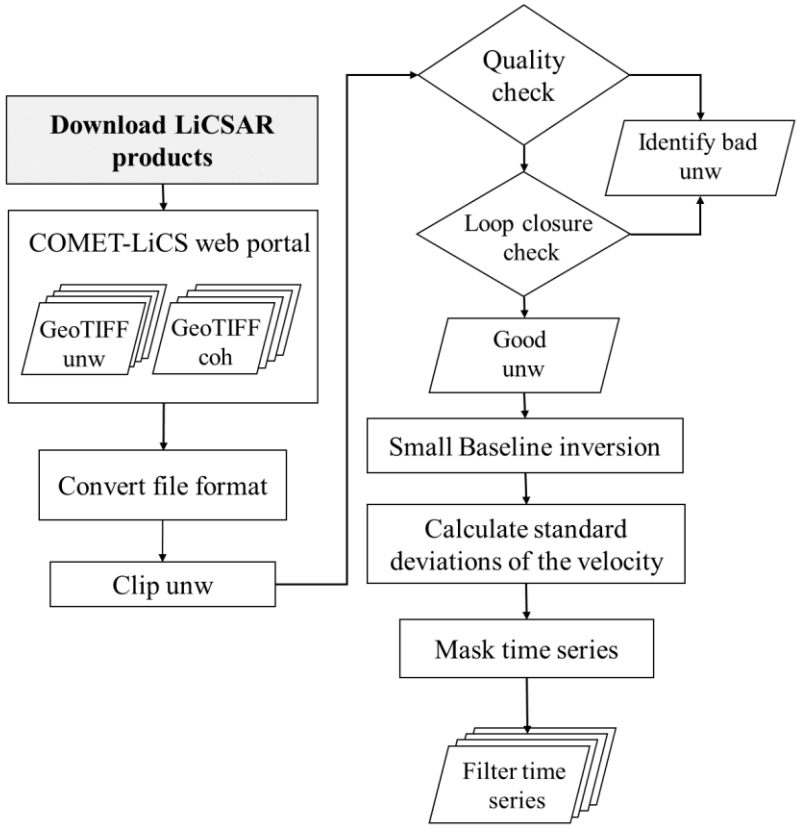

Figure 13. Workflow of LiCSBAS time-series analysis (Morishita et al. 2020).

Initially, the method processes interferograms generated from InSAR data, with a focus on correcting unwrapping errors and masking noise sources. For a stack of M unwrapped interferograms derived from N images, the incremental displacements $\mathbf{m} = [m_1, ..., m_{n-1}]^T$ can be derived by solving $\mathbf{d} = \mathbf{G}m$, where $\mathbf{d} = [d_1,...,d_m]^T$ is the vector of unwrapped interferograms and **G** is a design matrix of zeros and ones M×(N-1). This setup assumes each unwrapped interferogram represents the cumulative displacement of successive incremental displacements (Schmidt et al., 2003). The cumulative displacements, forming the time series for each acquisition, are obtained by summing these increments, while mean displacement velocities are derived via least-squares.

Although Sentinel-1 frequently captures short-baseline data, network gaps can still occur, resulting from factors such as decorrelation caused by vegetation or snow cover or extended acquisition gaps (e.g., several months or more). In such cases, even if the interferogram network is technically connected image-by-image, gaps may persist at a pixel-by-pixel level due to coherence-based masking in LiCSAR products. Singular value decomposition (SVD) is used to solve these cases, but it yields zero displacements over

network gaps, which may not be realistic even for small intervals (e.g., 6 days) since interferogram noise over gaps could be non-zero.

To generate realistic time series despite disconnected networks, LiCSBAS incorporates a temporal constraint following the NSBAS approach (Agram et al., 2013; López-Quiroz et al., 2009; Doin et al., 2011).

$$\begin{bmatrix}\mathbf{d}\\ \mathbf{0}\end{bmatrix} = \begin{bmatrix} \begin{bmatrix} & & \mathbf{G} & & & \mathbf{0} & \mathbf{0} \end{bmatrix} \\ \gamma \begin{bmatrix} 1 & 0 & \dots & \dots & 0 & -t_1 & -1 \\ \vdots & \ddots & \ddots & & \vdots & -t_2 & \vdots \\ 1 & \dots & 1 & \ddots & \vdots & \vdots & \vdots \\ \vdots & & \vdots & \ddots & 0 & \vdots & \vdots \\ 1 & \dots & 1 & \dots & 1 & -t_{N-1} & -1 \end{bmatrix} \end{bmatrix} \begin{bmatrix}\mathbf{m}\\ v\\ c\end{bmatrix} \quad (5)$$

Here, the temporal constraint's weighting factor γ is set small (e.g., 0.0001), thereby only affecting displacements across network gaps, while leaving connected sections of the network largely unchanged. This method applies a linear temporal model (**d** = **vt+c**), but where observed displacement deviates from linearity (e.g., due to seismic activity), alternative functions such as Heaviside or exponential models could be more accurate if prior knowledge about the deformation pattern is available. Currently, however, LiCSBAS only supports linear solutions, and network gaps are flagged in the time series viewer for interpretation.

Spatial and Temporal Resolution: LiCSBAS processes LiCSAR interferograms at their native ~100-meter multilook resolution, providing sufficient spatial detail for highway infrastructure monitoring (embankments, bridge approaches, cut slopes extending tens to hundreds of meters) while maintaining computational tractability for statewide coverage. Temporal resolution follows Sentinel-1's 12-day repeat cycle, enabling seasonal pattern characterization and episodic event detection with sub-centimeter displacement accuracy for coherent pixels (Morishita et al., 2020; Ghorbani et al., 2022). LiCSBAS has demonstrated effectiveness across diverse geographic and deformation contexts, establishing confidence in its applicability to Alabama highway monitoring despite development.

3.1.1 Generate InSAR database

For this task, we utilized Sentinel-1 (C-band) satellite imagery spanning from October 2016 to the present, with data captured every 12 days. We processed interferograms generated from Sentinel-1 LiCSAR frames in the Ascending orbits over Alabama. These frames are accessible via the COMET-LiCS web portal (*https://comet.nerc.ac.uk/COMET-LiCS-portal/*). The "Looking inside the Continents from Space" (LiCS) initiative is led by the United Kingdom's Centre for the Observation and Modelling of Earthquakes, Volcanoes and Tectonics (COMET), under the Natural Environment Research Council. The project aims

to monitor tectonic and volcanic regions worldwide through Sentinel-1 InSAR, map tectonic strain with high spatial detail, and use the results to refine models of seismic and volcanic hazards. The LiCSAR processor, an automated Sentinel-1 InSAR tool utilizing GAMMA SAR and interferometry software (Wegmüller et al., 2016; Werner et al., 2000), was developed to support the LiCS project objectives. By November 2019, approximately 160,000 interferograms had been created, primarily covering the Alpine-Himalayan Belt and global volcanic regions, with availability on the COMET-LiCS portal (COMET-LiCS, 2019). The LiCSAR coverage is progressively expanding to include more globally deforming areas.

Within the LiCSAR processing chain, interferograms are produced automatically for each predefined LiCSAR frame (generally covering 13 bursts per subswath in IWS mode, about 250 km × 250 km). New data acquisitions are co-registered to a primary reference image with assistance from a secondary image (temporally close to the latest image) that was previously co-registered (if available), using the enhanced spectral diversity method (Scheiber and Moreira, 2000; Prats-Iraola et al., 2012). Interferograms are then generated with three images taken before and after each acquisition by default, though this number may be expanded. The interferograms are multilooked, with a 20 × 4 range × azimuth factor (resulting in a 46 × 56 m spacing) and filtered to minimize noise using a GAMMA adaptive power spectrum filter with an alpha setting of 1.0 (Goldstein and Werner, 1998). LiCSAR performs 2D phase unwrapping using a statistical cost-based approach with SNAPHU software (Hooper, 2009; Chen and Zebker, 2002). During unwrapping, low-coherence areas in the interferograms are masked out if the filtered interferogram's phase noise coherence is less than 0.5. The wrapped and unwrapped interferograms, along with coherence images, are geocoded at a pixel spacing of approximately 0.001 degrees (~100 m) and saved in GeoTIFF format. These GeoTIFF files and preview images are made publicly available on the COMET-LiCS Sentinel-1 InSAR portal for free download (COMET-LiCS Sentinel-1 InSAR Portal, 2019), along with additional metadata (e.g., line-of-sight (LOS) vectors and perpendicular baselines). **Figure 14** shows the LiCSAR frames that were used for analysis. Each image is geolocated and contains the unwrapped phase and coherence over an area of 100 square miles (250 km^2).

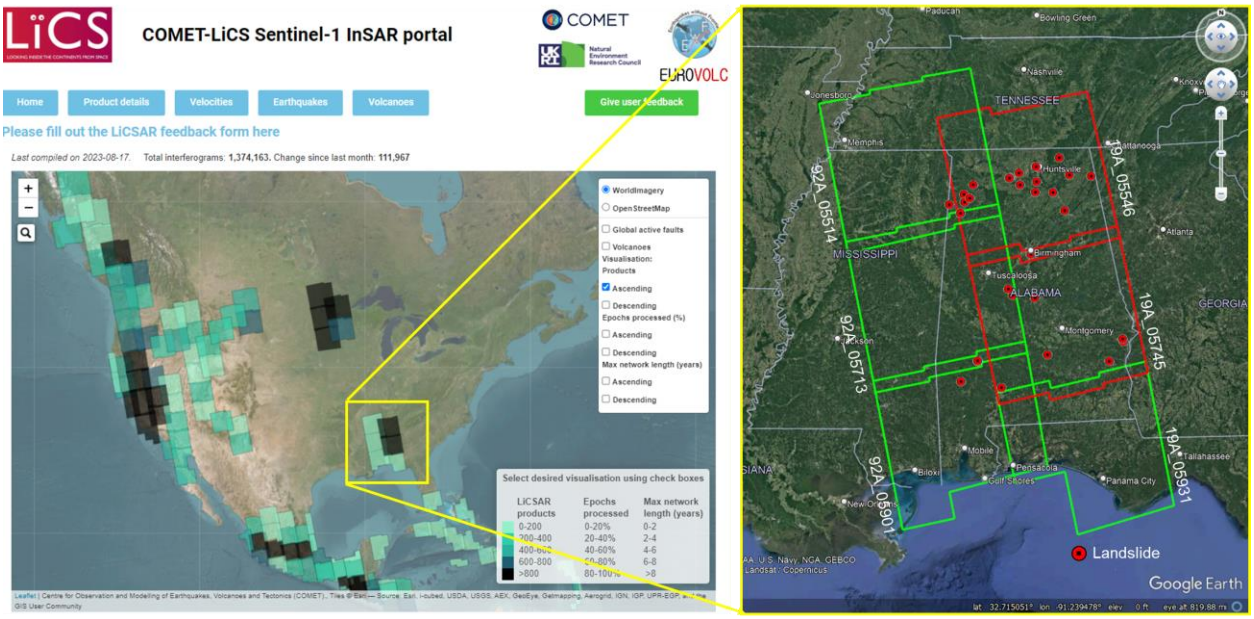

Figure 14. Geographical locations of Sentinel-1 images used to study land deformation in Alabama (*https://comet.nerc.ac.uk/COMET-LiCS-portal/*).

3.1.2 Deformation Analysis using LiCSBAS

We have completed the generation of interferograms over Sentinel-1 LiCSAR frames covering Alabama using the ascending orbit. The analysis of these frames was performed using the open-source SAR interferometry time series analysis package, LiCSBAS, to estimate detailed deformation time series with high spatial and temporal resolutions. A total of six frames was required to determine deformation across the entire state. During the initial analysis, we encountered some processing challenges related to phase unwrapping errors, particularly in heavily vegetated areas of Alabama, where signal coherence was degraded. To address these challenges, we successfully applied re-unwrapping techniques that significantly improved the quality of our deformation maps. The re-unwrapping process involved reprocessing the interferometric phase data using enhanced algorithms that better handle phase discontinuities and ambiguities caused by dense vegetation cover. This approach proved highly effective in resolving the unwrapping errors and producing high-quality, reliable deformation measurements across the entire state.

An example of analysis results for this task is presented in **Figure 15**, which demonstrates the improvement achieved through re-unwrapping. This figure shows the state's mean LOS velocity maps obtained from LiCSAR products from April 2016 to December 2023. As can be seen in the Figure, intriguing patterns of ground deformation are observed in several regions of the state.

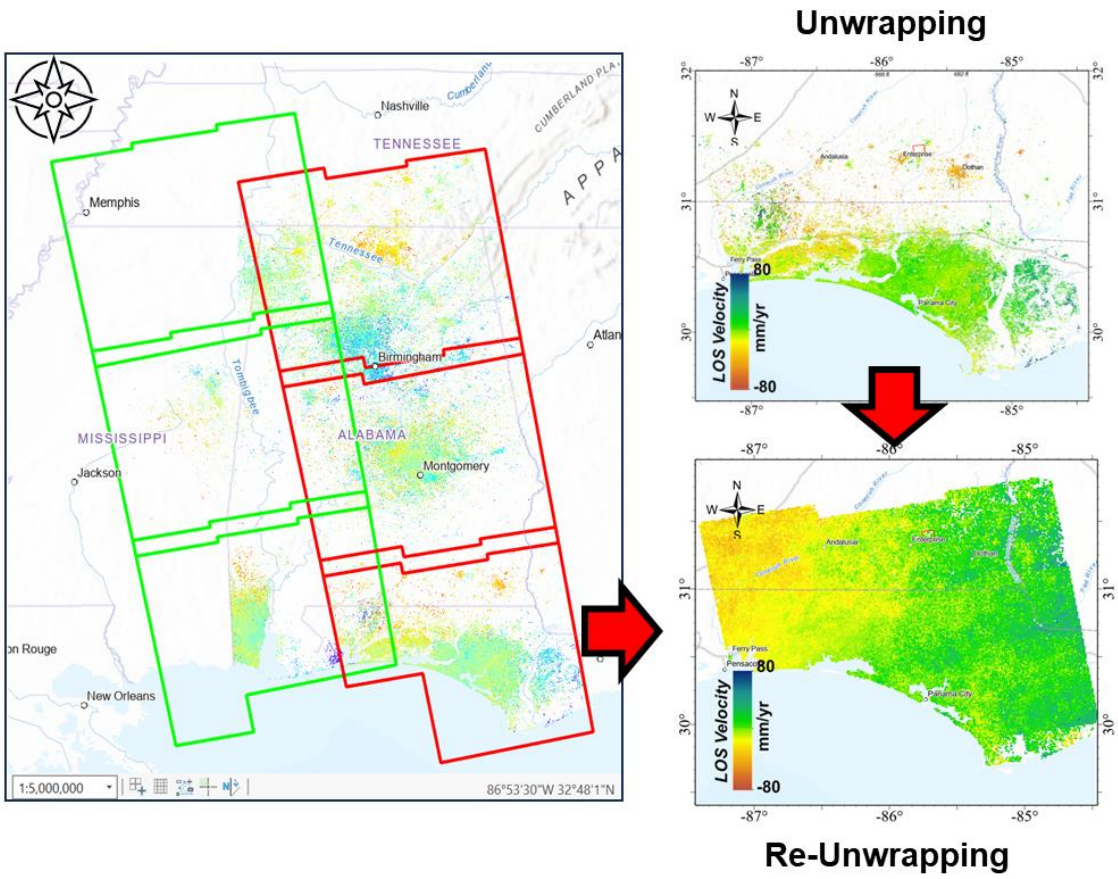

Figure 15. The mean LOS velocity maps obtained from LiCSAR products by LiCSBAS from April 2016 to December 2023.

Although the standard-resolution analysis (~100 m pixel spacing) provides valuable situational awareness and captures regional deformation patterns, it is not sufficient for reliable highway-scale assessment. The mixing of pixels between vegetated areas and narrow infrastructure may lead to the elimination of some pixels, resulting in loss of data at critical highway locations. This creates a gap in coverage for infrastructure monitoring and necessitates higher-resolution analysis approaches for detailed site investigations, as is discussed in the next section.

3.2 PS-InSAR Analysis using PyGMTSAR

To maximize spatial resolution at the most critical infrastructure sites, we employed PS-InSAR (Persistent Scatterer InSAR) methodology using the PyGMTSAR toolkit (Pechnikov, 2024). PyGMTSAR is a versatile Python-based InSAR toolkit that provides automated processing of Sentinel-1 data and supports multiple interferometric techniques, including SBAS, PS, and PS-SBAS, while automatically handling data retrieval, interferogram computation, and time-series analysis. The PS-InSAR approach fundamentally differs from

the SBAS strategy by focusing on identifying and tracking individual stable radar scatterers rather than processing spatially averaged interferograms. PyGMTSAR's advanced persistent scatterer identification utilizes amplitude dispersion index (ADI) calculations to identify points with stable backscatter characteristics throughout the observation period. The platform's distinctive 1D temporal unwrapping approach performs phase unwrapping sequentially through time for each identified persistent scatterer point rather than traditional 2D spatial unwrapping, significantly improving accuracy for point-wise displacement measurements in vegetated environments where traditional 2D unwrapping approaches often fail.

The PS-InSAR methodology enables deformation measurements at full Sentinel-1 resolution (~5×20 m single-look spacing) at persistent scatterer locations, including exposed rock outcrops, road surfaces, and infrastructure elements that maintain coherent phase characteristics throughout the observation period. This approach is particularly effective for infrastructure monitoring along narrow corridors where discrete stable targets provide reliable measurement points.

3.3 Validation Framework and Field Implementation

To ensure the reliability of InSAR-derived deformation measurements for engineering and operational decision-making, we implemented a multi-component validation framework combining satellite reference targets (corner reflectors), independent geodetic measurements (GNSS), and ground-based instrumentation (e.g., inclinometers and soil moisture sensors). This report emphasizes (1) quantitative validation using existing ALDOT ground-based instrumentation datasets at two previously monitored highway sites; (2) validation of the NSBAS approach using GNSS data, (3) two applications of localized displacement analysis for infrastructure monitoring, and (4) deployment of corner reflectors for future validation and improvement of data collection. The Corner reflectors and co-located field sensors at Littleville will serve as a primary validation reference as additional satellite acquisitions accumulate.

We originally planned to also use long-wavelength L-band SAR data for validation, but delays in acquisition and availability prevented this. Although the NISAR mission has now successfully launched (after a multi-year delay), analysis-ready datasets suitable for deformation validation were not available within the reporting window. To mitigate delays in the availability of analysis-ready NISAR data, we successfully obtained access to L-band SAR data from the ALOS program through a separate, complementary funding effort. This additional support enabled the acquisition of ALOS datasets intended to partially bridge the data gap created by the delayed NISAR release. However, full integration of ALOS L-band SAR into the current project phase was not feasible as access to ALOS-2 archived data was temporarily disrupted. This was caused by JAXA’s migration from the G-Portal system to the AUIG4 platform, limiting timely retrieval and processing. We were able to obtain ALOS-4 data for the study area,

but acquisition frequency and temporal coverage were insufficient for robust InSAR time-series analysis, as the site is not yet included in the mission's regular observation plan. These changes were beyond the control of the project team, but we were able to adapt and complete the planned validation activities using the other datasets described above. The issues with data collection and availability should be temporary, allowing the L-band data to be used in future phases of this research.

3.4 Validation with Inclinometer Data

Ground-based inclinometer measurements from existing ALDOT monitoring sites provided an independent benchmark for evaluating the accuracy and temporal reliability of satellite-based deformation measurements under Alabama environmental conditions. In this study, validation analyses were conducted at two representative landslide locations: the US-231 Lacey's Spring site in Morgan County, which experienced a major failure in February 2020, and the SR-219 (Selma Road) site near Centreville, where ongoing slope instability has been monitored through subsurface instrumentation. These datasets offer discrete measurements of horizontal displacement at depth and therefore serve as a robust reference for assessing the ability of InSAR time-series approaches to capture both long-term deformation trends and pre-failure acceleration behavior. Because inclinometer data represent localized subsurface deformation, they provide a critical framework for evaluating how different InSAR processing strategies resolve slope movement at both point and regional scales. The following sections separately assess the performance of Persistent Scatterer (PS) InSAR and NSBAS processing approaches, highlighting their respective strengths and limitations relative to in situ measurements.

3.4.1 US-231 Lacey's Spring Landslide Site

The US-231 site near Lacey's Spring in Morgan County represents one of the most critical landslide locations in northern Alabama. In February 2020, a major landslide occurred along this highway segment, causing significant pavement cracking, road closure, and requiring emergency repairs (Montgomery et al. 2026). This site has been continuously monitored by ALDOT using inclinometer installations (Rahimikhameneh et al., 2024) that provide horizontal displacement measurements at discrete borehole locations.

To enable direct comparison with inclinometer readings, which are typically collected at quarterly intervals, we implemented a dual-processing approach. First, the complete long-term InSAR time series spanning 2017-2025 was processed to capture the continuous evolution of slow-moving deformation patterns **(Figure 16)**. Second, to enable direct comparison with inclinometer readings, InSAR displacement values were extracted at dates corresponding to each available inclinometer measurement, preserving the irregular but approximately monthly sampling frequency of the field instrumentation.

Long-Term Continuous Monitoring (2017-2025):

Figure 16a presents the mean LOS velocity map derived from PyGMTSAR PS-InSAR analysis, overlaid on Google Earth imagery, illustrating the spatial distribution of ground deformation across the US-231 landslide area. The velocity field (−16 to +16 mm/yr) clearly delineates the extent of the unstable slope, with pronounced subsidence concentrated along the highway corridor. To systematically evaluate both deforming and non-deforming zones, five monitoring points (P1–P5) were deliberately selected to represent a range of deformation behaviors: points located within the active landslide body, points near the landslide margins, and points in adjacent areas expected to remain stable. A reference point (Ref) was placed in a geologically stable area outside the landslide zone to provide a consistent baseline for relative displacement measurements. In addition, three ALDOT-installed inclinometer locations (US-231, 52019, and 52020) are shown, corresponding to borehole sites where independent subsurface deformation measurements were collected.

Figure 16b presents the PS-InSAR cumulative displacement time series from 2017 to 2025 for the selected points. The temporal evolution reveals distinct and contrasting deformation patterns that collectively demonstrate the sensitivity and reliability of InSAR for both unstable and stable ground conditions. Point P2 exhibits the most dramatic behavior, with a clear acceleration phase beginning in late 2019 and cumulative displacement reaching approximately −60 mm by the February 13, 2020, landslide event, followed by continued subsidence to nearly −160 mm by 2025. Point P3 shows steady, progressive subsidence, reaching approximately −50 mm by 2025, indicative of ongoing slow slope movement. In contrast, points P1 and P5 remain stable around 0 mm throughout the observation period, confirming the ability of InSAR to correctly identify non-deforming regions adjacent to active failures. Point P4 remains stable until early 2020, after which it exhibits approximately −20 mm of displacement, consistent with post-failure slope adjustment following the landslide event.

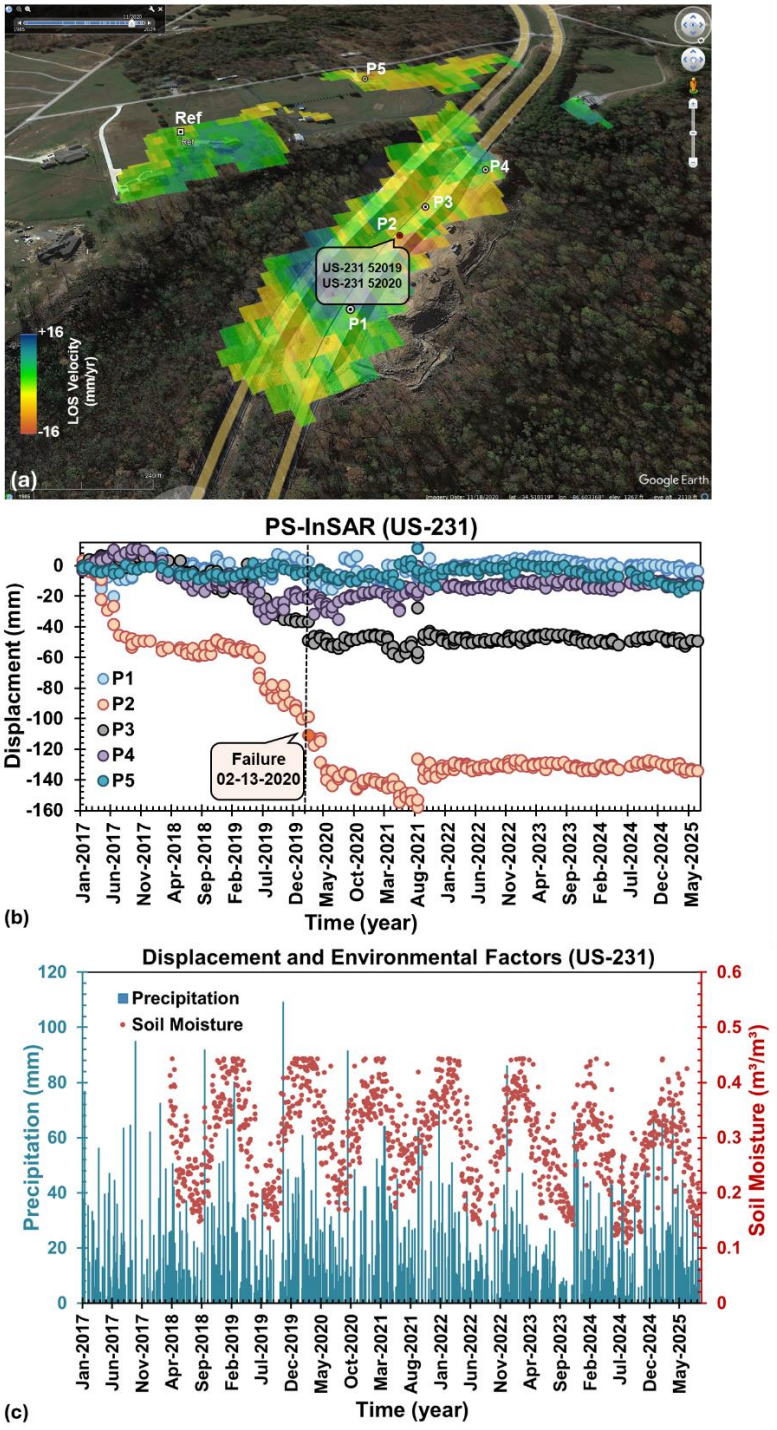

Figure 16. (a) PyGMTSAR PS-InSAR mean LOS velocity map, (b) Displacement time series for P1-P5 showing the February 13, 2020, failure event, (c) Environmental factors including CHIRPS daily

precipitation (blue bars, mm) and SMAP soil moisture (red circles, m^3/m^3) demonstrating hydrological control on slope deformation at US-231 site (2017-2025).

The contrasting behavior among these monitoring points highlights a key strength of the InSAR approach: its ability to simultaneously capture accelerating deformation in unstable zones while confirming stability in nearby areas. In particular, the pre-failure acceleration observed at P2 where displacement rates increased from approximately −2 mm/month to more than −10 mm/month in the months preceding failure demonstrates the capability of InSAR time series analysis to provide early warning signals well in advance of catastrophic slope failure.

To investigate the hydrological controls on slope deformation at the US-231 site, we integrated multi-source environmental datasets spanning 2017-2025 **(Figure 16c)**. Daily precipitation data were obtained from the CHIRPS (Climate Hazards Group InfraRed Precipitation with Station data) dataset via Google Earth Engine, providing high-resolution rainfall measurements (5 km spatial resolution) at the site location P2. Soil moisture measurements were derived from NASA's SMAP (Soil Moisture Active Passive) L3 Enhanced product (9 km spatial resolution), utilizing morning ascending pass retrievals filtered for quality flags to ensure measurement reliability. As previously demonstrated in Rahimikhameneh et al. (2024), hydrological saturation was identified as a primary trigger for the February 2020 landslide event. The InSAR time series presented in **Figure 16c** further corroborates these findings.

3.4.1.1 Direct Validation with Inclinometer Data

Figure 17 presents a direct comparison between PS-InSAR cumulative displacement time series and ALDOT inclinometer readings (Inc-2019) at the US-231 landslide site. For a full description of the site, see Montgomery et al. (2026). Notably, InSAR measurements extend back to January 2019, predating the installation of inclinometers in March 2019. The InSAR time series captures a change in displacement rate coinciding with the cracking reported in the southbound lanes in February 2019, a period for which no inclinometer data are available. Following inclinometer installation, both systems indicate relatively stable conditions through mid-2019. The acceleration observed in the inclinometer record during December 2019 through February 2020 corresponds temporally with the increase in InSAR-derived cumulative displacement, consistent with the pre-failure movements described in Montgomery et al. (2026). Note that the two systems are plotted on separate vertical axes because of differences in measurement geometry: inclinometers measure horizontal displacement at depth, while InSAR captures surface displacement along the satellite line-of-sight. The long-term continuous InSAR record demonstrates the potential of satellite-based monitoring to capture deformation trends between discrete field measurement campaigns.

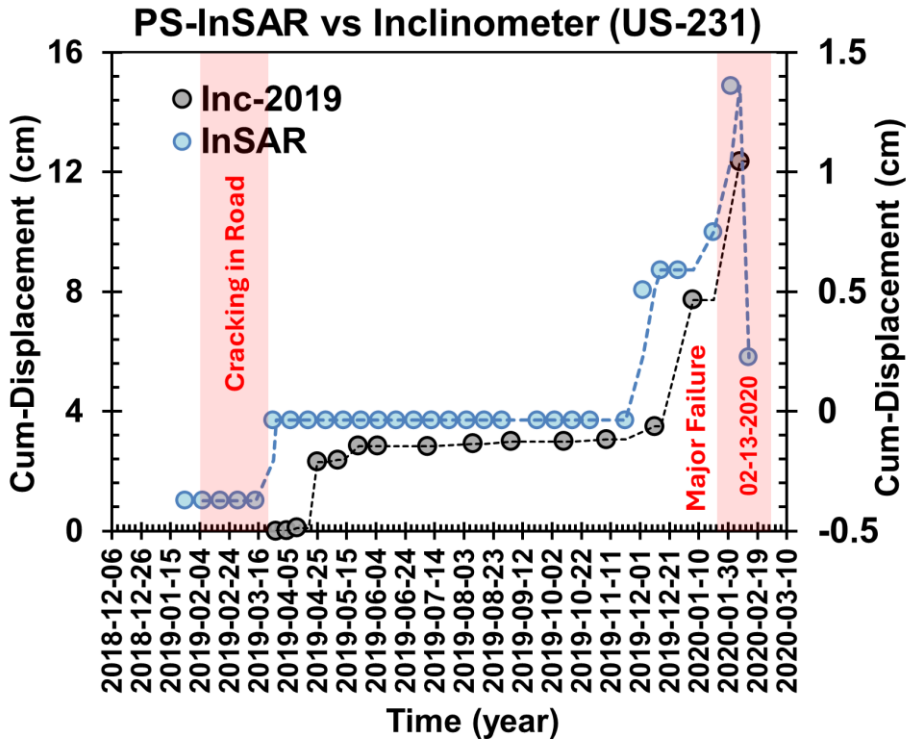

Figure 17. Comparison between PS-InSAR measurements and ALDOT inclinometer readings (2019), demonstrating close agreement in capturing pre-failure acceleration and progressive displacement during the February 2020 event.

The correlation between InSAR and inclinometer measurements demonstrates good agreement in both displacement magnitude and temporal trends. The differences reflect different measurement geometries as described earlier. The long-term continuous InSAR processing revealed subtle deformation patterns between inclinometer readings, demonstrating the potential of continuous InSAR monitoring to capture deformation trends between discrete field measurement campaigns.

3.4.1.2 NSBAS (LiCSBAS) Evaluation

Figure 18 presents a complementary analysis of the US-231 landslide site using LiCSBAS with the NSBAS processing approach, alongside the PS-InSAR results from PyGMTSAR. **Figure 18a** shows the mean LOS velocity map derived from LiCSBAS at 100-meter spatial resolution overlaid on Google Earth imagery. Despite the coarser resolution relative to the PS-InSAR output, the LiCSBAS velocity map successfully delineates a zone of negative LOS velocity coinciding with the mapped landslide area and the ALDOT inclinometer locations (US-231 52019 and 52020), confirming spatial consistency of the deformation signal across processing methods. **Figure 18b** compares the cumulative displacement time series extracted at the

same location using both approaches. The LiCSBAS time series (purple) exhibits a sustained negative displacement trend beginning in 2017, with acceleration preceding the February 13, 2020, failure event and continued post-failure subsidence reaching approximately -140 mm by 2025. The PS-InSAR time series (orange) shows more subdued displacement magnitudes with greater scatter, which is expected given that persistent scatterer selection at this vegetated site is sensitive to local surface conditions and may sample a different population of scatterers than the distributed scatterers used in the SBAS approach. The PS-InSAR time series (orange) clearly captures the pre-failure acceleration phase in late 2019, while the LiCSBAS time series (purple) exhibits a more gradual negative trend with greater scatter, making the pre-failure acceleration less discernible at this location. The larger cumulative displacements resolved by LiCSBAS reflect its sensitivity to distributed, low-coherence scatterers across the broader landslide mass, while PS-InSAR provides higher spatial resolution measurements tied to individual stable reflectors.

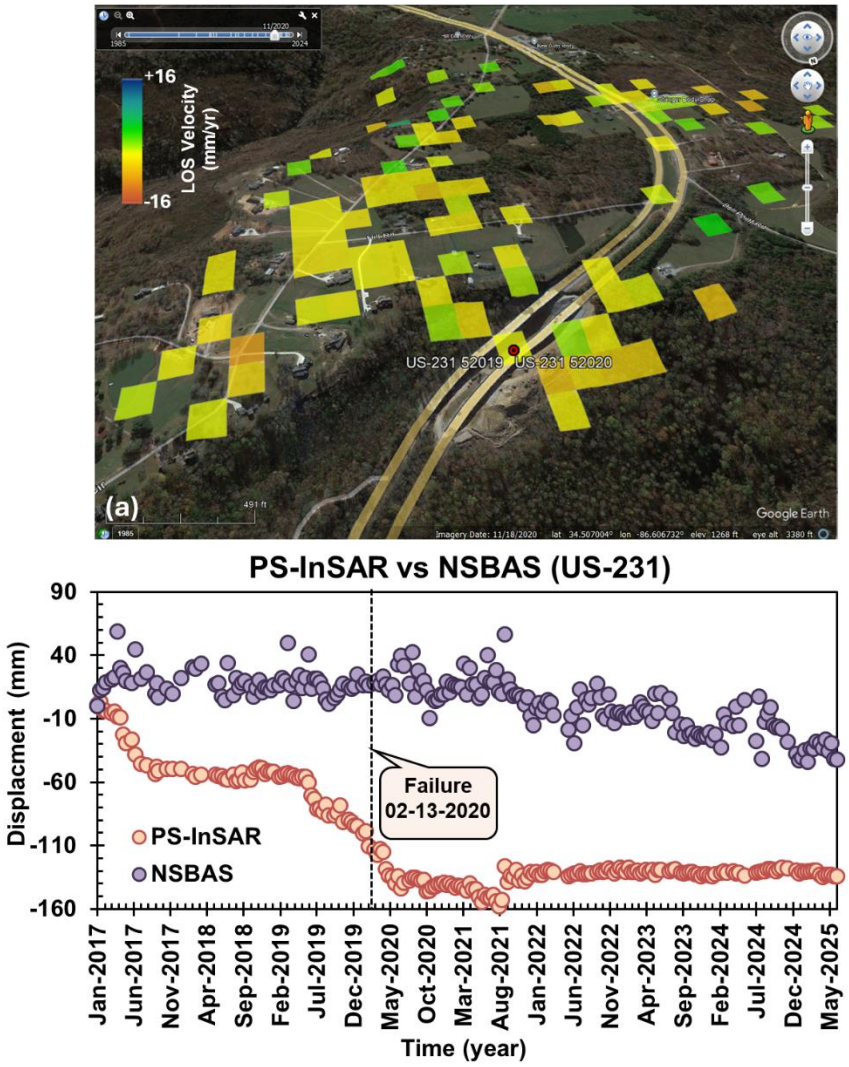

Figure 18. LiCSBAS and PS-InSAR comparison at US-231, showing (a) mean LOS velocity map and (b) cumulative displacement time series (2017–2025).

3.4.2 SR-219 (Selma Road, AL-219) near Centreville

The second validation site is located along SR-219 (also referred to as Selma Road or AL-219) in Bibb County near Centreville, Alabama. This site features a slow-moving landslide on the west side of the road that was first reported in 2010 and has continued moving since that time. ALDOT installed multiple monitoring boreholes equipped with inclinometers and groundwater wells to track the evolution of this slope instability. The site lies within the Gordo Formation of the Tuscaloosa Group, consisting of cross-bedded sand, gravelly sand, and clay layers that are particularly susceptible to landsliding under saturated conditions (Rahimikhameneh et al., 2024). Similar to US-231, a dual-processing approach was implemented: continuous long-term processing to capture slow-moving creep behavior characteristic of this site, and annual-interval processing for direct inclinometer comparison.

3.4.2.1 Validation of PS-InSAR Time Series with Inclinometer Data

Long-Term Continuous Monitoring (2017-2025)

Figure 19a presents the mean LOS velocity map from PyGMTSAR PS-InSAR analysis overlaid on Google Earth imagery along the SR-219 highway corridor. The results clearly delineate the spatial extent of deformation, with negative LOS velocities concentrated along the western side of the roadway. This deformation pattern coincides precisely with the mapped landslide zone and the locations of ALDOT inclinometer boreholes (AL-219 40002, 40003, and 40004), confirming that the InSAR signal reflects genuine slope instability rather than noise or decorrelation artifacts. The presence of dense vegetation in the background imagery further highlights the robustness of the PS-InSAR processing under challenging coherence conditions. Two monitoring points (P1 and P2) were deliberately selected to represent contrasting deformation regimes. Point P2 is located within the core of the deforming zone identified in the LOS velocity map, while P1 is positioned near the inclinometer cluster at the landslide boundary. This selection strategy enables simultaneous evaluation of InSAR performance in both actively deforming and relatively stable areas, demonstrating the method's ability to distinguish unstable slopes from adjacent stable ground.

Figure 19b shows the corresponding displacement time series from 2017 to 2025. Progressive subsidence is observed at both locations, with P2 exhibiting larger cumulative displacement and more pronounced acceleration, consistent with its position deeper within the landslide body. Seasonal oscillations superimposed on the long-term trend are evident at both points, reflecting hydrologically driven

deformation typical of slow-moving landslides in the Gordo Formation. In contrast, the lower displacement magnitude at P1 confirms that InSAR correctly identifies zones of reduced movement adjacent to active deformation.

To evaluate the hydrological controls on slow-moving landslide behavior at the SR-219 site, we integrated environmental datasets spanning 2017-2025 following the same methodology applied at US-231 **(Figure 19c)**. The temporal relationship between precipitation events (blue bars), soil moisture variations (red circles), and InSAR-detected displacement patterns demonstrate sustained hydrological forcing of slope creep behavior. Unlike the catastrophic failure observed at US-231, the SR-219 site exhibits persistent seasonal oscillations in both soil moisture (typically ranging 0.15-0.45 m^3/m^3) and displacement, with progressive subsidence accelerating during prolonged wet periods (notably 2020-2021 and 2023-2024). The consistent correlation between elevated soil moisture levels and increased displacement rates confirms that precipitation-driven pore pressure changes represent the dominant control on slow-moving landslide dynamics at this location, characteristic of clay-rich formations in the Tuscaloosa Group.

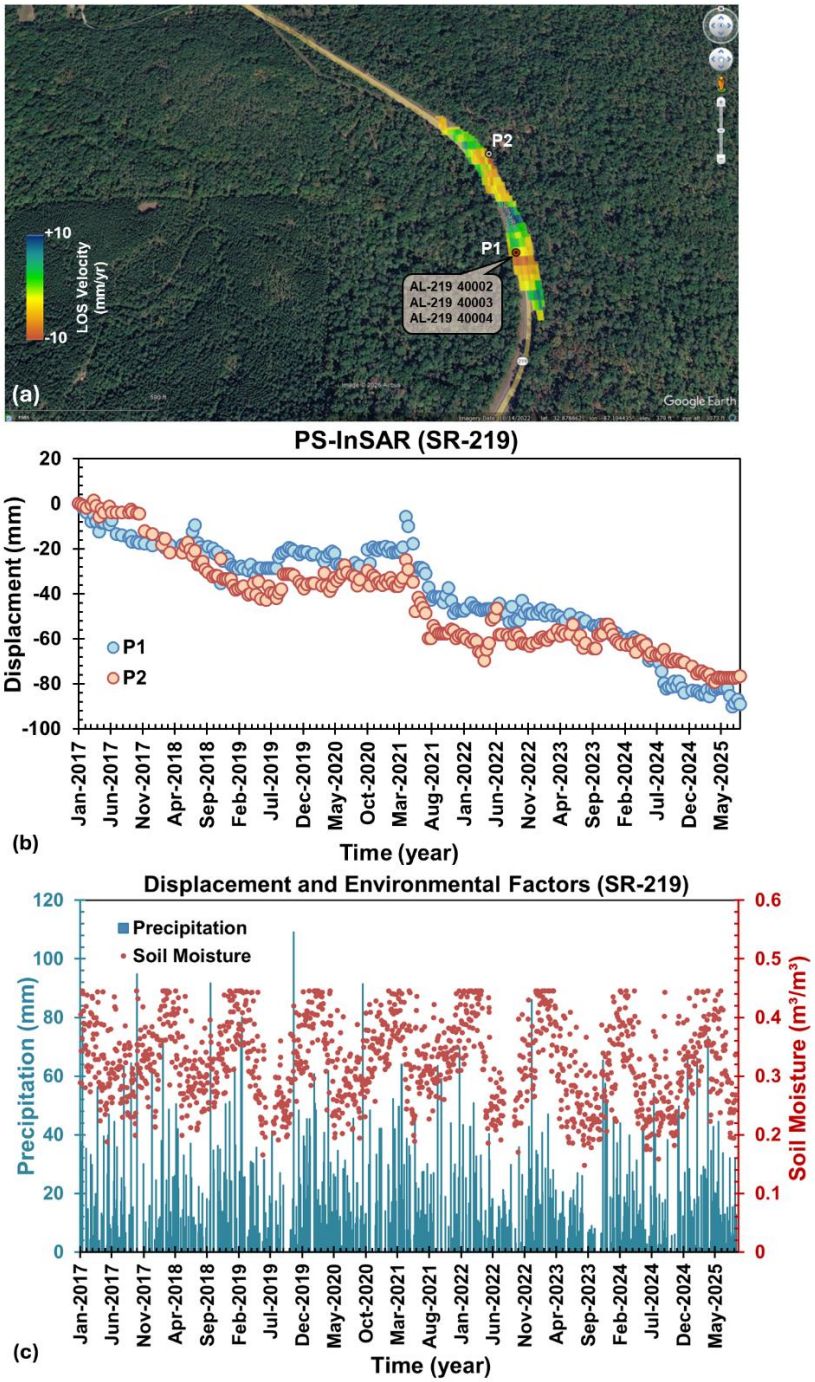

Figure 19. (a) PyGMTSAR PS-InSAR mean LOS velocity map of SR-219 slow-moving landslide site near Centreville showing monitoring points P1-P2 and ALDOT inclinometer location (AL-219). (b) Displacement time series (2017-2025) showing progressive subsidence and seasonal variations characteristic of slow-moving creep behavior. (c) Environmental factors including CHIRPS daily precipitation (blue bars, mm) and SMAP soil moisture (red circles, m^3/m^3) demonstrating persistent hydrological control on landslide dynamics.

3.4.2.1 Direct Validation with Inclinometer Data

Direct validation against ALDOT inclinometer data is shown in **Figure 20**. The two datasets are plotted on separate vertical axes, reflecting the differences in measurement geometry described before (inclinometers record cumulative horizontal displacement at the shear zone depth, while InSAR captures surface displacement in the satellite line-of-sight direction). Both datasets exhibit a generally increasing cumulative displacement trend over the 2016–2021 monitoring period, with seasonal oscillations consistent with hydrological forcing at this site, as documented by Rahimikhameneh et al. (2025). The InSAR-derived cumulative displacements are smaller in magnitude than inclinometer readings, which is expected given these geometric differences. The temporal patterns, however, show general consistency, particularly during periods of accelerated movement in 2019–2020.

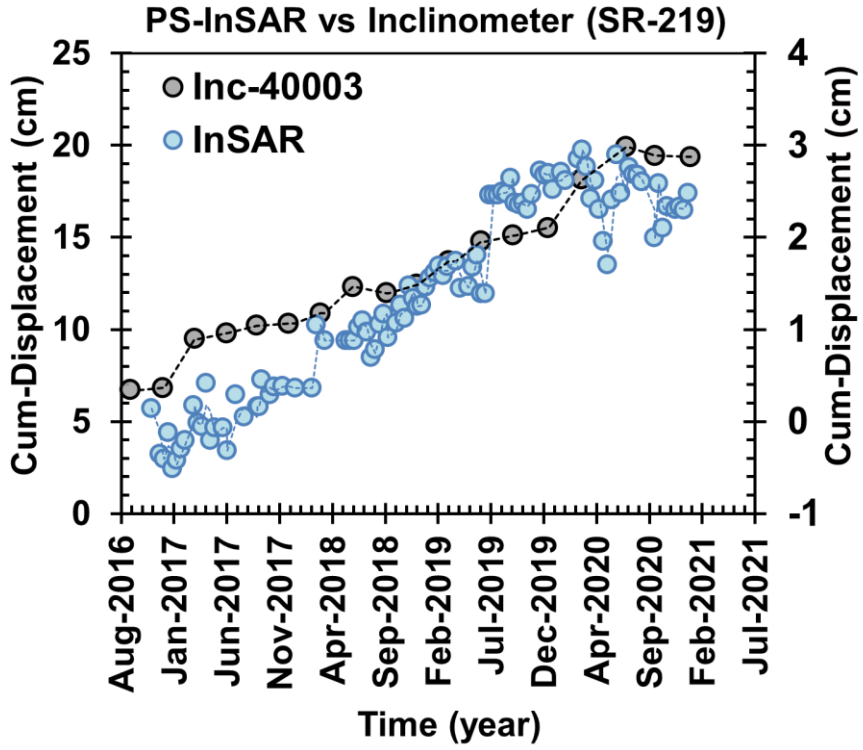

Figure 20. Comparison between PS-InSAR measurements and ALDOT inclinometer readings at SR-219 site, showing generally consistent temporal trends in cumulative displacement, with differences in magnitude reflecting the distinct measurement geometries of the two systems.

Comparison of InSAR and inclinometer measurements at both US-231 and SR-219 sites demonstrates that satellite-based monitoring can capture the same general deformation trends observed by ground instrumentation, including pre-failure acceleration at US-231 and seasonal creep behavior at SR-219. The degree of quantitative agreement varies between sites and is inherently limited by differences in

measurement geometry and depth sensitivity. These results nonetheless support the use of InSAR as a complementary monitoring tool for identifying spatial patterns and temporal trends in slope deformation along Alabama highway corridors.

3.4.2.2 NSBAS (LiCSBAS) Evaluation

To provide consistency with the validation framework applied at the US-231 site, NSBAS processing using LiCSBAS was also performed for the SR-219 landslide area. However, unlike the US-231 case, the NSBAS processing did not yield sufficient coherent points within the active landslide zone to enable meaningful time-series extraction or comparison with inclinometer measurements (**Figure 21**). The absence of valid NSBAS measurements at SR-219 is primarily attributed to the strict coherence masking and distributed scatterer requirements inherent to the NSBAS approach. The site is characterized by dense vegetation cover and persistent seasonal moisture variations, which significantly reduce interferometric coherence. Under these conditions, the NSBAS quality filtering removed most candidate pixels, resulting in sparse or absent deformation observations within the area of interest.

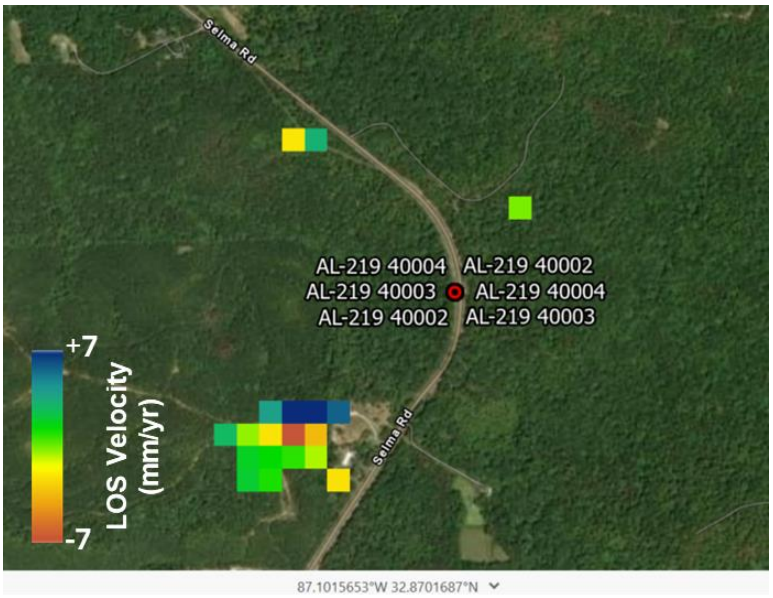

Figure 21. LiCSBAS and PS-InSAR comparison at SR-219, showing (a) mean LOS velocity map and (b) cumulative displacement time series (2017–2025).

In contrast, the PS-InSAR processing implemented in PyGMTSAR successfully identified persistent scatterers along localized stable reflectors near the roadway and instrumentation locations, allowing continuous deformation monitoring and validation with inclinometer data. This difference highlights an important methodological distinction between the two approaches: while NSBAS provides robust regional deformation products in areas with sufficient distributed scatterer coherence, PS-InSAR

demonstrates greater resilience for localized monitoring in challenging, vegetation-dominated environments.

3.4.3 Use of GNSS Data for NSBAS Data Validation

While inclinometer measurements provide a robust benchmark for validating high-resolution PS-InSAR results at localized slope locations, their suitability for NSBAS validation is limited due to differences in spatial sampling scale and the distributed scatterer nature of the NSBAS products. In particular, the reduced spatial resolution and stricter coherence requirements of NSBAS lead to weaker correspondence with discrete borehole measurements, and in some cases (e.g., SR-219), insufficient coherent pixels for direct comparison. To provide an independent and scale-appropriate validation framework for NSBAS-derived deformation, we therefore employed continuous GNSS observations, which provide spatially representative, long-term geodetic displacement measurements compatible with the regional nature of NSBAS products.

Our dataset for this purpose encompasses approximately 50 GNSS continuous operating reference stations distributed across Alabama **(Figure 22)**. This dense spatial network spans diverse geological and environmental settings, enabling evaluation of whether InSAR-observed deformation reflects regional ground motion or localized site-specific effects. From this network, two representative stations AL10 and ALCU were selected for detailed validation analysis based on the following criteria: (1) long-term continuous operation (since 2010), (2) high-quality daily solutions processed by the Nevada Geodetic Laboratory (NGL) using GipsyX Precise Point Positioning in the IGS20 reference frame, (3) proximity to primary InSAR analysis frames, and (4) location in distinct geological settings.

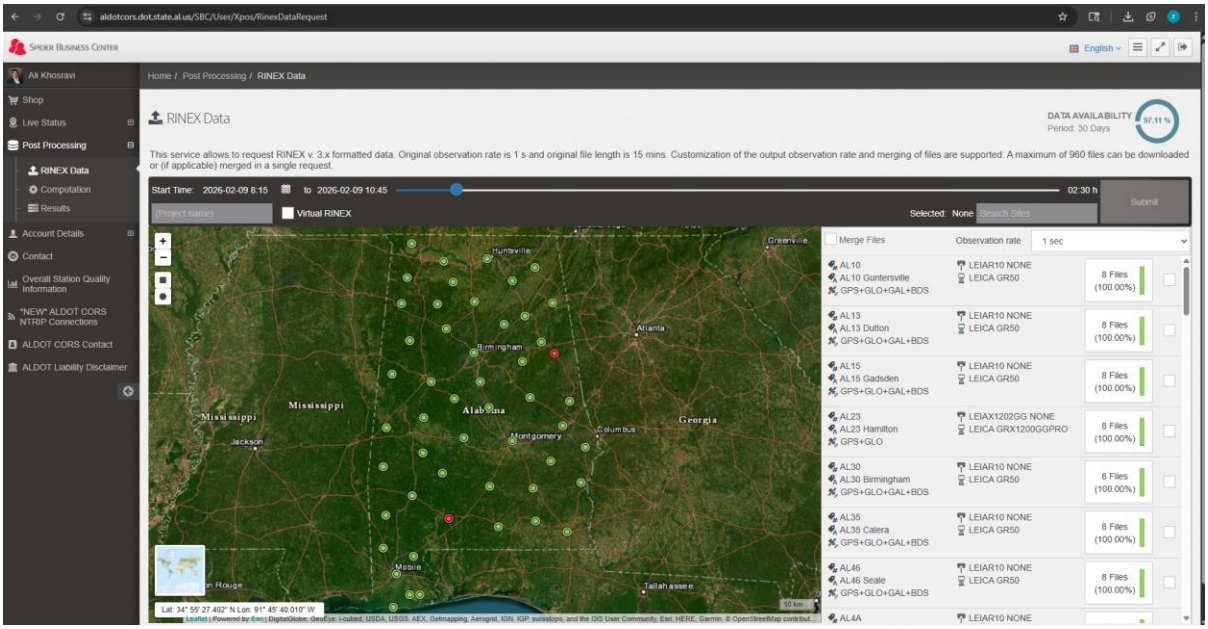

Figure 22. GNSS survey stations.

Station AL10 (34.435°N, 86.268°W; elevation 167.154 m) has operated continuously since June 30, 2010, providing 5,451 daily observations through January 2026 (**Figure 23**). Station ALCU (34.180°N, 86.845°W; elevation 222.830 m), located approximately 60 km west of AL10, provides an independent validation point in a different geologic context (**Figure 24**). This spatial separation enables assessment of whether detected deformation patterns are regionally coherent or attributable to localized effects such as monument instability. Both stations experienced documented equipment changes during their operational histories. AL10 underwent an antenna replacement affecting the vertical component in 2023, while ALCU experienced antenna and elevation cutoff adjustments. The ALCU events were recorded in the NGL metadata and critical for interpretation of apparent offsets (*https://geodesy.unr.edu/NGLStationPages/stations/ALCU.sta*). Daily GNSS position time series were downloaded in tenv3 format from the NGL public repository. These data include East, North, and Up components with formal uncertainties and quality metrics. Importantly, NGL preprocessing using GipsyX and final IGS orbits already accounts for ionospheric and tropospheric delays, solid Earth tides, and ocean loading (Blewitt et al., 2018), ensuring that observed displacements primarily reflect true ground motion rather than geophysical noise. This allows the validation effort to focus on geometric consistency and temporal agreement with InSAR rather than atmospheric correction.

To make GNSS observations directly comparable to InSAR, several preprocessing steps were required. First, quality control filtering removed observations with formal uncertainties exceeding 10 mm or missing components; over 99.9% of observations passed these criteria. Second, absolute coordinates were converted to relative displacements referenced to the first observation epoch, consistent with InSAR's relative measurement framework, as $\Delta(t) = X(t) - X(t_0)$ where X represents each coordinate component.

To separate secular trends from seasonal variability, each GNSS component was modeled using a combined linear and harmonic trajectory:

$$y(t) = a + b \cdot t + c \cdot \sin(2\pi t) + d \cdot \cos(2\pi t) + e \cdot \sin(4\pi t) + f \cdot \cos(4\pi t) \quad (6)$$

where b represents long-term velocity and the sinusoidal terms capture annual and semiannual signals related to hydrological loading, thermal expansion, and atmospheric pressure effects.

The original three-component GNSS position time series from the Nevada Geodetic Laboratory (NGL) are shown in **Figures 23** and **24**, illustrating the East, North, and Up displacement components for stations AL10 and ALCU, with NGL's fitted trajectory models overlaid as red curves. These time series demonstrate both the high quality of the GNSS data, and the long-term kinematic trends as processed using the GipsyX Precise Point Positioning software. For station AL10, NGL-published velocities are −13.544 ±

0.138 mm/yr (East), +0.767 ± 0.129 mm/yr (North), and +0.322 ± 0.606 mm/yr (Up). Station ALCU exhibits nearly identical horizontal motion, with −13.542 ± 0.130 mm/yr (East) and +0.861 ± 0.136 mm/yr (North), consistent with the stable westward motion of the North American plate. A notable vertical offset of approximately 60–80 mm is observed in AL10 during 2023, which is attributed to antenna replacement and monument disturbance documented in the station metadata. In contrast, ALCU shows no comparable offset and remains vertically stable throughout the observation period, providing a useful reference site for validation interpretation.

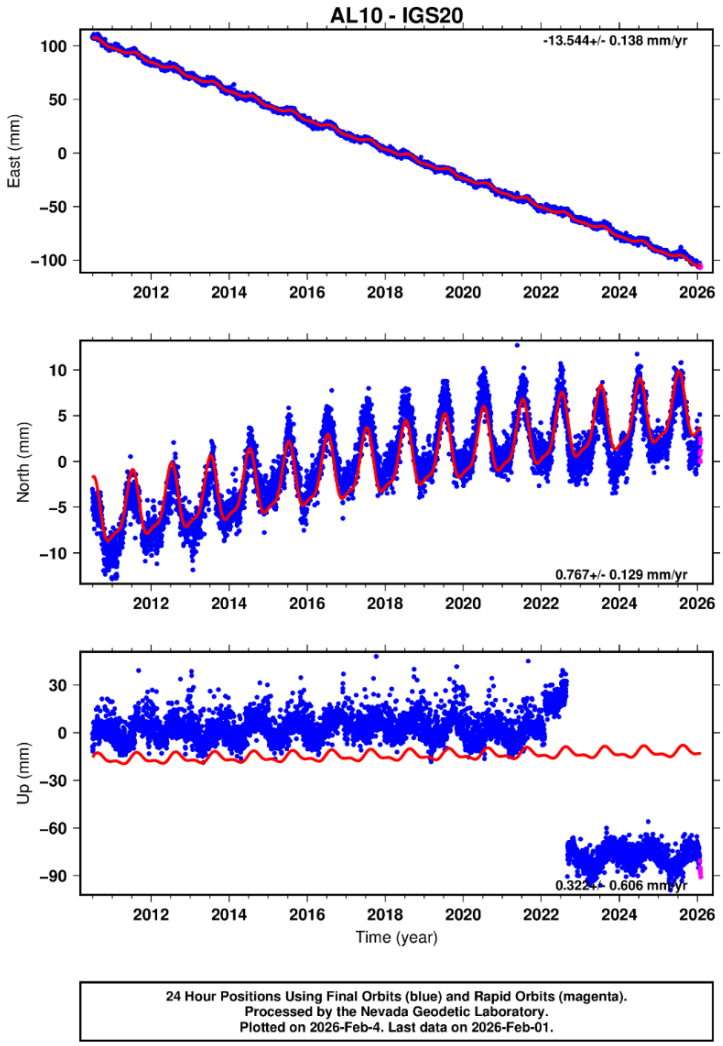

Figure 23. GNSS-AL10 station (2010 to 2026).

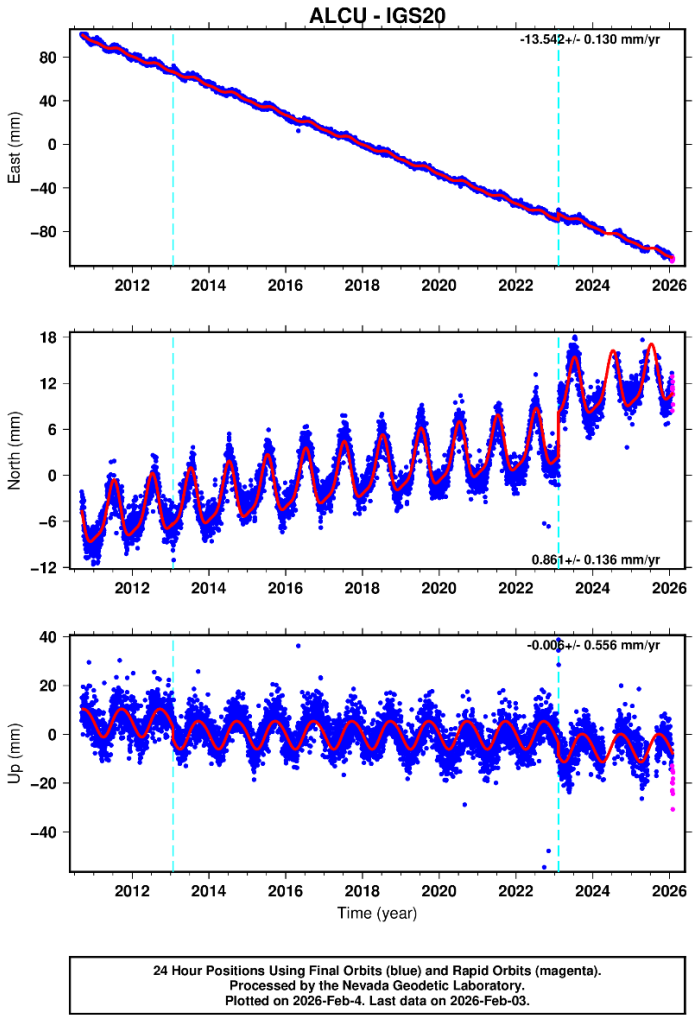

Figure 24. GNSS-ALCU station (2010 to 2026).

Because InSAR satellites measure ground deformation only along their specific viewing geometry, recording changes in range between the satellite and ground surface, it is necessary to project the three-dimensional GNSS displacements into the satellite line-of-sight (LOS) direction for meaningful comparison. For Sentinel-1 ascending-orbit acquisitions, the satellite travels from south to north with a heading angle of $\alpha = -10.2°$ (clockwise from north) and observes the surface at an incidence angle of $\theta = 39.5°$ from vertical. The corresponding LOS unit vector components are given by:

$$u_E = -\sin(\theta) \cdot \sin(\alpha) = +0.113 \quad (7)$$

$$u_N = -\sin(\theta) \cdot \cos(\alpha) = -0.627$$

$$u_U = \cos(\theta) = +0.771$$

The GNSS displacement vector projected into line-of-sight is then:

$$\mathrm{LOS}_{\mathrm{GNSS}} = E \cdot u_E + N \cdot u_N + U \cdot u_U = 0.113 \cdot E - 0.627 \cdot N + 0.771 \cdot U \quad (8)$$

This projection highlights the relative sensitivity of Sentinel-1 InSAR measurements: approximately 77% of the LOS signal is controlled by vertical motion, 63% by north–south displacement, and only 11% by east–west motion. Consequently, vertical deformation and north–south trends dominate the InSAR response, while east–west motion contributes minimally. The InSAR dataset used for calibration consists of 232 Sentinel-1 acquisitions spanning April 2016 to August 2025, processed using the NSBAS-InSAR methodology implemented in LiCSBAS**. Figure 25** shows the spatial distribution of mean LOS velocity across Alabama, with GNSS stations AL10 and ALCU overlaid as reference locations.

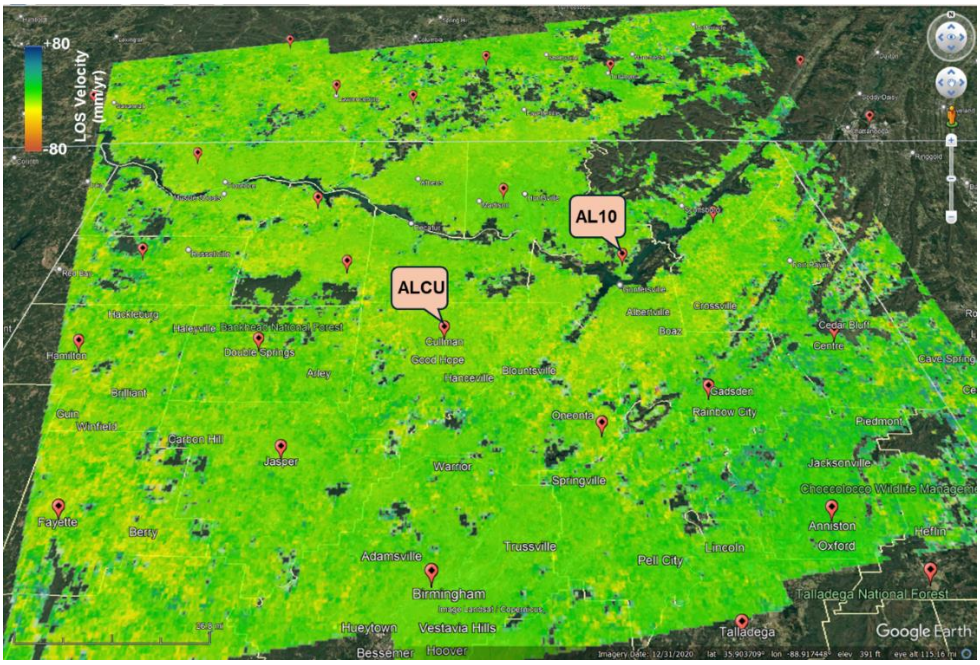

Figure 25. The mean LOS velocity map obtained from NSBAS-InSAR by LiCSBAS and GNSS Stations AL10 and ALCU from April 2016 to August 2025.

Direct comparisons between GNSS-derived LOS displacements and the InSAR LOS time series are presented in **Figures 26** and **27**. The statistical evaluation indicates a moderate point-by-point correlation for AL10 (Pearson R = +0.424, R^2 = 0.18, RMSE = 38.7 mm, $p < 0.001$). In contrast, ALCU exhibits a weaker and negative correlation (R = −0.262, R^2 = 0.069, RMSE = 14.4 mm). **Figure 28 (a, b)** presents the corresponding scatter plots of GNSS versus NSBAS-InSAR LOS displacements for AL10 and ALCU, respectively.

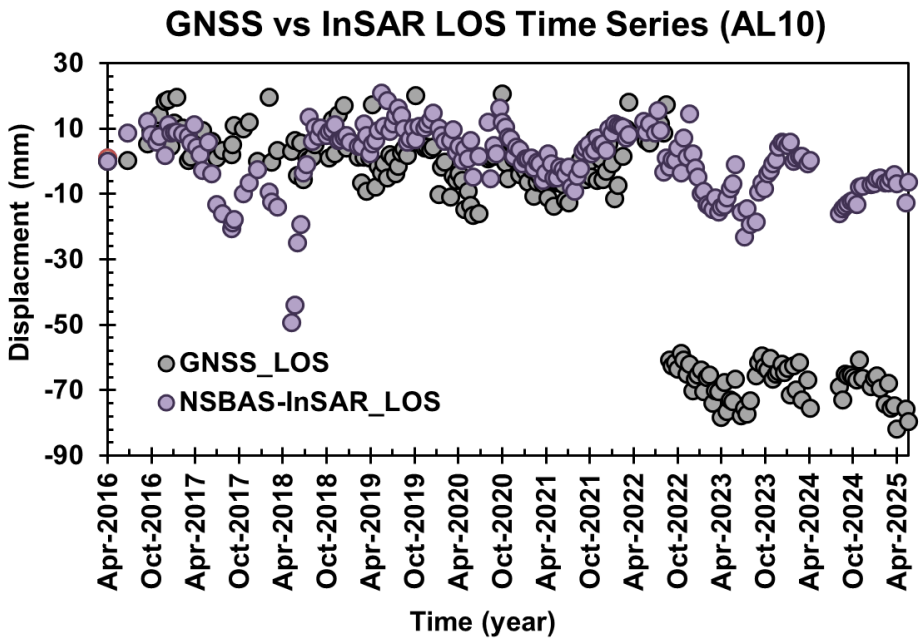

Figure 26. Evaluation between NSBAS-InSAR observations with GNSS-AL10 station (2016 to 2025).

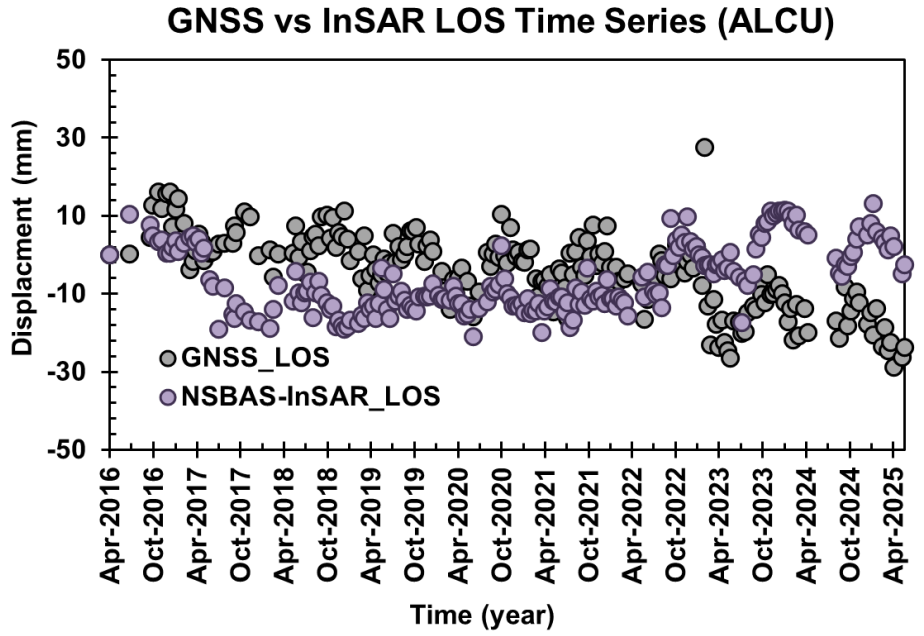

Figure 27. Evaluation between NSBAS-InSAR observations with GNSS-ALCU station (2016 to 2025).

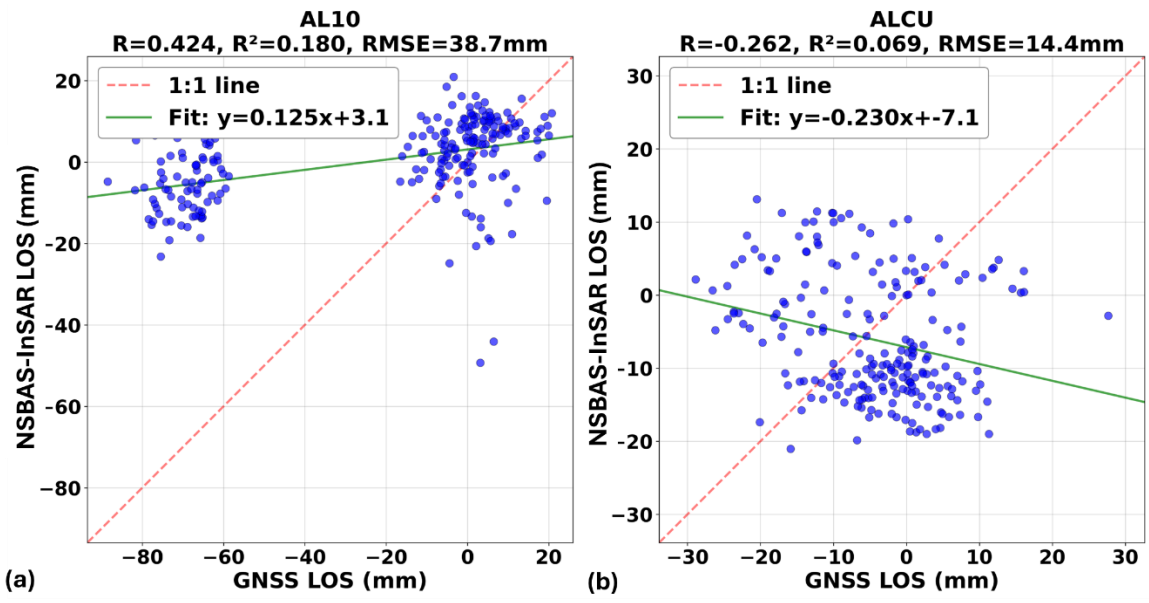

Figure 28. Scatter plot of differential GNSS versus differential InSAR displacements (AL10 and ALCU)

While these individual station correlations are not expected to be high due to fundamental differences in spatial sampling (point-based GNSS versus distributed InSAR pixels), temporal resolution, and monument stability, both datasets consistently capture long-term trends and seasonal oscillations. The pronounced vertical offset at AL10 during 2023 coincides with a documented antenna replacement at the GNSS monument. This offset is primarily an instrument-related event in the GNSS record, and its absence at ALCU confirms the localized nature of the disturbance.

To reduce the influence of spatially correlated atmospheric phase delays and to provide a more robust assessment of InSAR measurement accuracy, a differential comparison was performed between the two GNSS stations. Rather than comparing InSAR time series at individual pixels directly with the corresponding GNSS stations, we computed the difference between the two GNSS-derived LOS time series and compared it with the corresponding difference between the InSAR time series at those station locations:

$$\Delta GNSS(t) = LOS_{GNSS}(AL10, t) - LOS_{GNSS}(ALCU, t) \quad (9)$$

$$\Delta InSAR(t) = LOS_{InSAR}(AL10, t) - LOS_{InSAR}(ALCU, t) \quad (10)$$

This differential approach effectively cancels spatially correlated errors, including tropospheric and ionospheric delays that affect both stations similarly on any given acquisition date. From 215 common acquisition dates, the differential comparison yielded a Pearson correlation coefficient of $R = +0.718$ ($R^2 = 0.515$, RMSE = 29.9 mm, $p < 0.001$), representing a substantial improvement over the individual station

correlations. **Figure 29** presents the differential time series, while **Figure 30** shows the corresponding scatter plot of ΔGNSS versus ΔNSBAS-InSAR.

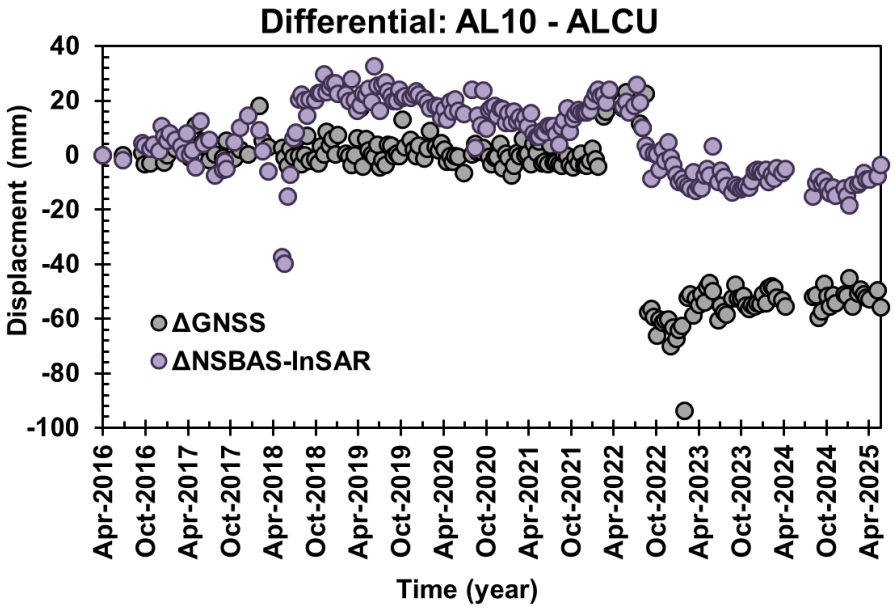

Figure 29. Differential time series: ΔGNSS (AL10−ALCU) versus ΔInSAR (AL10−ALCU) from 2016 to 2025.

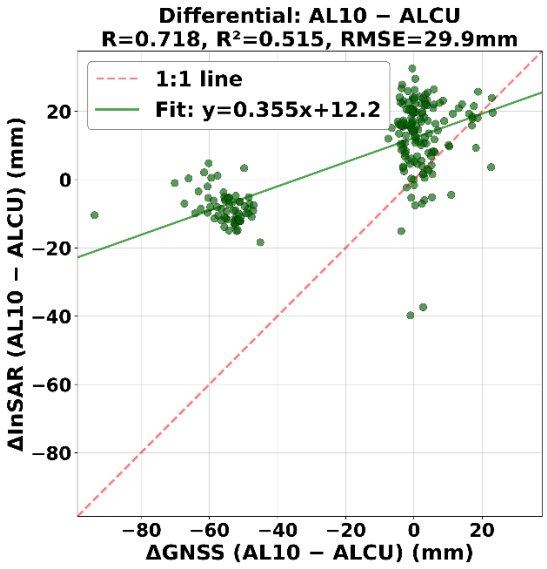

Figure 30. Scatter plot of differential GNSS versus differential InSAR displacements (AL10−ALCU), showing R = 0.718 (R^2 = 0.515), and RMSE = 29.9 mm.

The marked improvement in correlation R = 0.718 (differential) demonstrates that a significant portion of the discrepancy in the direct comparison is attributable to spatially correlated atmospheric

artifacts rather than fundamental measurement error. The differential results show that the NSBAS-InSAR processing workflow effectively captures the relative deformation behavior between the two stations, with $R^2 = 0.515$, meaning that more than 51% of the variability in the differential GNSS measurements is accounted for by the differential InSAR observations.

The differential time series also reveals that the 2023 antenna offset at AL10, which appears as a systematic ~50 mm shift in the ΔGNSS record, is not mirrored in the ΔNSBAS-InSAR signal. This provides independent confirmation that the 2023 offset is a GNSS monument artifact rather than a real ground deformation event, further validating the InSAR measurements at both stations. These results are consistent with published GNSS–InSAR validation studies that report improved correlation using differential baseline approaches (e.g., Alonso-Díaz et al., 2026), and they support the use of the NSBAS-InSAR deformation time series for operational monitoring applications in Alabama.

3.5 Localized Infrastructure Case Studies

Following the validation analyses presented in the previous sections, localized case studies were conducted to demonstrate how InSAR methods can be applied to real-world infrastructure monitoring scenarios across Alabama. While validation using inclinometer and GNSS data established the reliability of the processing approaches at different spatial scales, practical infrastructure monitoring often requires resolving deformation along narrow roadway corridors and engineered earth structures under diverse environmental and geological conditions. This section presents two complementary case studies designed to illustrate these challenges. The first focuses on the Littleville corridor, where full-resolution PS-InSAR analysis is used to resolve deformation associated with natural slope instability along a highway corridor. The second examines the Lake Tholocco levee system in southern Alabama, representing a contrasting engineered embankment environment influenced by standing water and strong hydrologic forcing, where high-resolution NSBAS processing is evaluated alongside PS-InSAR results. Together, these case studies demonstrate how InSAR performance depends on spatial scale, processing methodology, and site-specific geological and environmental conditions, highlighting the potential for operational infrastructure monitoring across varying terrain and infrastructure types.

3.5.1 Localized Displacement Analysis using pyGMTSAR – Littleville AL Case Study

The Littleville corridor along US-43 in Colbert County was selected as a primary case study to evaluate localized deformation monitoring along a highway segment affected by documented slope instability and recurring maintenance interventions by ALDOT. To resolve deformation patterns along narrow infrastructure elements and landslide-prone slopes, PyGMTSAR PS-InSAR processing was performed

using full-resolution Sentinel-1 imagery (~5 × 20 m single-look spacing). Persistent scatterers were identified using amplitude dispersion metrics, combined with 1D temporal unwrapping to improve robustness in densely vegetated terrain and narrow roadway geometry. The analysis spans 2017 through August 2025, providing more than eight years of continuous displacement monitoring **(Figure 31)**.

Figure 31a presents the mean LOS velocity field overlaid on high-resolution imagery and highlights spatially variable deformation along the corridor, including localized zones of negative LOS velocity consistent with slope movement adjacent to the roadway. To evaluate PyGMTSAR's ability to distinguish stable versus unstable behavior, and to support subsequent predictive modeling and early warning development, we selected three monitoring points (P1–P3) representing distinct displacement regimes **(Figure 31a–b)**: P1 as a comparatively stable reference region (stable infrastructure), P2 within the core deformation zone (critical movement), and P3 capturing intermediate behavior (moderate movement). The displacement time series **(Figure 31b)** demonstrates clear separation between these regimes, with P2 exhibiting the largest cumulative displacement and the most persistent downward trend over the monitoring period, while P1 remains comparatively stable and P3 shows intermediate subsidence. This point-selection strategy mirrors the validation-site approach used in sampling both moving and minimally moving areas, to demonstrate that PS-InSAR can resolve true deformation gradients rather than producing uniformly biased signals.

To interpret deformation mechanisms and quantify environmental forcing at Littleville, we integrated precipitation and soil moisture datasets over the same observation period (2017–2025) using the same methodology applied at the validation sites **(Figure 31c)**. Daily precipitation from CHIRPS (blue bars) and soil moisture from NASA SMAP L3 Enhanced (brown markers) were extracted at the site location and evaluated alongside the InSAR displacement record (pink markers). The combined time series shows seasonal coupling among precipitation, soil moisture, and displacement, with rainfall events followed by increases in soil moisture and amplified displacement, particularly during prolonged wet periods. Ground observations at the Littleville corridor indicate recurring slope instability along US-43, though the precise onset of movement at this location has not been documented. The InSAR record beginning in 2017 captures an already-active deformation signal, suggesting that slope movement predates the satellite monitoring period.

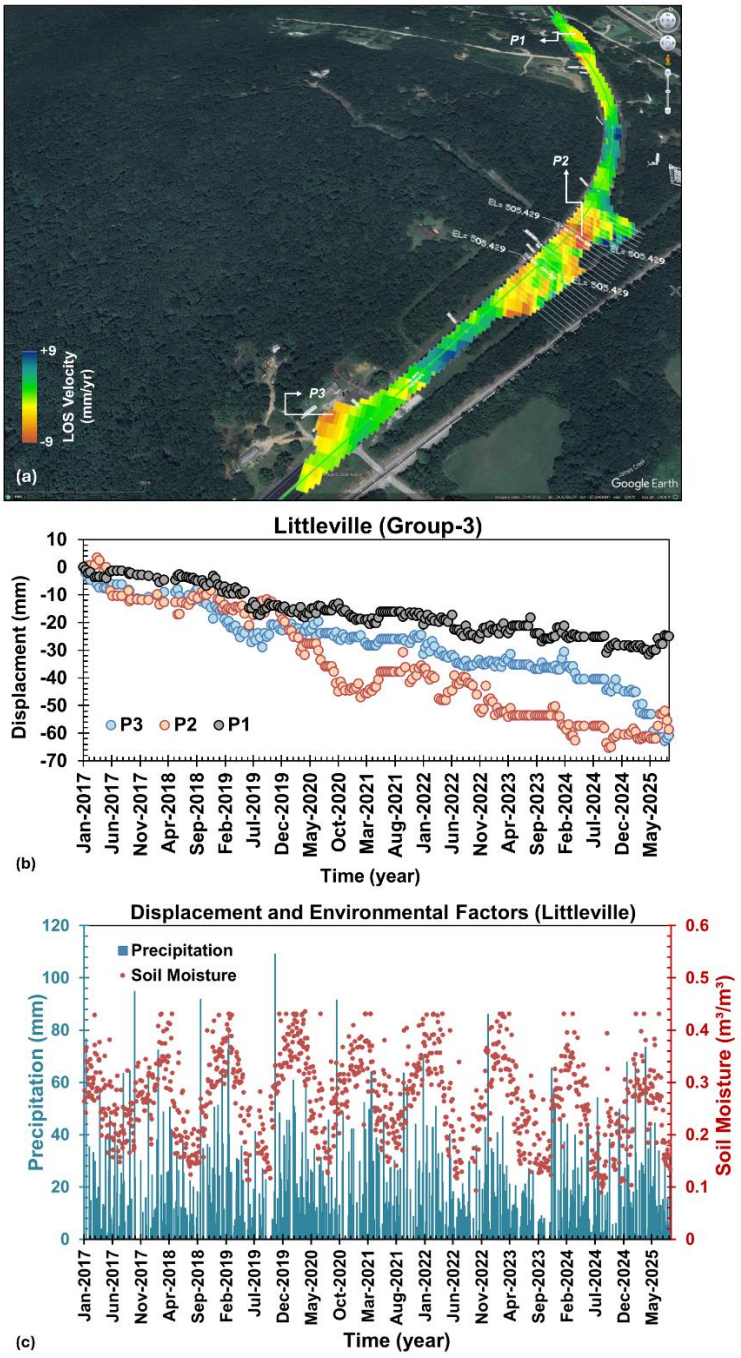

Figure 31. Littleville deformation map with planned near CRs locations, PS-InSAR time series plots, and landslide boundaries overlaid on Sentinel-1 satellite imagery.

3.5.2 High-Resolution NSBAS Analysis for Localized Infrastructure Monitoring: Lake Tholocco Levee System

The preceding analyses demonstrated that InSAR performance depends strongly on spatial scale and processing methodology. While the Littleville case study highlighted the capability of full-resolution PS-InSAR to resolve localized slope deformation along narrow highway corridors, this section presents a complementary case focused on distributed-scatterer analysis within a levee-roadway environment.

The Lake Tholocco levee system, located in southern Alabama, was selected as a contrasting infrastructure case study to evaluate roadway deformation monitoring under a markedly different geological and hydrologic setting (**Figure 32**). Unlike the Littleville corridor, which represents natural slope instability in a hillside environment, the Lake Tholocco site consists of a narrow roadway constructed atop an engineered levee adjacent to standing water. These conditions introduce unique challenges for InSAR monitoring, including mixed land–water pixels, limited coherent scatterers, and strong moisture-driven deformation. To better represent the narrow roadway footprint, NSBAS processing was performed using reduced multilooking, yielding an effective spatial resolution of approximately 20 m and enabling direct comparison with high-resolution PS-InSAR results.

In this analysis, Sentinel-1 SAR data spanning from April 2016 to July 2023 were processed utilizing PyGMTSAR's advanced persistent scatterer identification through amplitude dispersion index (ADI) calculations and 1D temporal unwrapping and NSBAS-LiCSBAS following procedure mentioned earlier. For this road, due to the mixing of pixels between vegetated areas and the levee at 100 m resolution (standard), some pixels were removed and the standard-resolution data failed to capture deformation at the levee location **(Figure 32a)**. To deal with this problem and to improve spatial detail at priority sites,

processing was repeated using reduced multilooking factors, producing deformation products with approximately 20 m effective pixel spacing **(Figure 32b)**.

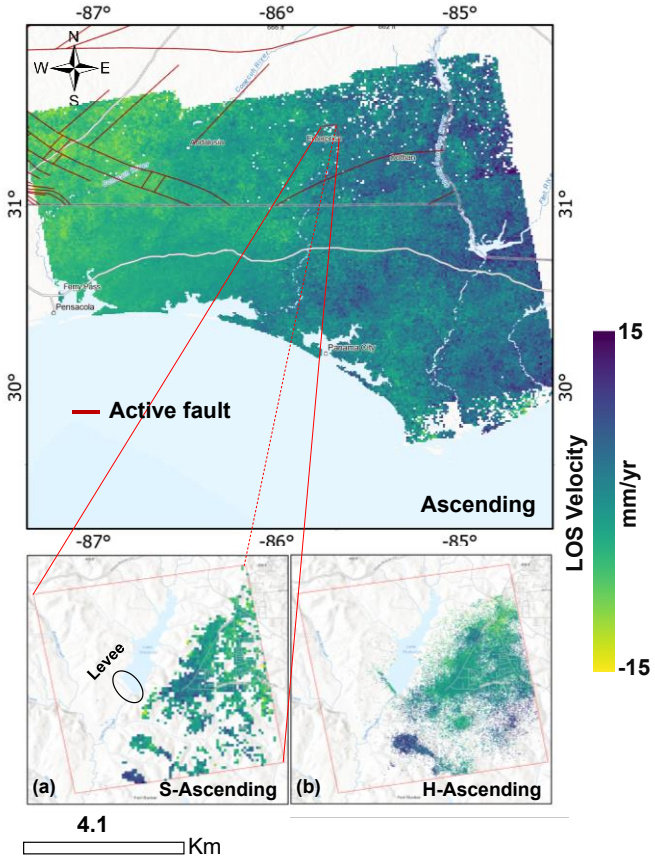

Figure 32. InSAR-derived LOS velocity maps of the Lake Tholocco levee system (a) standard resolution ascending track and (b) higher resolution ascending track.

This approach retained the automated LiCSAR/LiCSBAS workflow while improving the ability to resolve localized deformation along highway corridors. However, the reduced spatial averaging increased noise levels in densely vegetated areas, and coverage remained limited for very narrow infrastructure features. Results were also compared with the results of Persistent Scatterer InSAR (PS-InSAR) analysis using the PyGMTSAR framework **(Figure 33)**.

Cross-comparison between NSBAS-LiCSBAS **(Figure 33a)** and PS-PyGMTSAR **(Figure 33b)** results was also conducted to evaluate consistency and measurement reliability. At the Lake Tholocco levee system, both methods identified similar spatial patterns of localized subsidence, with PS-InSAR estimating

subsidence rates of 8.6 mm/yr and LiCSBAS estimating approximately 10 mm/yr near the levee structure. Observed displacement rates consistently ranged between 7 and 10 mm/yr.

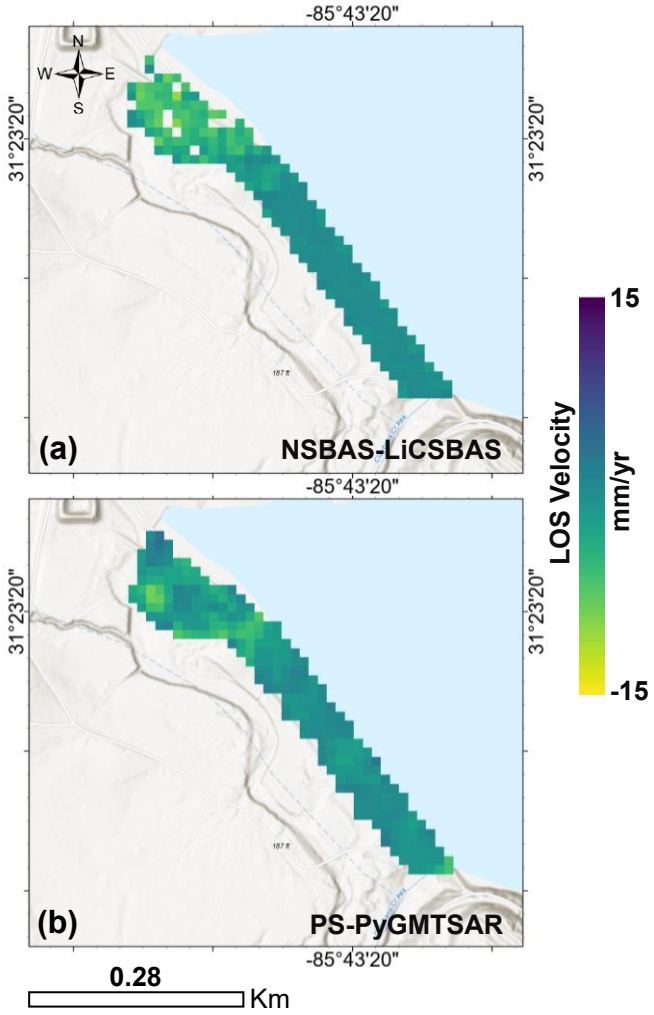

Figure 33. Comparison of InSAR displacement measurements at Lake Tholocco levee system (April 2016 - July 2023). (a) NSBAS-LiCSBAS analysis. (b) PS-PyGMTSAR validation.

Quantitative comparison yielded a root mean square error (RMSE) of 2.9 mm/yr and a mean absolute error (MAE) of 2.0 mm/yr between the two methods **(Figure 34)**, values well within acceptable ranges for engineering-scale deformation assessment. The scatter plot indicates strong agreement, with most observations clustering within ±2 mm/yr of the 1:1 reference line.

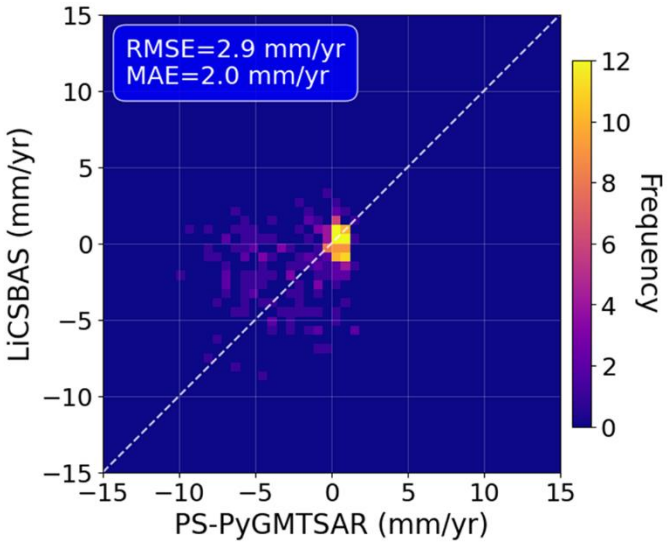

Figure 34. Statistical comparison between PS-PyGMTSAR and NSBAS-LiCSBAS displacement measurements at Lake Tholocco levee system showing scatter plot with RMSE and MAE values. The dashed line represents perfect 1:1 correlation.

Differences between the two approaches were most evident in heavily vegetated sections. In these areas, PS-InSAR either detected stable conditions or lacked persistent scatterers, while LiCSBAS identified deformation through its distributed scatterer methodology. These discrepancies reflect fundamental methodological differences: PS-InSAR relies on amplitude-stable point targets (Ferretti et al., 2001), whereas LiCSBAS exploits phase-based distributed scatterers and is more sensitive to spatial filtering effects, which may introduce phase bias in low-coherence regions (Maghsoudi et al., 2022).

To evaluate the influence of environmental factors on levee deformation at Lake Tholocco, multi-source remote sensing data from August 2016 to July 2023 were analyzed and compared with InSAR-derived displacement time series **(Figure 35)**. Three key environmental variables were examined: precipitation, surface soil moisture, and land surface temperature. Precipitation data were obtained from the GPM mission, soil moisture from NASA–USDA global datasets, and land surface temperature from MODIS, providing consistent long-term coverage.

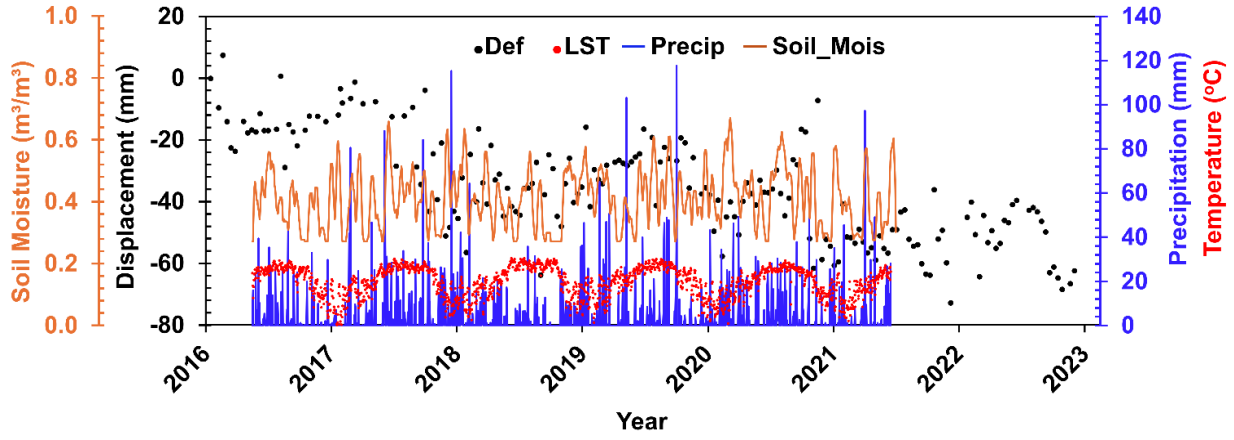

Figure 35. Evaluation between InSAR observations with precipitation and soil moisture in levee location for the Lake Tholocco dam and levee system from August 2016 to July 2023.

The InSAR time series reveals pronounced seasonal and long-term variability in levee displacement, with rates ranging from approximately −40 mm/yr to +10 mm/yr. Displacement patterns show strong correlation with precipitation and soil moisture. Periods of intense rainfall lead to increased soil moisture and are associated with upward ground movement, reflecting swelling behavior in the clay-rich levee materials. In contrast, dry periods correspond to reduced soil moisture and increased subsidence, indicating shrinkage and consolidation. The deformation response exhibits a measurable time lag relative to precipitation events, consistent with delayed infiltration and soil volume adjustment processes. Superimposed on these seasonal cycles is a gradual long-term subsidence trend, suggesting ongoing consolidation within the levee structure. Land surface temperature follows expected seasonal variations and modulates the soil moisture–deformation relationship by influencing evaporation rates and moisture retention.

To interpret the observed InSAR-derived deformation at the Lake Tholocco levee, a geotechnical analysis was conducted to link seasonal climate variability to subsurface soil behavior. Unlike cement-stabilized levees, the Lake Tholocco levee is composed primarily of clay loam and sandy clay loam soils, providing a relatively homogeneous earthen system well suited for hydromechanical interpretation. This soil composition enables direct correlation between satellite-observed deformation and unsaturated soil mechanics. The analysis integrated satellite-derived soil moisture estimates, laboratory-measured soil hydraulic properties, and unsaturated soil mechanics theory. Multi-temporal Sentinel-1 SAR data (2016–2023) were processed to estimate volumetric water content using an ensemble of polarization-based methods, constrained by laboratory-measured soil properties (Zulfeqar et al., 2025) **(Figure 36)**. The same approach was used by Javid and Bulut (2019). These moisture estimates were converted to matric suction

using a van Genuchten soil-water retention model developed from laboratory testing of levee soils. The resulting suction stress fields were compared with InSAR-derived line-of-sight deformation rates. Then, using the suction stress framework of Lu and Likos (2004), seasonal changes in degree of saturation were translated into suction stress variations, providing a mechanistic link between moisture dynamics and deformation.

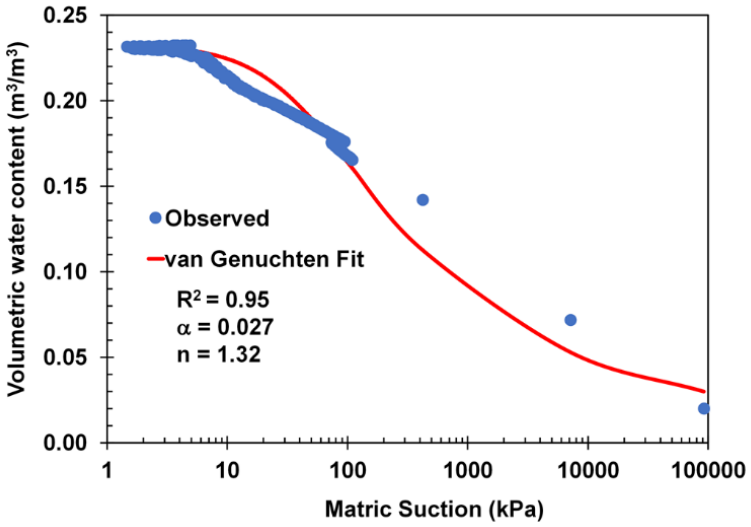

Figure 36. Soil water retention curve for Lake Tholocco levee.

Figure 37 links suction stress and degree of saturation **(Figure 37a)** with InSAR-derived LOS velocity **(Figure 37b)**. An 8-year average period, aligned with the InSAR record, was used to capture the full spectrum of seasonal wet-dry cycles while filtering out short-term fluctuations. The analysis clearly shows that zones with high suction stress and low degrees of saturation correspond to areas of greater ground deformation, emphasizing the strong hydromechanical coupling within the levee structure. Across the levee, suction stress varies from 0 to 60 kPa, while the degree of saturation ranges from 0.03 to 0.23 (m^3/m^3). Areas with the highest suction stress (50–60 kPa, yellowish zones) correspond to the lowest saturation levels (below 0.15) and exhibit the largest deformation rates (LOS velocity from −10 to 0 mm/yr). In contrast, sections with higher saturation (above 0.20, blue zones) show minimal suction stress (0–20 kPa) and remain stable. These results confirm that levee deformation is primarily controlled by seasonal fluctuations in soil moisture: wet periods reduce matric suction and suction stress, limiting settlement, whereas dry periods increase suction stress, leading to shrinkage and localized deformation. The close match between suction stress patterns and InSAR measurements highlights the soil moisture as the dominant factor driving seasonal deformation.

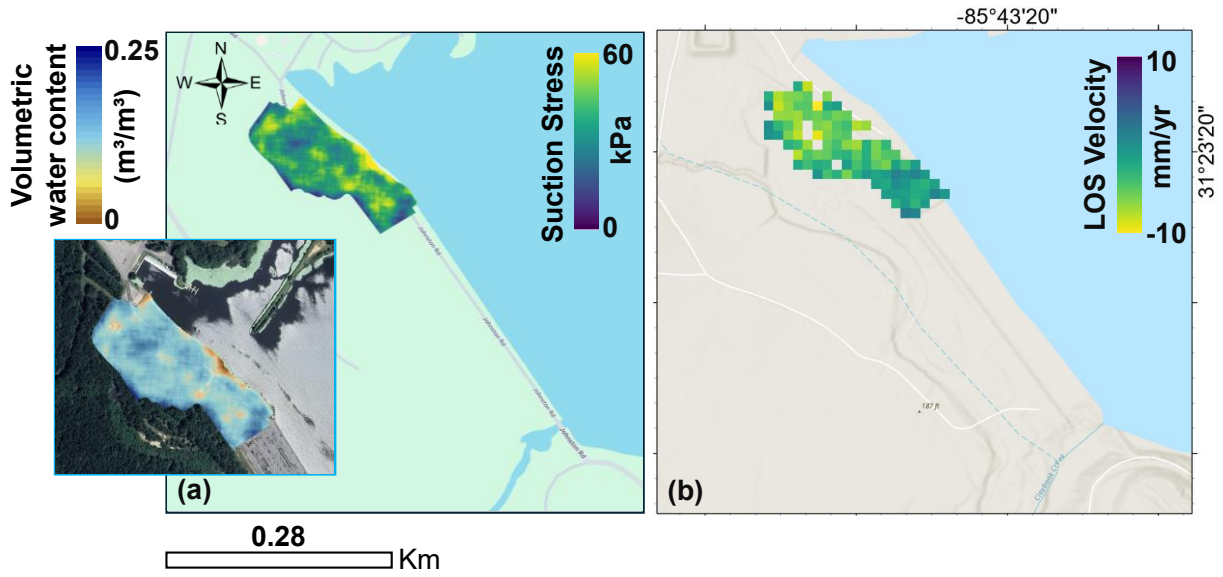

Figure 37. Suction stress, soil moisture, and InSAR-derived deformation for the Tholocco levee (2016–2023) (a) High suction stress corresponds to low moisture content and (b) The LOS velocity map shows greater deformation in zones of high suction.

3.6 Field Deployment of a Corner Reflector Network

To support future validation and long-term operational monitoring, a network of corner reflectors (CRs) was designed and deployed in coordination with ALDOT. Although sufficient post-installation time series are not yet available for quantitative validation, this deployment establishes a stable ground reference framework intended to enable millimeter-level validation of InSAR-derived displacement products as the dataset matures. The deployment strategy was developed in consultation with ALDOT personnel and engineers to identify locations that satisfy both InSAR technical requirements and field accessibility constraints (Figure 38). Initial planning included campus-based installations for calibration and visibility testing, followed by installation of multiple reflectors along the Littleville corridor (US-43), where ongoing landslide monitoring activities are underway. This staged deployment approach ensured proper reflector alignment, satellite visibility, and reproducibility of field procedures prior to large-scale deployment.

Figure 38. Corner reflector deployment and possible installation locations.

Corner reflectors are passive devices designed to reflect radar signals directly back to the satellite, creating bright, stable targets in SAR imagery **(Figure 39)**. These reflectors significantly enhance the accuracy and repeatability of InSAR measurements by serving as consistent ground reference points. Compared to GNSS stations, they offer higher spatial resolution and broader applicability across diverse monitoring zones. To ensure long-term reliability, we procured advanced corner reflectors from EO59, a European company specializing in InSAR monitoring systems. EO59 was selected after evaluating multiple vendors based on technical specifications and field-proven performance. The reflectors are trihedral, passive metal structures oriented to align with both ascending and descending satellite line-of-sight geometries. Each unit includes a robust anchoring system to ensure that recorded displacements reflect true ground movement rather than device instability. No power source is required.

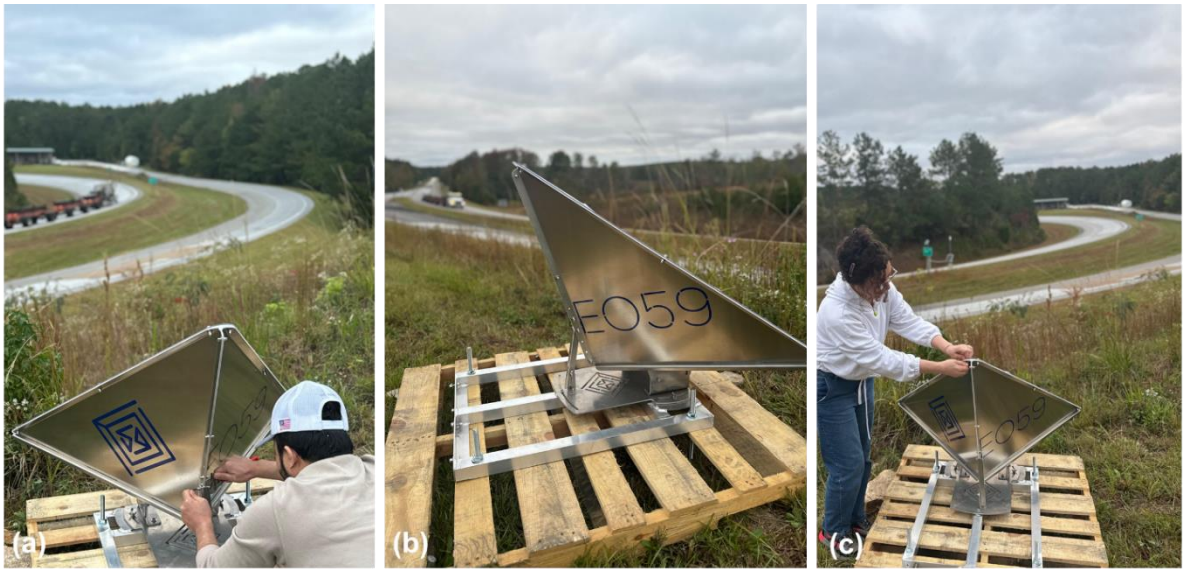

Figure 39. Field installation and alignment of the corner reflector: (a) tightening the mounting bolts and nuts to secure the reflector, (b) checking and adjusting the level of the assembly to ensure proper horizontal alignment, and (c) fine-tuning the reflector orientation to achieve the required angle toward the satellite line of sight.

The campus-based corner reflector (CR) installation for calibration and visibility testing was located at the geotechnical field-testing facility near the NCAT (National Center for Asphalt Technology) test facility. The CR was installed in early December 2025 to verify satellite visibility and optimize installation procedures. As shown in **Figure 40**, the CR (GCP2) was clearly detected by Sentinel-1, appearing as a bright, high-amplitude target in SAR amplitude imagery. The normalized backscatter intensity timeseries (Sigma0_IW3_VV) confirms a sharp increase in radar response following installation, rising from near-zero values to normalized intensity levels exceeding 0.8, demonstrating successful reflector orientation and consistent detection across multiple post-installation acquisitions (December 7, 2025 – January 24, 2026).

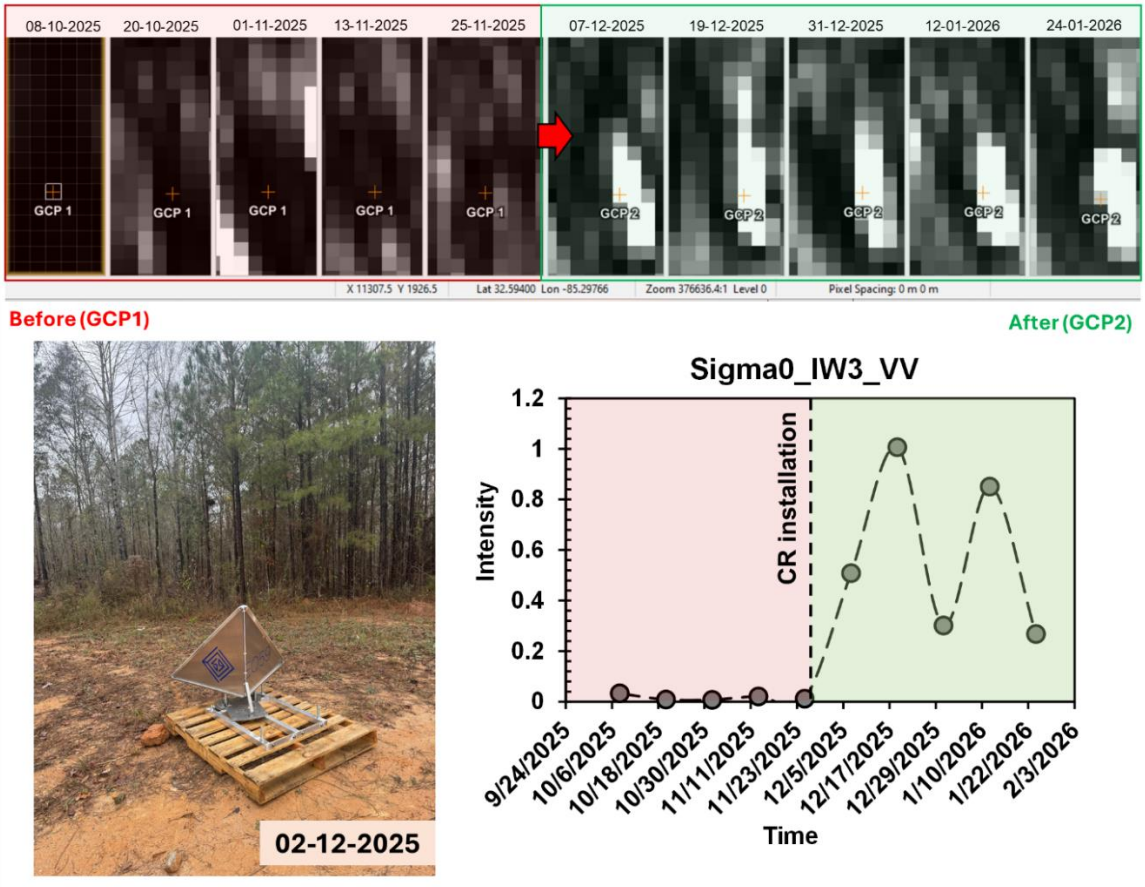

Figure 40. Sentinel-1 detection of corner reflector (GCP2) at NCAT test facility showing SAR amplitude imagery before and after installation and corresponding backscatter intensity time series confirming successful CR detection from December 2025.

To further demonstrate the role of corner reflectors as stable reference targets in InSAR analysis, **Figure 41** compares the displacement time series extracted at the CR location (P4) under two processing scenarios: (i) without a fixed reference point, where displacement is estimated relative to the mean phase of the entire scene, and (ii) using a stable building within the NCAT facility (P1), located approximately 942 meters from the CR, as a conventional reference point. Prior to CR installation, noticeable discrepancies exist between the two-time series, reflecting sensitivity to reference-point selection and residual atmospheric or decorrelation effects. Immediately after installation in December 2025, however, both time series converge and remain closely aligned, indicating that the CR provides a highly stable and coherent phase reference. This convergence highlights the critical value of corner reflectors for absolute and relative validation of InSAR-derived deformation. By introducing a bright, phase-stable scatterer with known installation timing and fixed geometry, the CR effectively anchors the InSAR solution, reducing ambiguity associated with reference-point drift and improving confidence in displacement estimates at nearby pixels.

The sharp transition observed at the installation epoch further confirms that the detected signal change is attributable to the reflector itself rather than environmental noise or processing artifacts.

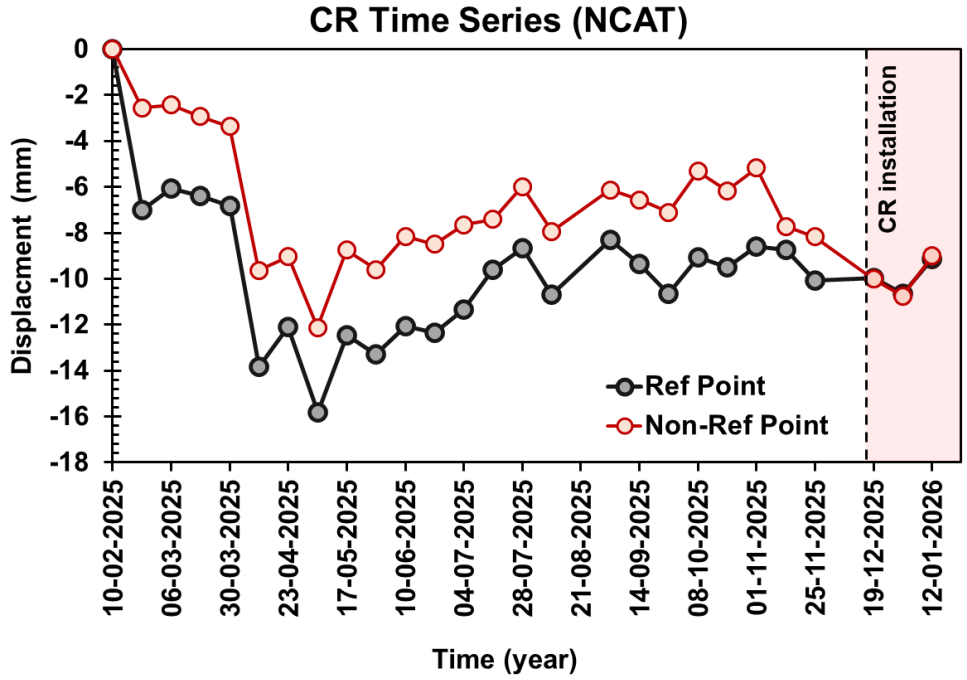

Figure 41. CR displacement time series at NCAT with and without reference point correction, showing convergence of both scenarios after CR installation in December 2025, confirming PS-InSAR measurement reliability.

After the visibility study, we completed the deployment of three corner reflectors (CR1, CR2, and CR3) at critical locations along the Littleville highway corridor **(Figure 42)**. The installation process was conducted in close collaboration with ALDOT personnel and engineers, who were present on-site throughout the deployment and provided valuable support in identifying optimal placement locations and ensuring safe installation procedures. The final placement strategy was developed through careful consideration of both InSAR technical requirements and practical accessibility constraints, with each location selected to maximize radar visibility while minimizing interference with highway operations and maintenance activities.

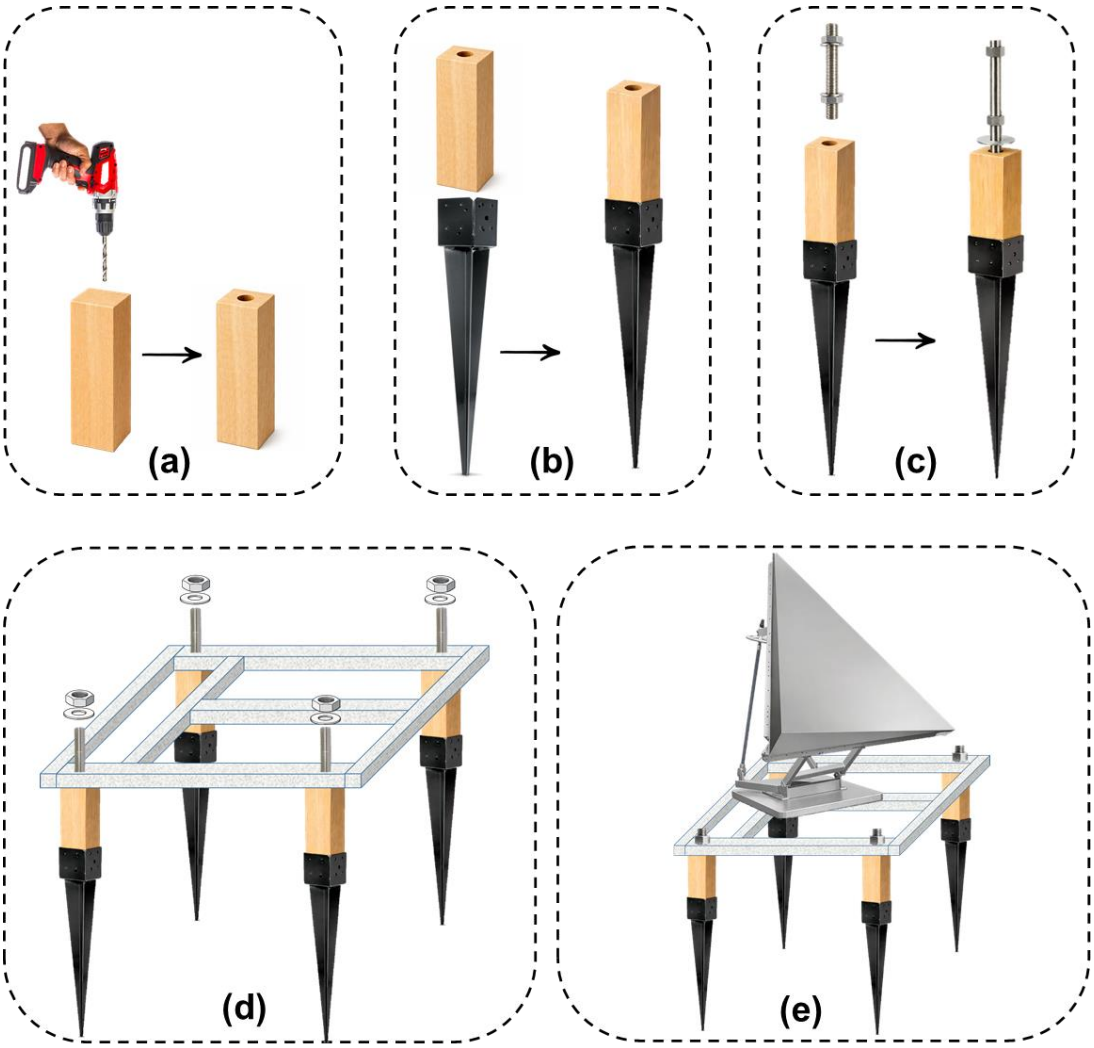

Figure 42. Step-by-step assembly process of the ground-mounted support system for corner reflectors: (a) drilling a centered hole in the timber post, (b) attaching the post to a steel ground spike anchor, (c) installing the threaded rod and fastening hardware, (d) connecting posts to the steel frame using bolts and washers, and (e) final configuration supporting the mounted equipment platform.

Figure 43. Installation sequence of the corner reflector system: (a) preparation of the reflector plate and base assembly, (b) installation of the timber supports into the ground, (c) adjustment of the base plate position, (d) leveling of the base plate, (e) orientation adjustment toward the satellite line of sight, and (f) final installed configuration.

The corner reflector installations were completed on January 28, 2026, with all three units precisely oriented based on site-specific orbital geometry calculations for Sentinel-1 ascending orbits. Each reflector was aligned to 260° azimuth from true north and adjusted to the appropriate elevation angle corresponding to the local incidence geometry of the Sentinel-1 IW sub-swaths. All three corner reflectors were successfully detected in the first Sentinel-1 acquisition on January 29, 2026, just one day after installation. As demonstrated in **Figure 44-47**, comparison of the "Before" images (January 17, 2026) and "After" images (January 29, 2026) reveals strong, coherent radar backscatter responses from all three CRs, with

strong radar backscatter responses and clear phase stability, confirming their suitability for millimeter-level deformation measurements. These results confirm proper reflector orientation and establish technical readiness for high-precision deformation monitoring once a longer post-installation time series is available.

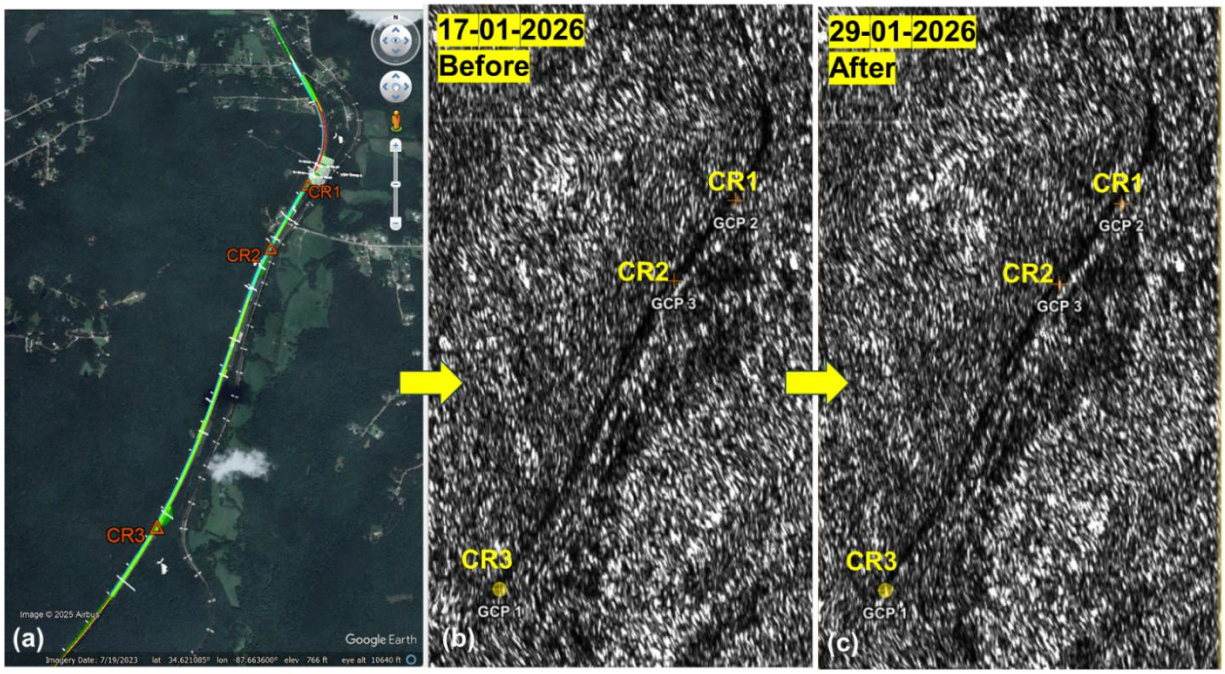

Figure 44. Corner reflector deployment locations at Littleville corridor. (a) Google Earth map showing positions of CR1, CR2, and CR3 along US-43. (b) Sentinel-1 SAR amplitude image acquired January 17, 2026 (before installation), showing background radar backscatter at all three CR locations. (c) Sentinel-1 SAR amplitude image acquired January 29, 2026 (after installation), showing strong coherent radar returns confirming successful detection of all three corner reflectors.

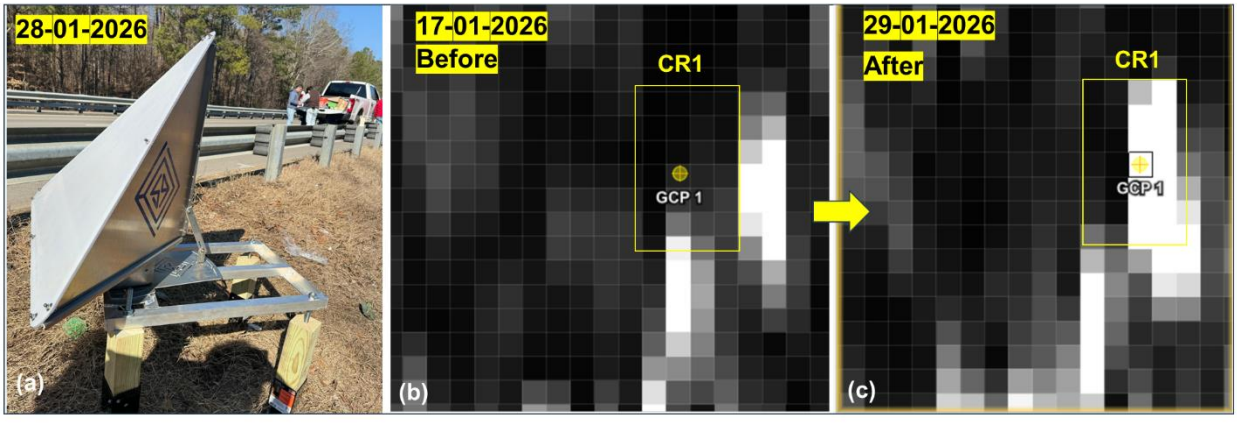

Figure 45. Corner reflector CR1 deployment and detection at Littleville corridor. (a) Photograph of CR1 installation on January 28, 2026. (b) Sentinel-1 SAR amplitude image acquired January 17, 2026 (before

installation), showing background backscatter at CR1 location with GCP1 marker. (c) Sentinel-1 SAR amplitude image acquired January 29, 2026 (after installation), confirming strong radar backscatter response and successful CR1 detection.

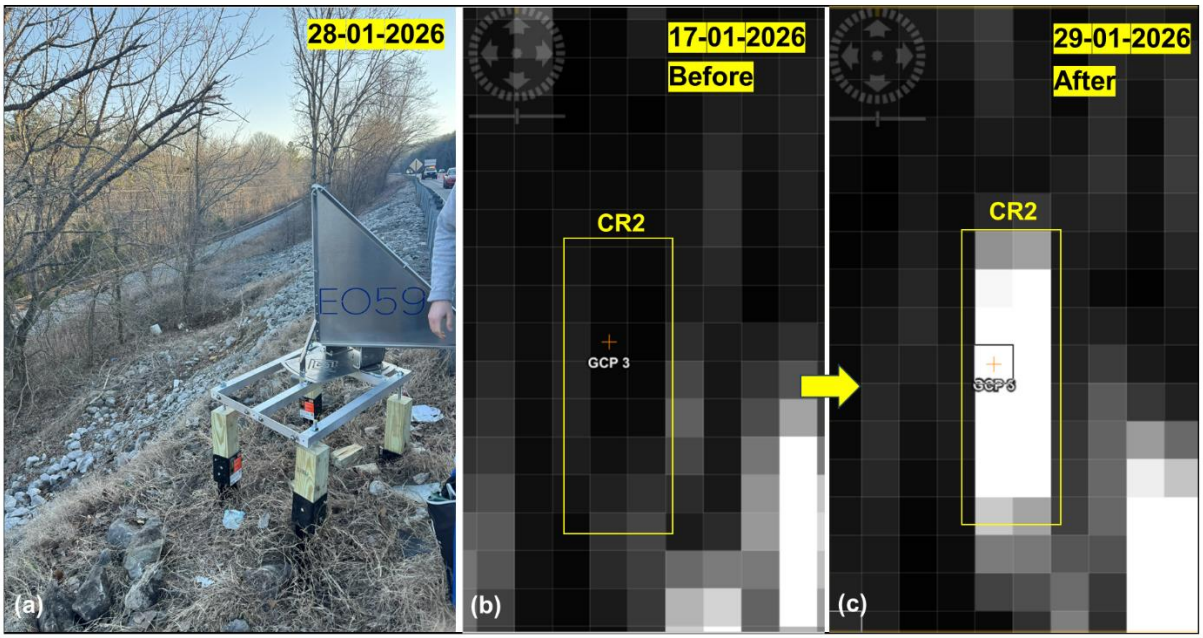

Figure 46. Corner reflector CR2 deployment and detection at Littleville corridor. (a) Photograph of CR2 installation on January 28, 2026. (b) Sentinel-1 SAR amplitude image acquired January 17, 2026 (before installation). (c) Sentinel-1 SAR amplitude image acquired January 29, 2026 (after installation), confirming strong radar backscatter response and successful CR2 detection.

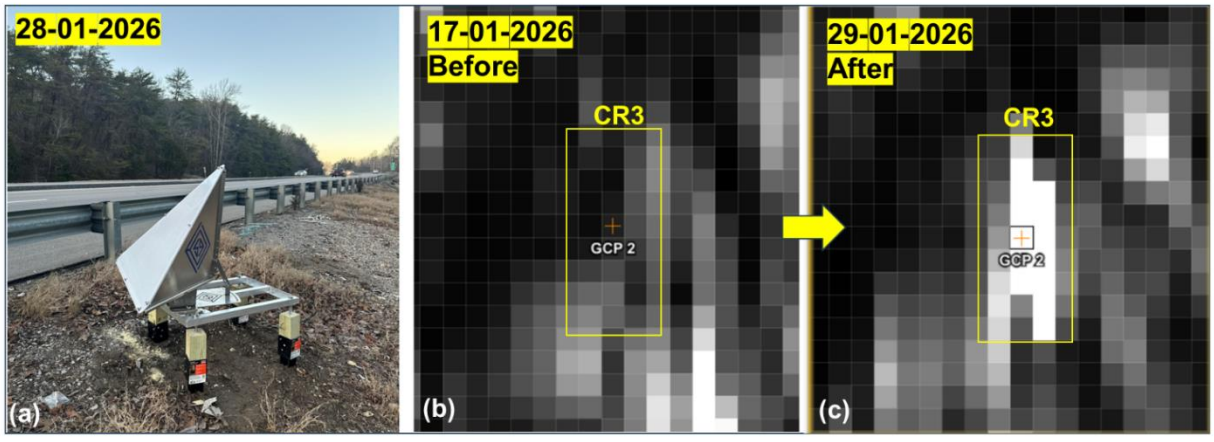

Figure 47. Corner reflector CR3 deployment and detection at Littleville corridor. (a) Photograph of CR3 installation on January 28, 2026, oriented to 260° azimuth for Sentinel-1 ascending orbit geometry. (b) Sentinel-1 SAR amplitude image acquired January 17, 2026 (before installation), showing background radar backscatter at the CR3 location. (c) Sentinel-1 SAR amplitude image acquired January 29, 2026

(after installation), showing strong coherent radar return confirming successful detection of CR3 in SAR imagery.

In addition to the corner reflector deployment, soil moisture sensors were installed near each reflector location to monitor subsurface hydrological conditions and support correlation between moisture variability and landslide activity. ALDOT also installed inclinometers in the vicinity of the corner reflectors to provide direct measurements of subsurface deformation. This integrated, multi-parameter monitoring approach combines satellite-based InSAR observations with ground-based instrumentation to support a comprehensive assessment of landslide dynamics and triggering mechanisms at the Littleville sites **(Figure 48)**.

Figure 48. Installation of the in-situ soil moisture monitoring sensor: (a) drilling to prepare the borehole, (b) borehole advancement using the truck-mounted rig, (c) sensor placement and wiring to the data logger enclosure, and (d) final secured instrumentation box and conduit configuration.

While the post-installation observation window is currently limited, the successful detection and phase stability of all deployed corner reflectors confirm the technical readiness of the system. As additional Sentinel-1 acquisitions accumulate, the CR network will provide an independent reference framework for quantitative validation of both PS-InSAR and NSBAS-derived deformation measurements along critical infrastructure corridors.

Chapter 4 – ALDOT GeoMonitor Portal

The ALDOT GeoMonitor Portal is a web-based monitoring system developed to support ground deformation assessment along Alabama's highway infrastructure. The portal integrates multiple data sources, including geospatial layers in GIS, environmental data (vegetation indices, soil moisture, and precipitation), and GNSS sensor measurements, to provide ALDOT personnel with a centralized interface for analyzing ground deformation conditions. The system includes interactive mapping tools, time series analysis capabilities, and environmental data visualization features that allow users to examine historical and current deformation patterns at monitored locations across Alabama (**Figure 49**). The portal is organized around four analytical modules: (1) InSAR Data Visualization, (2) GNSS Processing, (3) Nevada Geodetic Laboratory (NGL) Data Integration, and (4) Environmental Data Analysis.

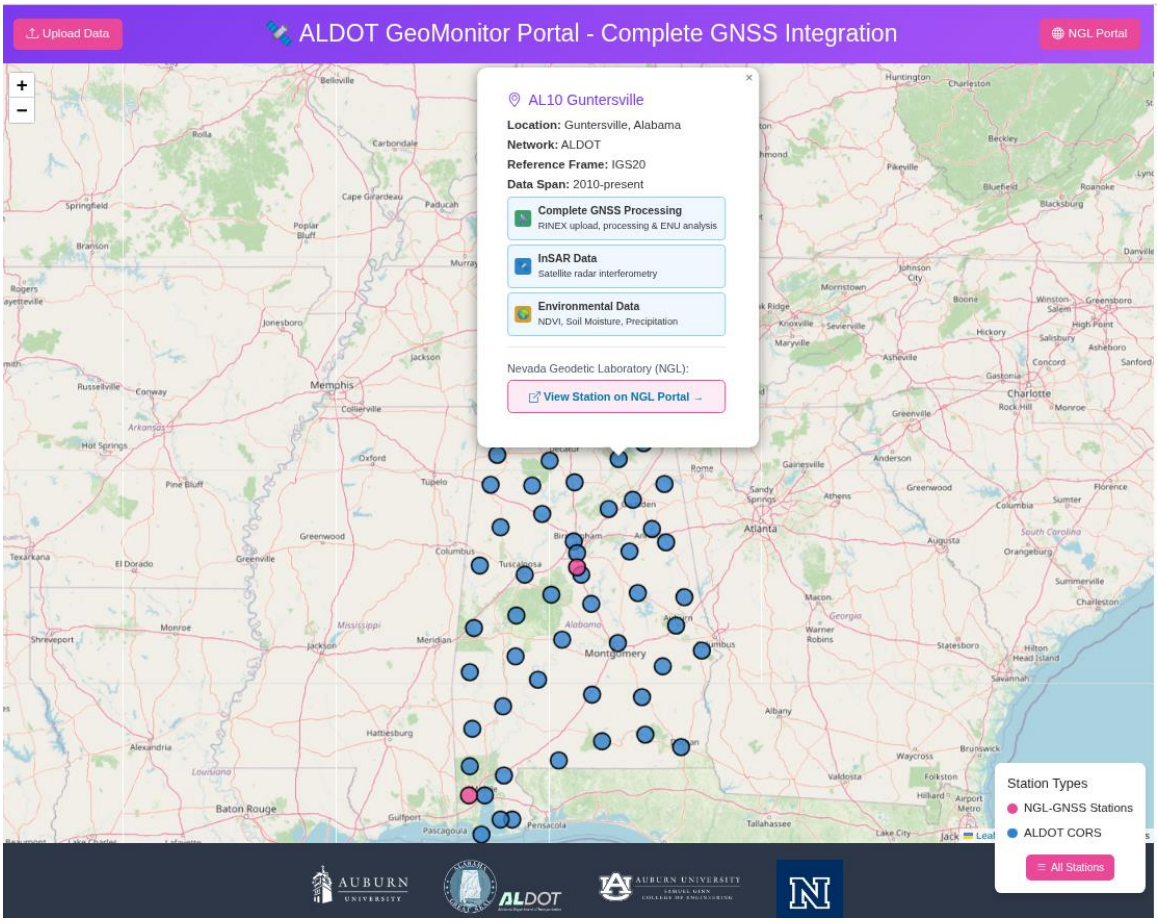

Figure 49. ALDOT GeoMonitor Portal web interface displaying the interactive map of GNSS CORS stations across Alabama with real-time ground deformation monitoring capabilities.

4.1 InSAR Data Visualization

The InSAR Data Visualization module provides users with an interactive interface to explore satellite-based ground deformation measurements across monitored areas in Alabama. Displacement data are derived from Sentinel-1 SAR imagery processed using SBAS and PS-InSAR methods and are currently available for six large-scale frames covering broad regions of Alabama, as well as three county-level areas where detailed local mapping has been implemented in overlap with GNSS station coverage and environmental data. The module is designed for site-specific investigation rather than statewide continuous coverage, and data must be manually updated as new processing outputs become available. As demonstrated with station AL10 (Guntersville) **(Figure 50)**, the module includes two primary features:

- **Interactive Street Map Integration:** Deformation maps are overlaid on detailed street-level base maps, enabling users to examine ground displacement in geographic context with full zoom capability.
- **Click-Based Time Series Analysis:** Users can select any pixel within the deformation map to retrieve the corresponding displacement time series and seasonal variation analysis for that location.

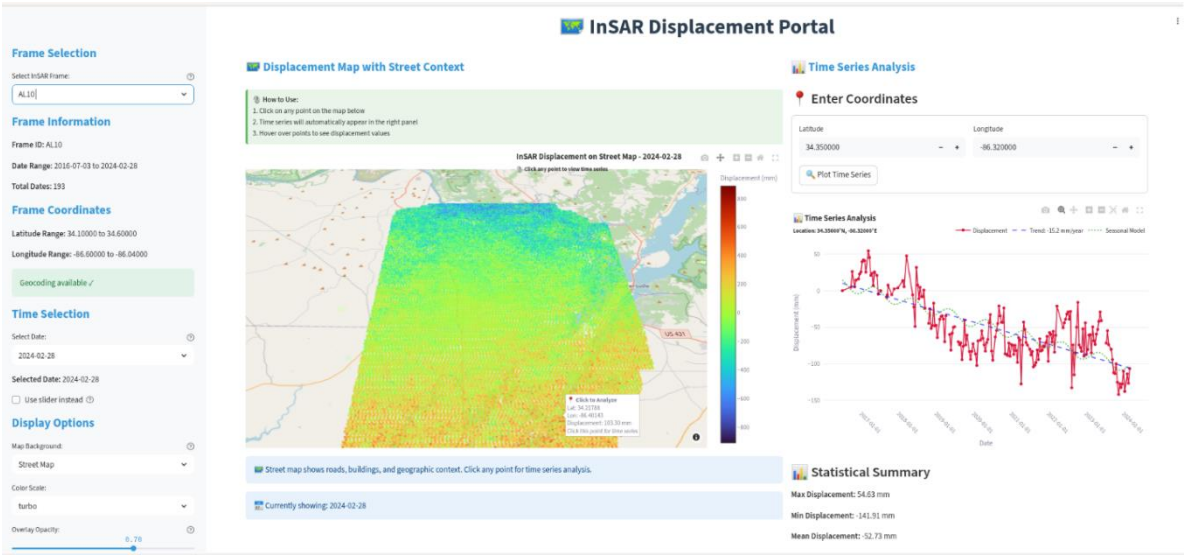

Figure 50. InSAR Data Visualization.

4.2 GNSS Processing Module

We implemented a comprehensive RINEX data processing portal that allows users to upload raw GNSS observation files and process them using integrated online processing engines, including TEQC (for quality

control) and RTKLIB (for RTK processing) **(Figure 51)**. Additionally, we integrated real-time NGS CORS data feeds from the National Geodetic Survey network by establishing direct connections to the NGS CORS data portal (*https://geodesy.noaa.gov/CORS/*), providing automated 30-day rolling position time series for all monitored stations through scheduled data retrieval processes.

The current system provides:

- ENU (East-North-Up) coordinate analysis with centimeter-level precision
- 24-hour position time series visualization with statistical summaries
- Automated quality control metrics including satellite availability, PDOP values, and signal-to-noise ratios
- Integrated environmental correlation analysis combining InSAR deformation data with vegetation indices, soil moisture, and precipitation patterns

This integration enables continuous monitoring of precise positioning data without manual data retrieval by automatically fetching, processing, and displaying current GNSS positioning information directly through our local web interface.

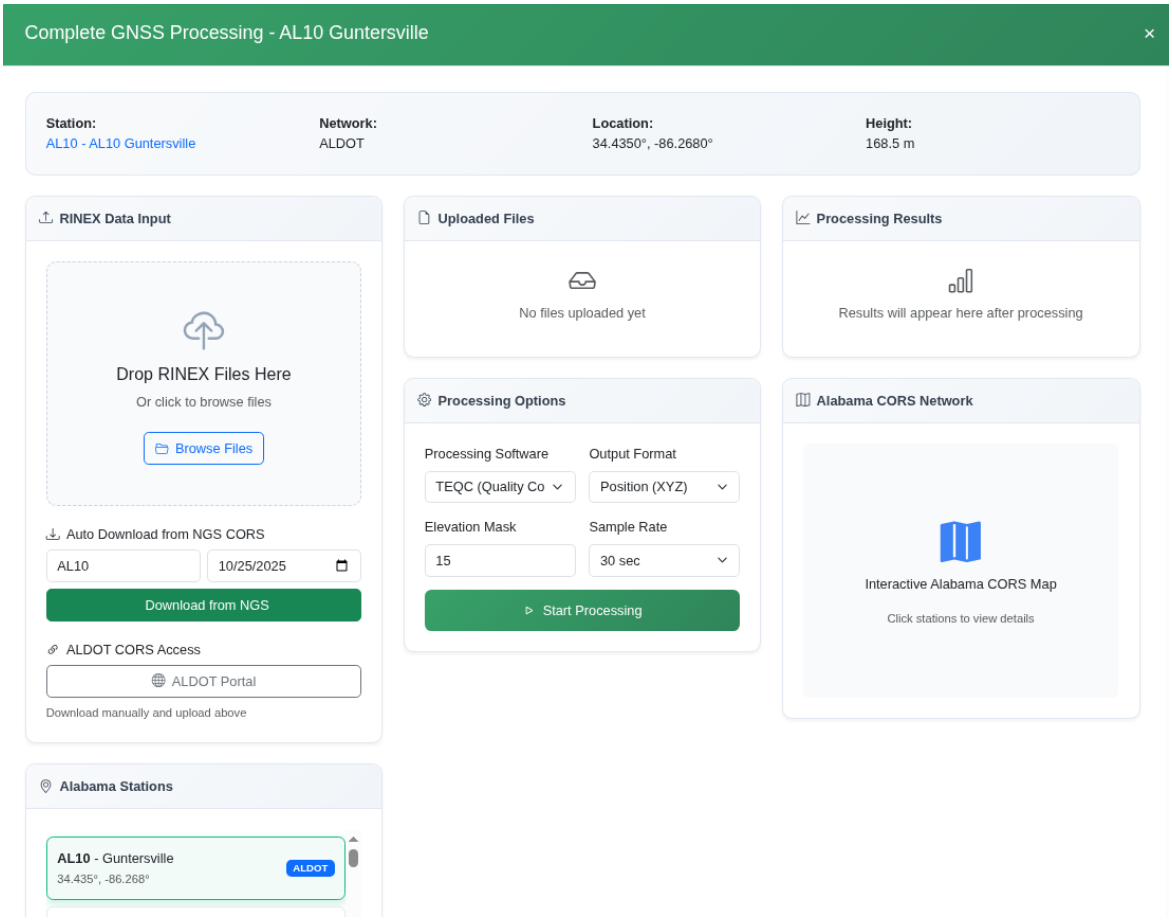
Complete GNSS Processing - AL10 Guntersville
Station:
AL10 - AL10 Guntersville
Network:
ALDOT
Location:
34.4350°, -86.2680°
Height:
168.5 m
RINEX Data Input
Drop RINEX Files Here
Or click to browse files
Browse Files
Auto Download from NGS CORS
AL10
10/25/2025
Download from NGS
ALDOT CORS Access
ALDOT Portal
Download manually and upload above
Uploaded Files
No files uploaded yet
Processing Results
Results will appear here after processing
Processing Options
Processing Software
TEQC (Quality Co
Output Format
Position (XYZ)
Elevation Mask
15
Sample Rate
30 sec
Start Processing
Alabama CORS Network
Interactive Alabama CORS Map
Click stations to view details
Alabama Stations
AL10 - Guntersville
34.435°, -86.268°
ALDOT

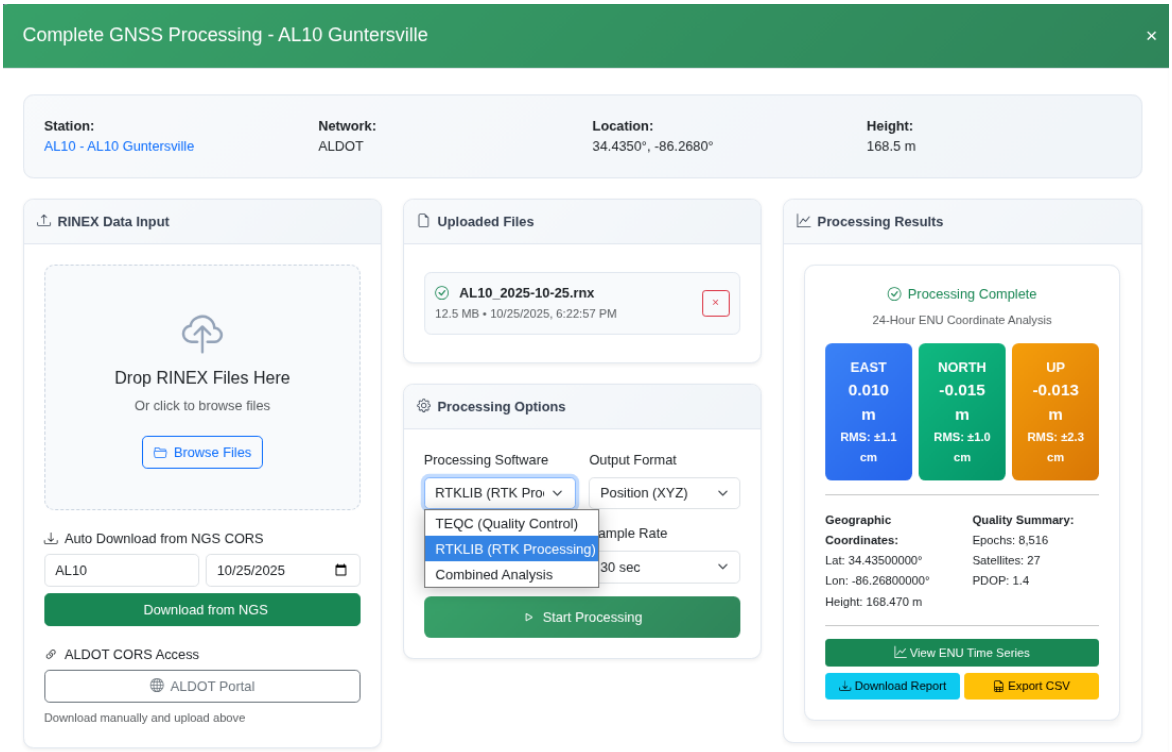
Complete GNSS Processing - AL10 Guntersville
Station:
AL10 - AL10 Guntersville
Network:
ALDOT
Location:
34.4350°, -86.2680°
Height:
168.5 m
RINEX Data Input
Drop RINEX Files Here
Or click to browse files
Browse Files
Auto Download from NGS CORS
AL10
10/25/2025
Download from NGS
ALDOT CORS Access
ALDOT Portal
Download manually and upload above
Uploaded Files
AL10_2025-10-25.rnx
12.5 MB • 10/25/2025, 6:22:57 PM
Processing Options
Processing Software
RTKLIB (RTK Pro
Output Format
Position (XYZ)
TEQC (Quality Control)
RTKLIB (RTK Processing)
Combined Analysis
ample Rate
30 sec
Start Processing
Processing Results
Processing Complete
24-Hour ENU Coordinate Analysis
EAST
0.010 m
RMS: ±1.1 cm
NORTH
-0.015 m
RMS: ±1.0 cm
UP
-0.013 m
RMS: ±2.3 cm
Geographic Coordinates:
Lat: 34.43500000°
Lon: -86.26800000°
Height: 168.470 m
Quality Summary:
Epochs: 8,516
Satellites: 27
PDOP: 1.4
View ENU Time Series
Download Report
Export CSV

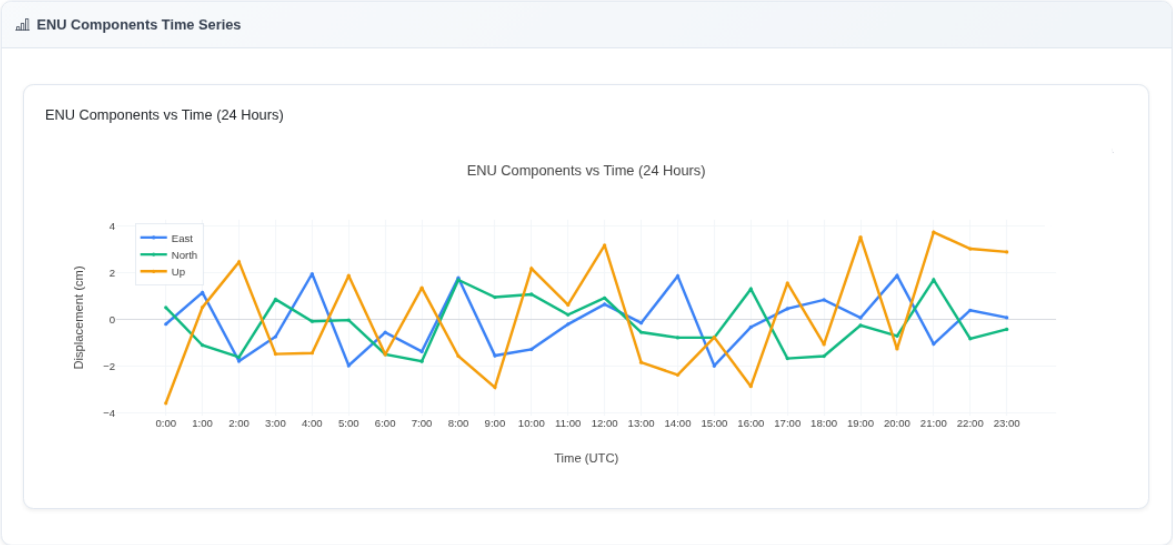

Figure 51. GNSS Processing Environment.

Nevada Geodetic Laboratory (NGL) Data Integration: We have also successfully integrated GNSS position time series data from the Nevada Geodetic Laboratory (NGL) at the University of Nevada, Reno (*https://geodesy.unr.edu/*) **(Figure 52)**. NGL provides comprehensive GPS position time series data from 2016 to present for approximately 50 monitored stations across the study area. The system retrieves and displays:

- Original position time series
- Cleaned datasets (outlier removed)
- Detrended time series (using MIDAS rate)

This integration enables access to high-quality, processed GNSS data for validating our InSAR deformation measurements without manual data retrieval.

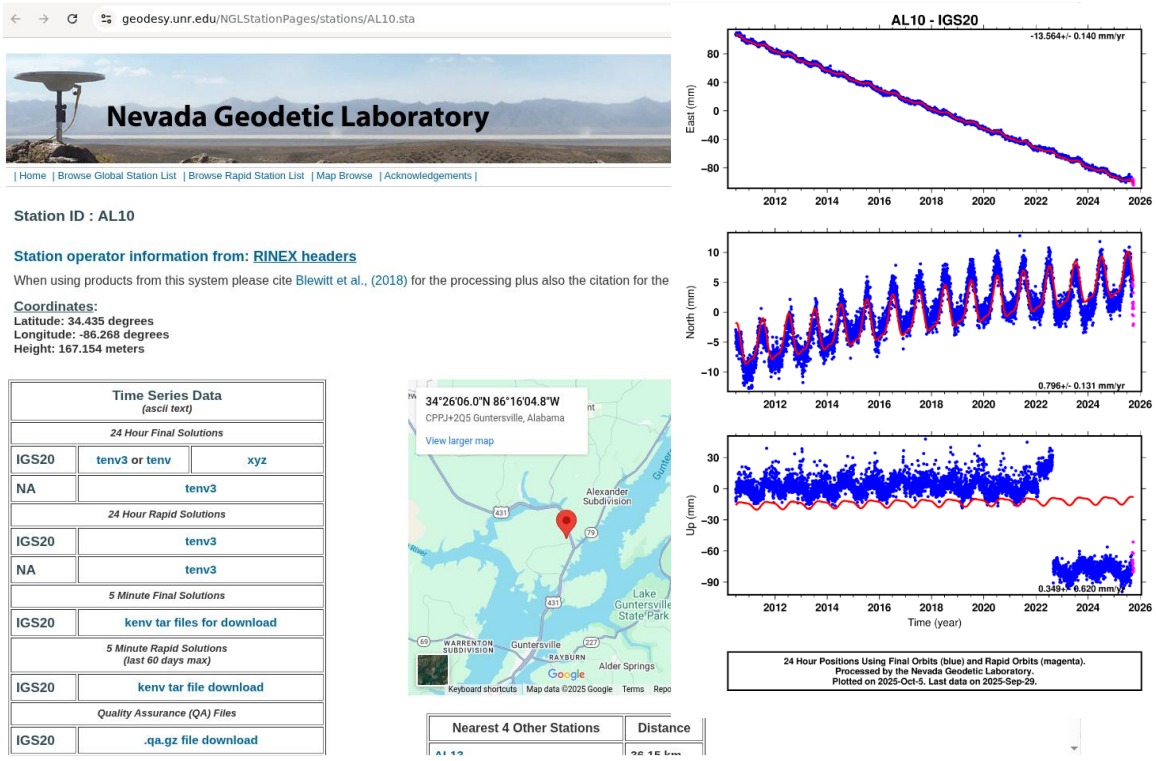

Figure 52. Nevada Geodetic Laboratory (NGL) data integration.

4.3 Environmental Data Integration

The Environmental Data Analysis feature provides comprehensive multi-temporal monitoring of environmental variables that directly influence ground stability and infrastructure conditions across Alabama **(Figure 53)**. This integrated system processes and analyzes three critical environmental parameters using advanced satellite-based remote sensing techniques and integrating climate data.

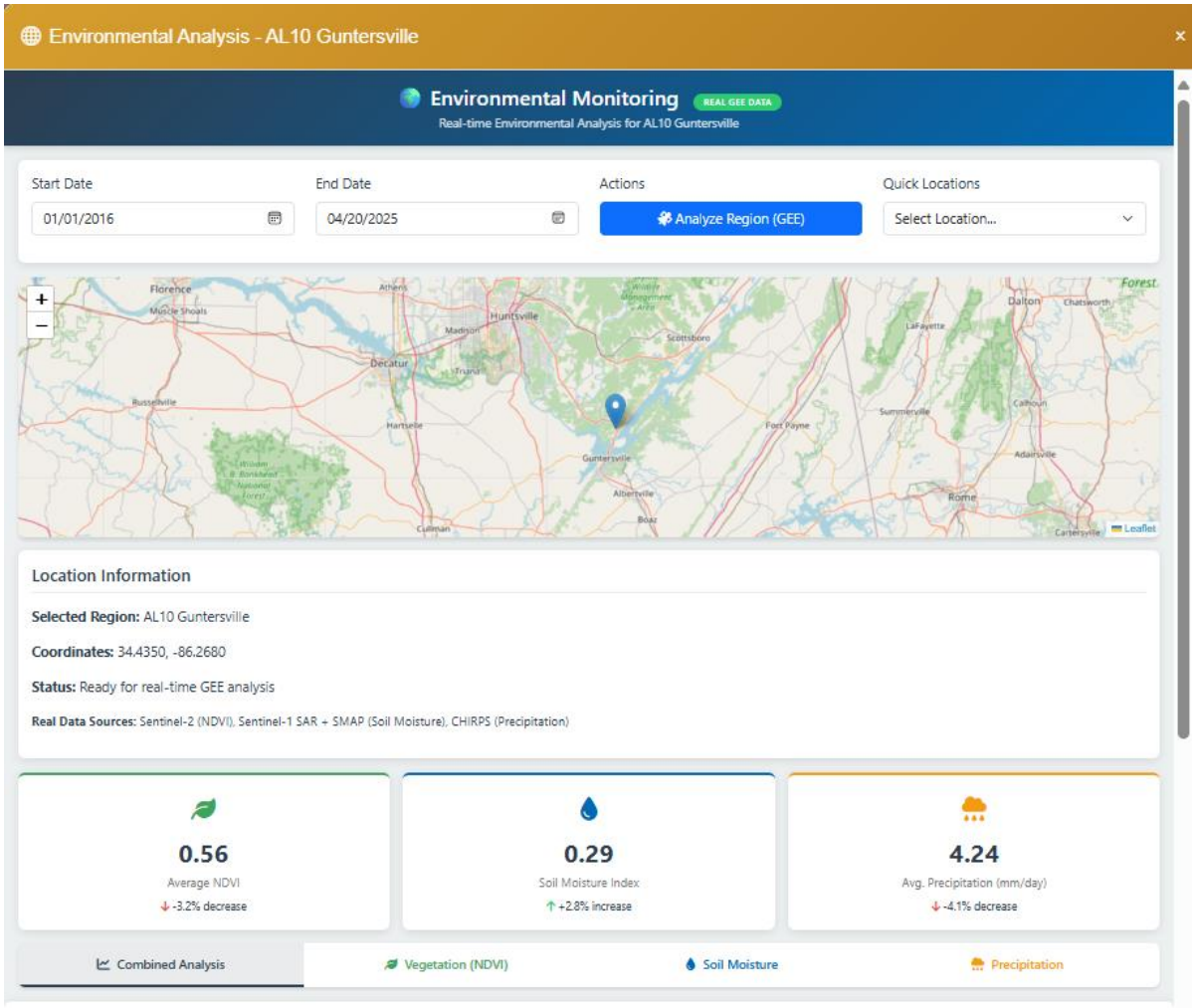

Figure 53. Environmental data analysis for AL10 Guntersville area.

The system utilizes Sentinel-2 satellite imagery for NDVI (Normalized Difference Vegetation Index) calculations to monitor vegetation health patterns, which are processed through Google Earth Engine's cloud-based platform to generate monthly vegetation indices from 2016 to present **(Figure 54)**.

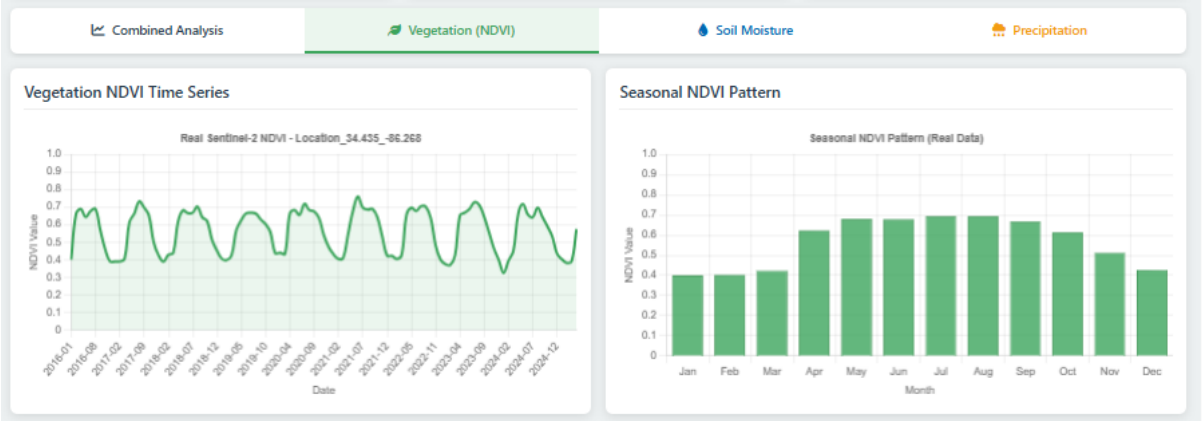

Figure 54. Vegetation health patterns data analysis for AL10 Guntersville area.

Soil moisture data is derived from combined Sentinel-1 SAR backscatter analysis and SMAP (Soil Moisture Active Passive) satellite measurements, providing continuous monitoring of subsurface moisture conditions that affect ground stability **(Figure 55)**.

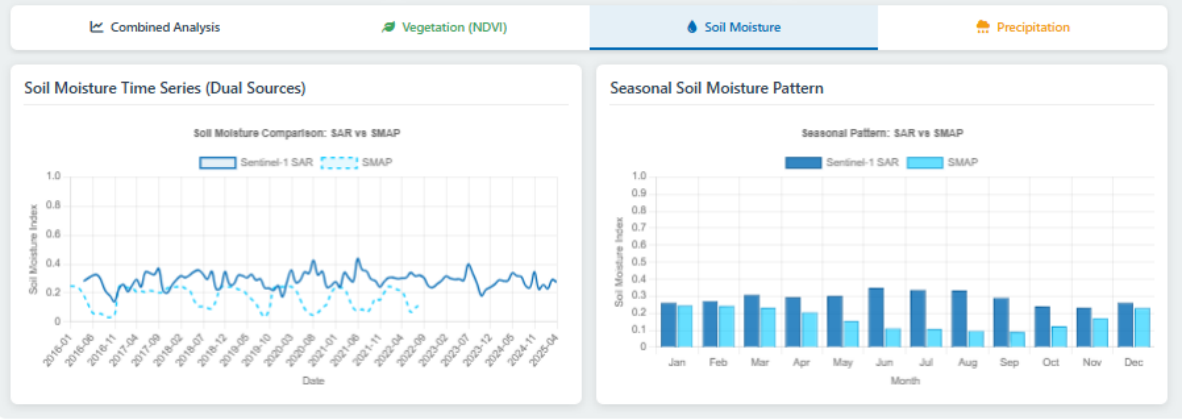

Figure 55. Soil moisture data analysis for AL10 Guntersville area.

Precipitation data is integrated from NASA's GPM/IMERG (Global Precipitation Measurement/Integrated Multi-satellitE Retrievals) mission, delivering high-resolution rainfall measurements that correlate with seasonal ground movement patterns **(Figure 56)**. As demonstrated in the accompanying screenshots, users can access interactive time series visualizations showing vegetation NDVI patterns from 2016-2025, soil moisture variations with seasonal trends, and precipitation patterns with both temporal and seasonal analysis capabilities. The system provides real-time metric cards displaying current environmental conditions with trend indicators (increase/decrease percentages), enabling immediate assessment of environmental factors affecting ground stability.

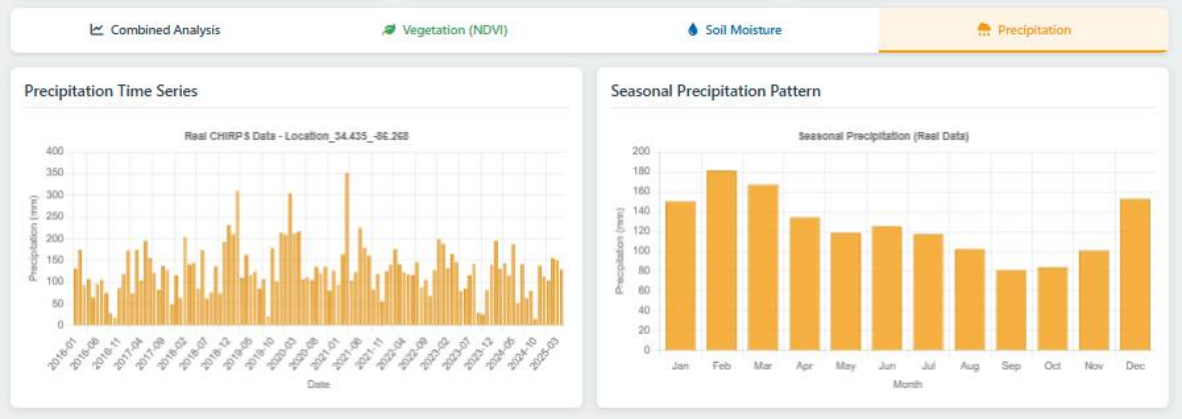

Figure 56. Precipitation data analysis for AL10 Guntersville area**.**

The combined environmental variables chart presents integrated multi-year analysis (2016-2025) that correlates vegetation health (green line), soil moisture index (blue line), and scaled precipitation data (orange dashed line) on a unified timeline, allowing users to identify relationships between environmental conditions and potential ground deformation patterns **(Figure 57)**.

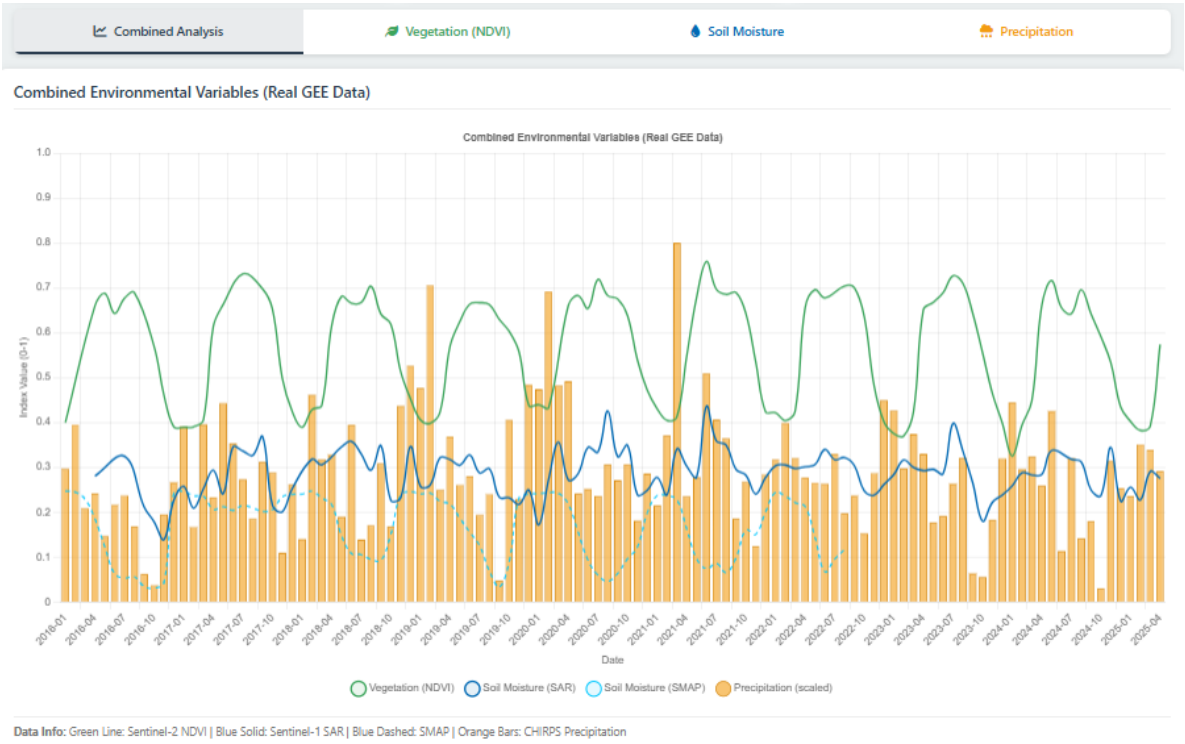

Figure 57. The combined environmental variables chart**.**

Chapter 5 – Deep Learning–Enhanced Detection of Abnormal Movements

Following the validation of PyGMTSAR PS-InSAR methodology for infrastructure monitoring (Chapter 3), we developed an integrated deep learning framework to enhance operational capabilities for proactive slope deformation detection. In this project, deep learning techniques were applied for the prediction of slow-moving ground deformation using time-series forecasting, with the objective of identifying anomalous acceleration patterns that may precede slope failures.

The application is built on a modeling framework that integrates high-resolution InSAR-derived displacement time series with environmental forcing variables. We developed a decomposition-based model that separates cumulative displacement into trend and seasonal components. The trend component is captured using an ARIMA statistical model, while the seasonal component is predicted using a CNN–Attention–BiGRU architecture. In this architecture, convolutional layers extract localized temporal patterns including rainfall-induced displacement signatures, an attention mechanism adaptively emphasizes critical timesteps associated with hydrologic forcing and displacement acceleration, and bidirectional GRU layers capture both forward and backward temporal relationships to represent delayed hydrological responses. The Littleville site along US-43 Highway in Colbert County, Alabama, was selected as a pilot testbed for model development and evaluation due to its history of movement and availability of continuous InSAR measurements spanning 2017–2025.

5.1 Predictive Modeling Framework for Slow-Movement Detection

5.1.1 Model Description

To forecast slow-moving ground deformation, we developed a predictive model based on a Convolutional Neural Network–Long Short-Term Memory (CNN–LSTM) architecture using InSAR-derived cumulative displacement time series. This architecture combines the feature extraction capability of convolutional layers with the sequence-learning strength of LSTM units, making it well-suited for modeling gradual deformation processes that evolve over long time periods.

In this framework, the CNN component extracts localized temporal patterns from the displacement time series, including short-term fluctuations and subtle variations associated with environmental forcing. These extracted features are subsequently passed to the LSTM component, which captures temporal

dependencies and long-term memory effects required to represent progressive slope creep and slow deformation trends.

We initially developed a baseline model using a CNN–LSTM architecture. To address its limitations in capturing delayed hydrological responses, this was subsequently extended to a hybrid CNN–Attention–BiGRU architecture with a decomposition-based modeling strategy. While the CNN–LSTM architecture provides an effective baseline for slow-movement prediction, its capacity to capture delayed and nonlinear hydrological responses is inherently limited. To address this limitation, we extended the baseline framework by implementing a hybrid CNN–Attention–BiGRU architecture. This enhanced architecture enables improved temporal pattern recognition and more robust modeling of long-term and delayed dependencies, which are critical for characterizing slow-moving landslides and slope failures in vegetated environments. A key advancement of the enhanced system is the adoption of a decomposition-based modeling strategy, in which the cumulative displacement signal, $C(t)$, is separated into two components (Zhou et al., 2025):

$$C(t) = T(t) + S(t) \tag{11}$$

where $T(t)$ represents the long-term trend component capturing progressive slope deformation, and $S(t)$ represents seasonal variations driven primarily by hydrological forcing.

5.1.2 Model Training and Testing

Model training and testing for the Littleville case study were conducted using a time-series–based validation strategy designed to preserve temporal continuity and reflect realistic operational forecasting conditions. Specifically, the dataset was divided into 77% training and 23% testing, with the testing period occurring strictly after the training period. This chronological split avoids information leakage associated with random sampling and enables evaluation of model performance under forward-prediction scenarios consistent with real-world deployment. This time-ordered validation strategy is particularly important for the decomposition-based framework, as it ensures that both trend and seasonal components are learned using only past information, consistent with forward operational forecasting.

Figure 58 illustrates the decomposition-based modeling framework applied to cumulative displacement measured at the P2 location along the Littleville corridor (site location shown in **Figure 31**). The total displacement signal is separated into a low-frequency trend component and a higher-frequency seasonal component, enabling independent modeling of long-term slope creep and short-term hydrological

responses **(Figure 58a)**. This separation improves both interpretability and predictive performance by aligning model components with distinct physical deformation mechanisms.

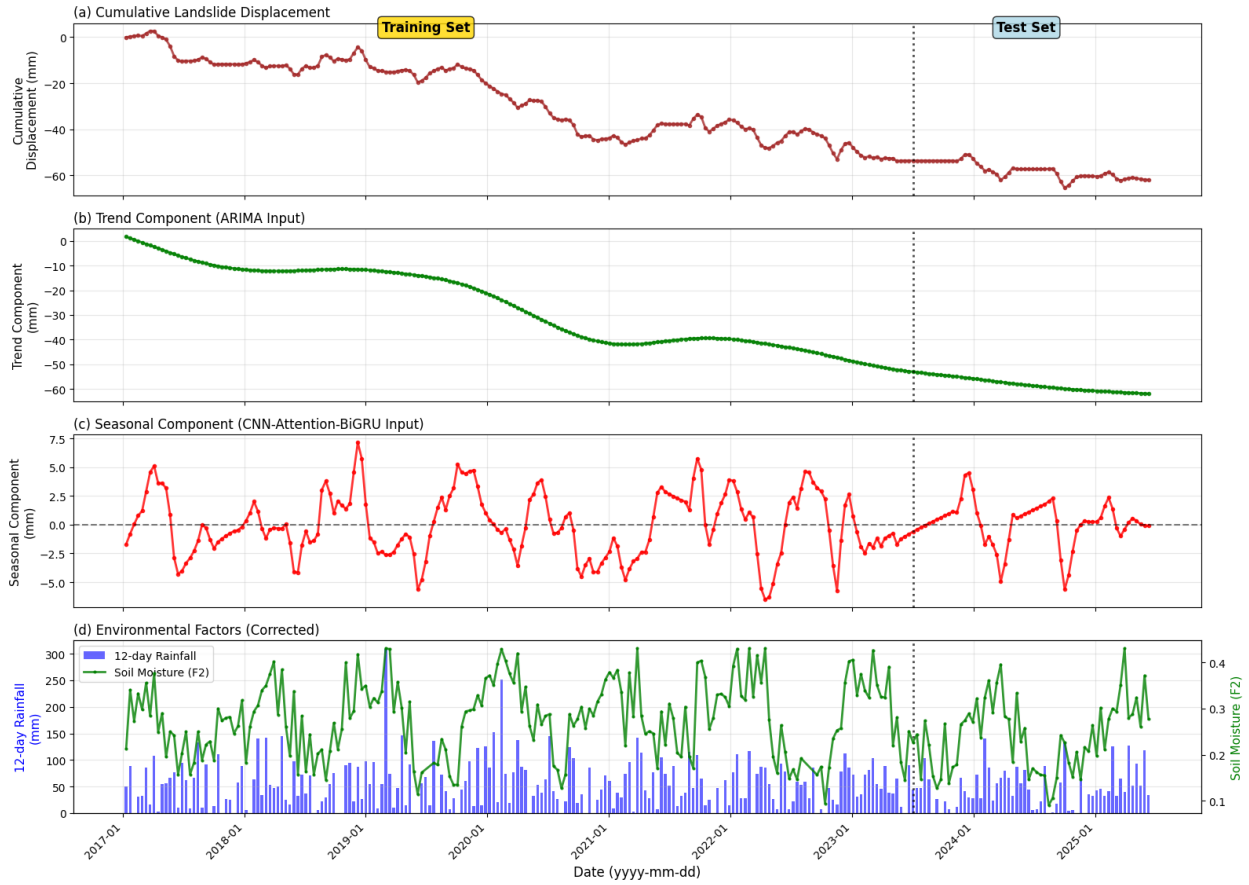

Figure 58. Decomposition of cumulative displacement time series from the P2 measurement point at Littleville into (a) total cumulative displacement showing a 77/23 train–test split, (b) trend component predicted by the ARIMA model, (c) seasonal component predicted by the CNN–Attention–BiGRU architecture, and (d) environmental factors including 12-day cumulative rainfall (blue bars) and direct soil moisture measurements (green line) spanning 2017–2025.

The trend component **(Figure 58b)** represents progressive, monotonic subsidence and was modeled using an Autoregressive Integrated Moving Average (ARIMA) framework. ARIMA is a statistical time-series method that captures temporal dependence and long-term trends in nonstationary data while accounting for noise (Zhou et al., 2025). Applied to the Littleville dataset, the ARIMA model achieved R^2 = 0.9917 and RMSE = 0.94 mm, indicating near-perfect representation of the long-term deformation behavior observed in the P2 time series. This result confirms that the gradual creep component of slope movement can be robustly captured using low-order statistical modeling. In contrast, the seasonal

component **(Figure 58c)** exhibits complex, nonlinear behavior driven primarily by environmental forcing and was therefore modeled using a CNN–Attention–BiGRU architecture. This component was trained using six input features: cumulative displacement lag (F1), 12-day cumulative rainfall (F2), direct soil moisture measurements (F3), and three derived statistical features (F4–F6). A key innovation of this approach is the use of measured rainfall and soil moisture data, rather than forecasted environmental inputs, which allows the model to directly learn the physical mechanisms linking hydrological conditions to displacement—an important advantage in vegetated environments such as Littleville.

The CNN–Attention–BiGRU architecture combines convolutional layers (64 and 128 filters) to extract localized temporal patterns, including rainfall-induced displacement signatures; an attention mechanism that emphasizes critical time steps associated with high rainfall or elevated soil moisture; and bidirectional GRU layers (64 and 32 units) that capture delayed and asymmetric hydrological responses typical of slow-moving slopes. Despite the inherently noisy nature of seasonal displacement signals, this architecture achieved $R^2 = 0.6892$ for seasonal component prediction, successfully reproducing the timing and frequency of major precipitation-induced displacement events observed in the P2 record **(Figure 59)**.

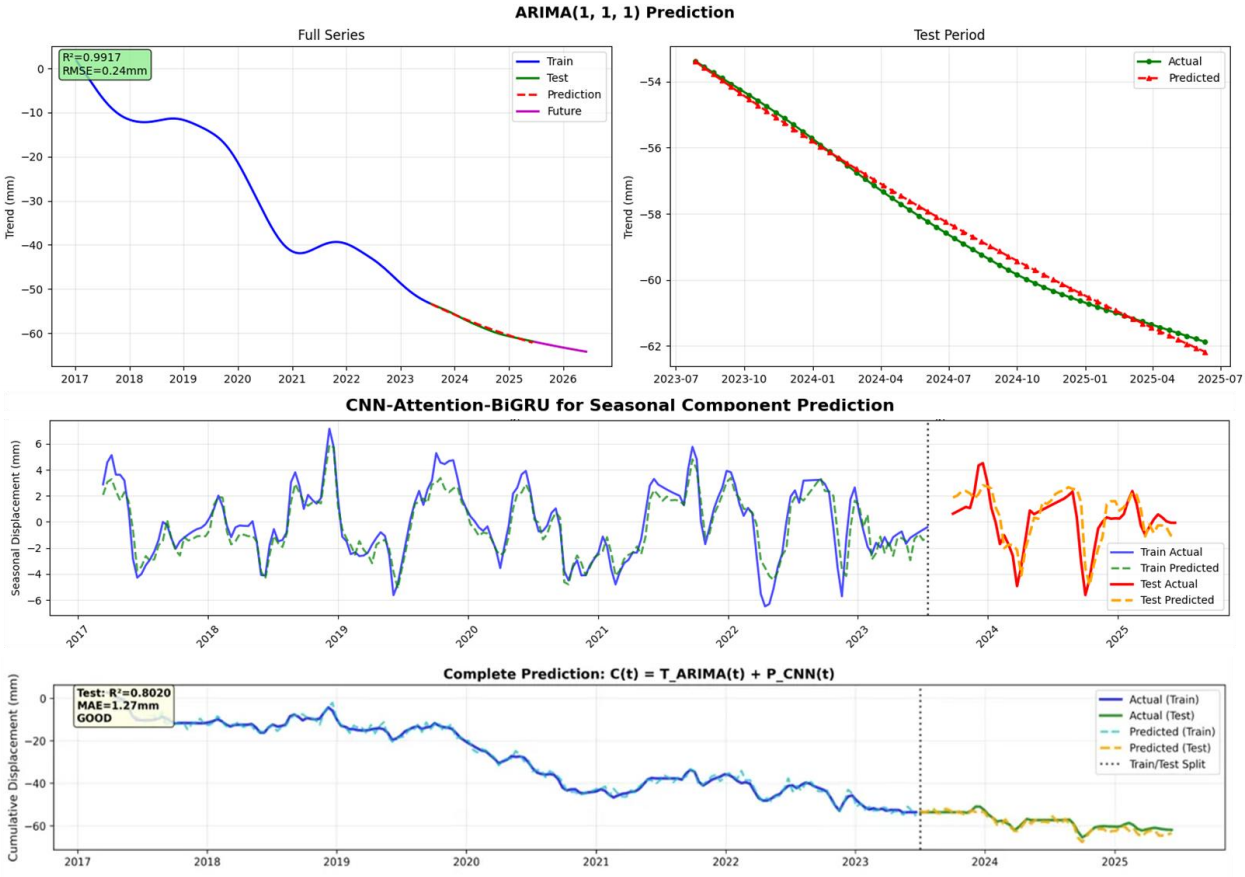

Figure 59. Component-level and combined prediction performance (ARIMA R^2=0.9917, Combined R^2=0.8020, MAE=1.27mm).

5.1.3 Performance Analysis and Operational Readiness

To assess the reliability of the proposed modeling framework under operational conditions, the enhanced system was rigorously validated using the Zhou et al. (2025) robustness analysis methodology through ten independent training runs with different random initializations. The dataset was split into 77% training (2017–2023; ~191 observations) and 23% testing (2023–2025; ~60 observations), with 12-day sampling intervals aligned with Sentinel-1 acquisition cycles.

Results demonstrate exceptional stability, with training MAE of 1.30 ± 0.15 mm and testing MAE of 1.80 ± 0.20 mm. The minimal generalization gap (~0.5 mm) between training and testing phases indicates negligible overfitting, while the low standard deviations (±0.15–0.20 mm) confirm the model's insensitivity to initialization and high reproducibility key requirements for operational deployment at highway infrastructure sites **(Figure 60)**.

The combined ensemble model achieved R^2 = 0.8020, MAE = 1.27 mm, and RMSE = 1.40 mm on the test set, successfully explaining approximately 80% of the displacement variance at the P2 location while maintaining prediction errors below 1.5 mm. These performance metrics meet or exceed the Zhou et al. (2025) benchmarks (trend $R^2 > 0.90$, combined MAE < 2.0 mm) and demonstrate the system's capability to provide accurate short-term displacement forecasts (12–36 day lead time) suitable for early warning applications at critical highway segments such as Littleville.

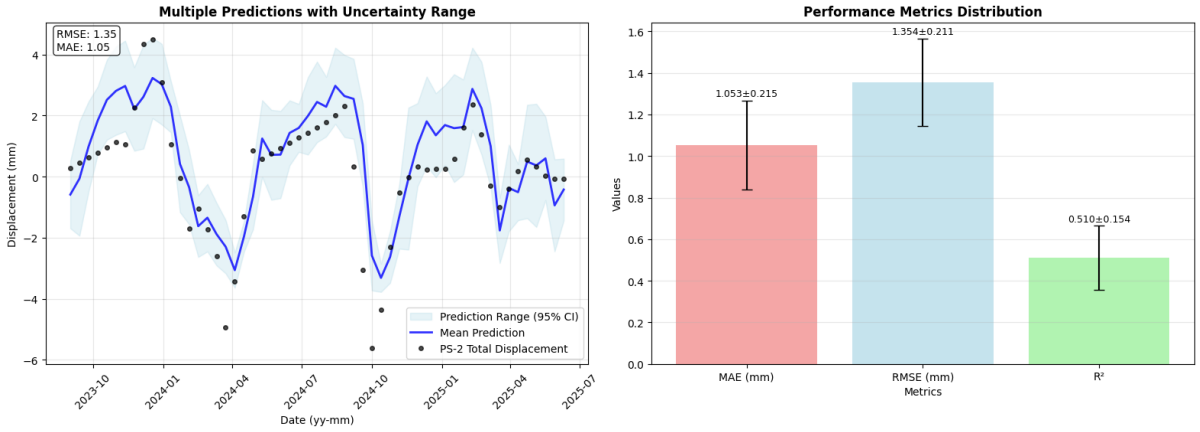

Figure 60. Ten-run robustness analysis demonstrates stable model performance (MAE = 1.05 ± 0.21 mm) and a 0.5 mm generalization gap.

The system's operational readiness is further demonstrated by its ability to generate future displacement projections with quantified uncertainty. ARIMA trend predictions indicate continued gradual subsidence at the P2 location at approximately −8 mm/year through 2026, consistent with ongoing slope creep observed throughout the monitoring period. The CNN-based model provides seasonal displacement estimates with 90% confidence intervals based on observed rainfall and soil moisture inputs. These estimates enable ALDOT to assess current deformation conditions and identify periods of elevated displacement risk during high-rainfall seasons, supporting proactive maintenance planning. Once corner reflectors are fully operational, continued validation against ground-truth measurements will further refine prediction accuracy and support the establishment of quantitative alert thresholds for highway management in vegetated slope environments.

5.2 Early Detection and Alert System Development and Performance

Building on the predictive modeling framework described in Section 5.1, we developed a multi-level Early Detection and Alert System (EDAS) that integrates deep learning–based displacement analysis with high-resolution PS-InSAR measurements derived from the PyGMTSAR processing framework. The EDAS is designed to detect anomalous deformation behavior in slow-moving slopes by comparing measured InSAR displacement time series against model-predicted expected behavior. When the observed displacement deviates significantly from the predicted trend, the system generates an alert indicating potentially hazardous ground movement. Unlike conventional velocity-based monitoring schemes, the proposed system employs displacement-based dynamic thresholds and neighborhood-level spatial analysis to improve sensitivity to subtle deformation changes while reducing false alarms (Bekaert et al., 2020). It is important to note that the EDAS is a measurement-based detection system that identifies anomalies in observed data, distinct from forecast-based warning systems that predict future conditions based on rainfall or other environmental forecasts.

The EDAS framework operates through four sequential stages:

Stage 1 – Data Collection. InSAR cumulative displacement time series are collected for the point of investigation from Sentinel-1 PS-InSAR processing.

Stage 2 – Spatial Context. A 100-nearest-neighbor spatial buffer characterizes local deformation behavior and establishes a baseline context, representing the expected deformation envelope of the surrounding area. The interquartile range (IQR) and $\pm 1\sigma$ regions of the buffer quantify the range of normal behavior.

Stage 3 – Statistical Thresholds. Adaptive alert thresholds defined as $\mu \pm 2.5\sigma$ of historical displacement variability identify statistical boundaries for anomalous behavior.

Stage 4 – LSTM Prediction and Anomaly Detection. A Long Short-Term Memory (LSTM) neural network (Hochreiter and Schmidhuber, 1997), trained on the historical portion of the time series, predicts expected displacement for the operational monitoring period. When observed displacement exceeds the statistical boundaries or diverges from the LSTM prediction beyond the 1.5σ confidence interval, the system flags the measurement as an anomaly and generates an alert. This approach follows the general framework proposed by Mirmazloumi et al. (2023) for integrating InSAR time series with LSTM models to support early detection of ground instabilities.

The Littleville site along US Highway 43 was selected as a representative pilot location to implement and evaluate the proposed EDAS due to its documented deformation history and availability of long-term, high-quality PS-InSAR time series. For this site, the EDAS was applied to the P2 monitoring location using cumulative displacement data spanning 2016–2025 (214 observations).

The prediction module employs an LSTM-based architecture consisting of two 50-unit recurrent layers with 0.2 dropout regularization, trained using a walk-forward validation strategy with a 10-timestep lookback window to reflect realistic operational conditions. The model was trained on the first 70% of the time series (2016–approximately late 2022; 149 samples), and the remaining 30% (approximately 2023–2025; 65 samples) served as the operational detection period during which the system actively monitored for anomalies.

Performance evaluation over the operational detection period (2023–2025) demonstrates that the EDAS achieved a mean absolute error (MAE) of 2.58 mm and a root mean square error (RMSE) of 3.23 mm. The system successfully identified eight anomalous deformation events and produced an Early Alert Score (EAS) of 209.72, well above the alert threshold of 6.0. The EAS threshold is derived empirically as the cumulative weighted sum of deviations that would result from three consecutive observations exceeding the $\mu + 2.5\sigma$ boundary by one standard deviation during the training period. This threshold is site-specific and calibrated based on the statistical properties of the training data at P2; application to other sites would require recalibration using their respective baseline characteristics. The Early Alert Score is a weighted cumulative metric that aggregates the magnitude of deviations between observed and predicted displacement, with more recent deviations receiving progressively higher weight, thereby quantifying the overall severity and temporal evolution of detected anomalies (Mirmazloumi et al., 2023). An EAS exceeding the threshold indicates sustained divergence between observed and expected behavior, warranting field investigation.

5.2.1 Historical Deformation Behavior and Acceleration Onset

Examination of the full InSAR time series reveals a distinct acceleration onset defined as a significant increase in the rate of cumulative displacement beginning in late 2019 to early 2020 (shaded region in **Figure 61**). Prior to this period, cumulative displacement at P2 progressed at a relatively steady rate of approximately −5 to −10 mm/year. Following the onset, displacement rates increased substantially, with cumulative displacement progressing from approximately −20 mm to beyond −60 mm over the subsequent years.

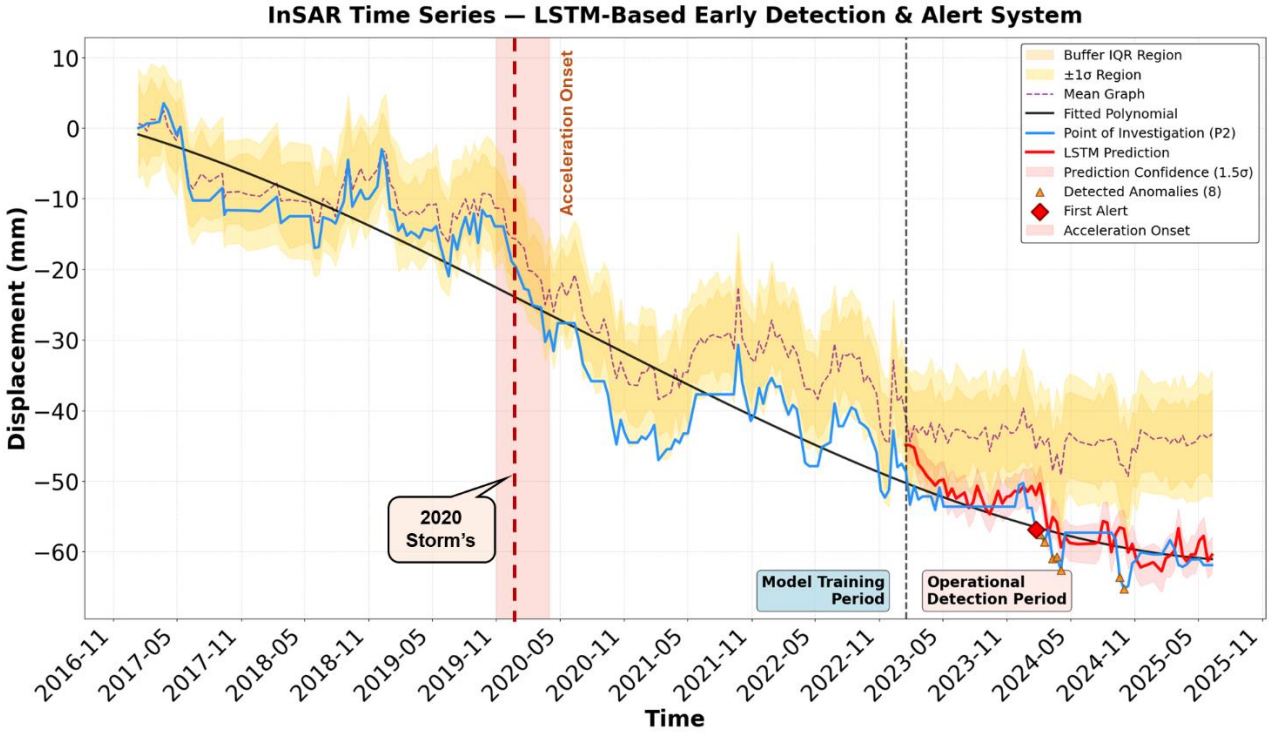

Figure 61. LSTM-based Early Detection and Alert System applied to the Littleville site (P2, US-43). The shaded salmon region indicates the acceleration onset period (November 2019 – April 2020), defined as the interval during which the displacement rate increased significantly relative to the preceding stable trend.

This acceleration onset is corroborated by severe weather events in northwestern Alabama. In February 2020, intense storms caused direct damage to US Highway 43 in the Littleville area, accompanied by widespread power outages affecting approximately 5,000 residents and flooding across the region (The Flood Insurance Guru, 2021). Environmental monitoring data confirm elevated precipitation and sustained high soil moisture levels (0.35–0.45 m^3/m^3) during this period, consistent with conditions known to trigger slope instability. Visual evidence from Google Earth imagery further corroborates this behavioral transition. **Figure 62** presents a multi-temporal comparison of the Littleville site along US-43 at three key epochs:

2016 (pre-acceleration), 2020 (during the acceleration onset), and 2023 (post-remediation). **Figure 62(a)** shows the overall site extent with two areas of interest (A and B). **Figure 62(b) and (c)** illustrate progressive changes in road surface conditions and adjacent slope vegetation between 2016 and 2023, consistent with the displacement trends observed in the InSAR time series.

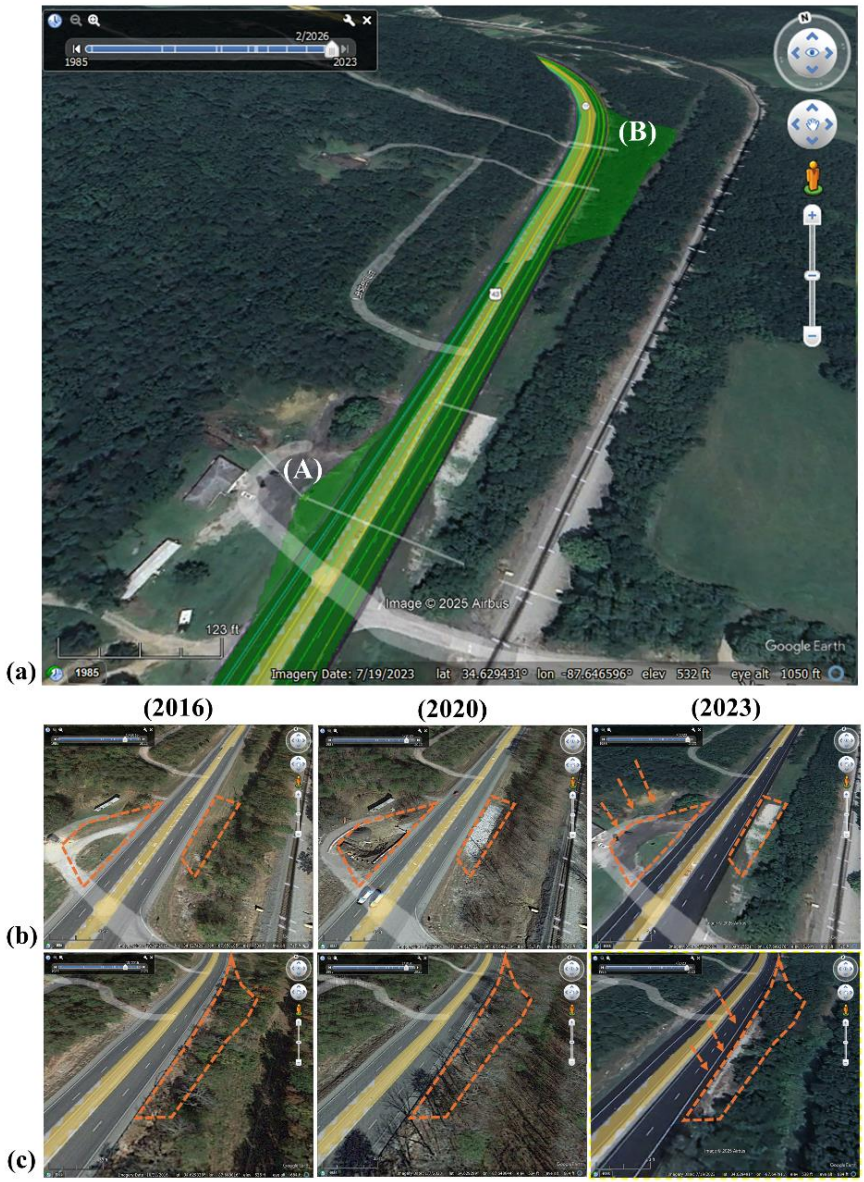

Figure 62. Multi-temporal Google Earth imagery of the Littleville site (US-43, Franklin County). (a) Overview showing areas of interest A and B along the highway corridor. (b–c) Close-up comparisons at three epochs: 2016 (pre-acceleration onset), 2020 (during acceleration onset period), and 2023 (post-remediation), illustrating progressive changes in road surface and slope conditions consistent with the InSAR-detected deformation trends.

It is important to note that this historical behavior change was observed in the InSAR data during the model training period and therefore does not constitute a detection by the EDAS. The model cannot detect patterns on which it was trained. Rather, it demonstrates the type of behavioral transition that the system is designed to identify when operating on new data during the operational detection period. The eight anomalies flagged during the 2023–2025 operational period represent genuine detections, in which measured displacement diverged from LSTM-predicted behavior. Progressive displacement evolution was captured through polynomial trend fitting and LSTM-based forecasts with 1.5σ confidence intervals, demonstrating the system's ability to track nonlinear deformation patterns (**Figure 61**). The EDAS provides a mechanism for automated identification of deformation anomalies from InSAR measurements, enabling alerts to be generated before conventional field inspection or periodic survey methods would typically identify the same changes.

While the EDAS has been developed and demonstrated using the Littleville site as a representative pilot, the framework is inherently scalable and transferable. The system architecture is site-agnostic: given any InSAR displacement time series of sufficient length, it can automatically establish baseline behavior, train the LSTM model, and begin operational anomaly detection. This scalability positions the EDAS for deployment across Alabama's highway network as additional PS-InSAR datasets become available.

6. Conclusions and Recommendations

6.1 Summary

This project developed and implemented a comprehensive InSAR-based deformation-monitoring framework to support operational infrastructure management for Alabama's transportation network. Consistent with established research demonstrating the value of multi-method InSAR processing for infrastructure monitoring, the workflow combines complementary time-series approaches to overcome the environmental challenges posed by Alabama's dense vegetation, high humidity, and strong soil-moisture variability, which commonly reduce interferometric coherence and increase atmospheric noise. To address these limitations, the study integrates NSBAS processing through LiCSBAS for computationally efficient regional monitoring, SBAS and Persistent Scatterer processing through PyGMTSAR for improved performance in semi-coherent environments, and full-resolution PS-InSAR analysis to capture localized deformation along narrow highway corridors and engineered structures. This multi-scale strategy enables simultaneous statewide situational awareness and high-resolution monitoring of critical sites, aligning with the broader InSAR literature emphasizing the importance of combining distributed-scatterer and persistent-scatterer methodologies to balance spatial coverage with measurement precision.

A validation framework was implemented to ensure that satellite-derived deformation products are suitable for engineering decision-making. Validation relied on multiple independent data sources, including ALDOT inclinometer measurements, continuous GNSS observations, and corner reflector deployments. The planned integration of L-band SAR datasets was not possible due to external delays in data availability. Comparison with inclinometer records demonstrated that PS-InSAR reliably captures temporal deformation evolution, including gradual creep and pre-failure acceleration behavior, while NSBAS products provided robust regional-scale trends but showed reduced sensitivity at localized, vegetation-dominated sites. GNSS-based evaluation confirmed that NSBAS-derived deformation products reproduce dominant long-term trends, seasonal variability, and regional motion patterns despite expected differences in sampling geometry between point-based geodetic data and spatially averaged InSAR pixels. These findings reinforce a key methodological conclusion supported by previous studies: NSBAS methods provide stable regional context, whereas PS-InSAR offers superior capability for localized infrastructure monitoring in challenging environments.

Application of the framework at representative validation sites and case studies further demonstrated its operational relevance. At the US-231 landslide site, PS-InSAR captured pre-failure acceleration preceding the documented February 2020 failure, highlighting the potential for early detection of slope movements and measurements at sites where inclinometers have not yet been deployed. At SR-

219, the methodology resolved slow-moving creep behavior and seasonal hydrologically driven deformation patterns, even under dense vegetation cover. Additional localized analyses at Littleville and the Lake Tholocco levee system illustrated how performance varies with infrastructure type, environmental setting, and spatial scale, while cross-comparison between PS-InSAR and NSBAS results showed consistent deformation trends at a location where both methods were applicable. Integration of environmental datasets, including precipitation, soil moisture, and land surface temperature, demonstrated strong coupling between hydrologic forcing and ground deformation, confirming that seasonal moisture variability is a dominant driver of deformation processes at many Alabama infrastructure sites.

Field deployment of corner reflectors established the foundation for future absolute calibration and long-term validation. Initial Sentinel-1 acquisitions confirmed strong reflector detection and phase stability, demonstrating technical readiness for high-precision monitoring as longer post-installation time series become available. Although limitations associated with data availability and mission timelines restricted full integration of L-band SAR datasets during this phase, successful acquisition efforts and initial deployments provide a clear path for expanded validation and improved monitoring performance in future phases of this research.

To translate these capabilities into practical decision-support tools, the ALDOT GeoMonitor Portal was developed as an operational web-based platform integrating InSAR-derived deformation layers, GNSS observations, and environmental data into a unified analytical interface. The portal enables interactive visualization, time-series exploration, and environmental correlation analysis, providing transportation personnel with centralized access to deformation information and supporting integration into routine maintenance and monitoring workflows. Building on the validated InSAR framework, machine-learning approaches were incorporated to enhance operational capability. A decomposition-based predictive modeling strategy separated long-term deformation trends from seasonal variability, combining ARIMA trend modeling with a deep learning architecture based on CNN, attention mechanisms, and bidirectional GRU networks. This hybrid approach demonstrated strong predictive performance and enabled development of a measurement-based Early Detection and Alert System capable of identifying anomalous displacement behavior relative to expected patterns, thereby supporting proactive inspection and risk management.

Overall, this work demonstrates that a unified framework combining multi-method InSAR processing, independent field validation, environmental data integration, and machine learning can provide a robust and scalable solution for infrastructure deformation monitoring in complex environmental conditions. The results show that PS-InSAR is particularly effective for localized monitoring of transportation assets in Alabama, while NSBAS approaches provide essential statewide context for

systematic screening. Together with the operational portal and automated detection framework, these developments establish a practical foundation for transitioning satellite-based deformation monitoring from research applications toward routine operational use for transportation infrastructure management.

6.2 Recommendations for ALDOT Implementation

Based on the outcomes of this project, we recommend that ALDOT adopt a **tiered implementation strategy** for satellite- and sensor-based ground deformation monitoring that builds directly on the validated workflows, analytical methods, and decision-support tools developed herein. A phased approach allows ALDOT to scale adoption in a controlled manner, balancing cost, staffing, and data maturity while progressively increasing monitoring capability and operational confidence.

Tier 1: Statewide Deformation Screening and Situational Awareness: As an initial step, ALDOT should institutionalize statewide deformation screening using Sentinel-1–based InSAR products as a routine component of its asset monitoring program. This project has demonstrated that standard-resolution LiCSBAS processing provides reliable, repeatable, and cost-effective situational awareness across large highway corridors. While not intended to resolve individual pavement features, this screening layer is highly effective at identifying broad zones of anomalous ground movement, seasonal instability, or progressive deformation trends before visible surface distress or structural damage occurs.

We recommend that this statewide screening be updated on a regular cadence (e.g., quarterly or semi-annually) and formally incorporated into planning and maintenance review cycles. Screening outputs can then be used to:

- Flag corridors or segments exhibiting unexpected deformation behavior
- Prioritize sites for higher-resolution InSAR analysis
- Guide targeted field inspections and geotechnical investigations
- Inform decisions on where permanent instrumentation would provide the greatest benefit

This screening approach will shift monitoring toward a proactive, data-driven posture rather than only capturing data after failures occur.

Tier 2: Operational Use of the ALDOT GeoMonitor Portal: As deformation screening identifies areas of concern, ALDOT should adopt the ALDOT GeoMonitor Portal as a decision-support platform for anomalous ground deformation. The portal integrates InSAR, GNSS, and environmental datasets within a unified, web-based interface and is well suited for internal use by ALDOT geotechnical, maintenance, and planning teams.

To ensure effective operational use, we recommend:

- Assigning designated ALDOT personnel responsible for routine portal review
- Incorporating portal outputs into existing inspection, maintenance, and asset review workflows rather than treating them as standalone analyses
- Using combined deformation trends and environmental correlations (precipitation, soil moisture, vegetation condition) to prioritize field investigations and preventive maintenance actions

Tier 3: Integration into Asset Management and Risk Assessment Frameworks: Finally, we recommend that ALDOT begin formal integration of deformation metrics into asset management and risk assessment frameworks. Even conservative, screening-level indicators, such as persistent acceleration, increasing seasonal amplitude, or deviation from historical deformation patterns, can be used to flag assets for closer review.

6.3 Recommendations for Future Research

While this project establishes a robust and operational foundation for satellite-based infrastructure monitoring in Alabama, several important research directions and system enhancements require continued investigation to fully realize the long-term potential of this approach. A subsequent project phase is strongly recommended to complete and expand the demonstrated framework and reach the goals highlighted in the previous implementation section.

6.3.1 Data Integration Enhancements

Future phases of this work should prioritize expanded data integration to improve monitoring robustness in challenging environments and extend both spatial and temporal coverage.

- **Incorporation of L-band SAR data (ALOS-2, ALOS-4, and NISAR):** This project originally planned to incorporate L-band SAR data to improve deformation monitoring in heavily vegetated regions of Alabama, where C-band Sentinel-1 coherence is often limited. Access to ALOS-2 and ALOS-4 data was successfully secured through a competitive JAXA selection process, and preliminary datasets were obtained. However, full implementation was not possible during this phase due to external technical constraints, including temporary suspension and migration of ALOS-2 data services and limited acquisition availability for ALOS-4 over the study area. Similarly, integration of NISAR data was planned as a key component for this phase, but routine, analysis-ready NISAR products were not

yet available during the project timeline due to launch and commissioning delays. Once fully operational, L-band SAR from ALOS-4 and NISAR is expected to significantly enhance deformation monitoring by improving coherence retention, reducing data gaps, and enabling more reliable long-term trend analysis in vegetated and soil-covered environments. Incorporating these datasets remains a high priority for future work.

- **Expanded environmental variables:** Future research should also incorporate additional environmental and subsurface datasets, including land surface temperature, groundwater levels, and evapotranspiration. These variables are critical for improving interpretation of deformation mechanisms and strengthening predictive modeling, particularly for sites where hydrological and thermal processes play a dominant role in seasonal or long-term ground movement.
- **Integration of ALDOT geotechnical instrumentation:** Although this phase focused on satellite-based monitoring and selected validation sites, broader integration of ALDOT's existing geotechnical instrumentation—such as inclinometers, piezometers, and other subsurface sensors—would significantly strengthen system validation and mechanistic understanding. Direct linkage of these measurements with InSAR and GNSS time series within the GeoMonitor Portal would support site-specific calibration, improve confidence in deformation interpretation, and enable development of tailored alert thresholds.
- **Corner reflector utilization and long-term validation:** Corner reflectors were successfully designed, installed, and detected by Sentinel-1 during this project, demonstrating technical feasibility and confirming correct deployment geometry. However, the short time span since installation limited their use for quantitative deformation validation within this phase. Continued monitoring over multiple acquisition cycles is required to fully leverage corner reflectors for precision calibration, accuracy assessment, and long-term performance evaluation. These activities are well-suited for a subsequent project phase.

6.3.2 Advanced InSAR Processing Framework Development

Results from this project indicate that Persistent Scatterer InSAR (PS-InSAR) processing using the PyGMTSAR framework provides significantly more reliable and spatially coherent deformation measurements in Alabama's vegetated and soil-covered environments compared to standard SBAS/NSBAS approaches. While SBAS-based statewide screening products (e.g., LiCSBAS) are effective for large-area reconnaissance and preliminary anomaly detection, PS-InSAR demonstrated superior performance in (1) maintaining coherence in densely vegetated slopes, (2) resolving deformation along narrow highway corridors, (3) distinguishing stable and unstable ground within short spatial distances, and (4) capturing gradual creep and pre-failure acceleration behavior. These findings suggest that PS-InSAR is the more appropriate operational method for detailed monitoring of Alabama's infrastructure corridors.

However, at the current stage, PS-InSAR processing requires manual configuration, site-by-site parameter tuning, and computational oversight using the PyGMTSAR workflow. This limits scalability for statewide deployment and prevents real-time automation within the ALDOT GeoMonitor Portal. A critical next step for future research is therefore the development of an automated PS-InSAR processing framework tailored to Alabama conditions. This should include:

- Automated frame selection and batch processing across Sentinel-1 acquisitions
- Standardized persistent scatterer selection criteria optimized for vegetated terrain
- Automated quality-control metrics (coherence stability, phase residual thresholds)
- Integrated reference point stabilization routines
- Direct linkage of processed time series outputs to the GeoMonitor Portal for near-real-time visualization and alerting

Developing such an automated pipeline would transition PS-InSAR from a research-grade analytical tool to an operational monitoring system capable of routine statewide deployment. This effort would significantly enhance scalability, reduce processing time, and enable systematic monitoring of multiple corridors without manual intervention.

6.3.2 Expanded Applications

Beyond slope instability, the methodologies developed in this project are directly transferable to other infrastructure assets and analysis objectives:

- **Extension to bridges and other transportation infrustructure:** Persistent scatterer InSAR and GNSS monitoring can be applied to detect subtle settlement, rotation, or differential movement at bridge approaches and abutments.
- **Seasonal deformation analysis by geologic region:** Comparative studies across Alabama's distinct geologic provinces would enable identification of region-specific deformation signatures and seasonal behavior, supporting tailored mitigation strategies.
- **Cost–benefit analysis of proactive monitoring:** A formal economic assessment comparing early detection and preventive maintenance against emergency repairs and closures would help quantify the return on investment of satellite-based monitoring and support long-term adoption within ALDOT.

6.3.3 Regional Collaboration

Finally, this work positions ALDOT to play a leadership role in broader infrastructure monitoring efforts:

- **Regional collaboration with neighboring state DOTs:** Sharing workflows, tools, and lessons learned with agencies in Mississippi, Georgia, and Tennessee would enable regional hazard assessment across shared geologic and climatic settings.
- **Participation in national monitoring initiatives:** The methodologies developed here align well with emerging federal efforts focused on infrastructure resilience, climate adaptation, and remote sensing–based monitoring.

References

Agram, P. S., Jolivet, R., Riel, B., Lin, Y. N., Simons, M., Hetland, E., Doin, M. P., & Lasserre, C. (2013). New radar interferometric time series analysis toolbox released. Eos, Transactions American Geophysical Union, 94(7), 69-70.

Alabama Department of Transportation. (2021). *State of Alabama Geotechnical Manual*. Alabama Department of Transportation. *https://www.dot.state.al.us/publications/Materials/pdf/ALDOTGeotechManual.pdf*

Alonso-Díaz, A., Roque, D., Lima, J.N., Rodríguez, J.L., and Solla, M. (2026). Improvement of InSAR displacements based on GNSS station calibration over corner reflector. Measurement, 118946.

Anantrasirichai, N., Biggs, J., Albino, F., & Bull, D. (2018). The application of convolutional neural networks to detect slow, sustained deformation in InSAR time series. Geophysical Research Letters, 45(21), 11850-11858.

Bai, S., Kolter, J. Z., & Koltun, V. (2018). An empirical evaluation of generic convolutional and recurrent networks for sequence modeling. arXiv preprint arXiv:1803.01271.

Bekaert, D. P. S., Walters, R. J., Wright, T. J., Hooper, A. J., & Parker, D. J. (2020). Statistical comparison of InSAR tropospheric correction techniques. Remote Sensing of Environment, 170, 40-47.

Berardino, P., Fornaro, G., Lanari, R., & Sansosti, E. (2002). A new algorithm for surface deformation monitoring based on small baseline differential SAR interferograms. IEEE Transactions on Geoscience and Remote Sensing, 40(11), 2375-2383.

Beshr, A. A. E. W. (2015). Structural deformation monitoring and analysis of highway bridge using accurate geodetic techniques. Engineering, 7(8), 488-498.

Billenberg, M. (2024). Precise displacement measurement of ground movement using a corner reflector and persistent scatterer interferometry (PSI) technique: A case study at the Mårtsbo Space Observatory.

Blewitt, G., Hammond, W., & Kreemer, C. (2018). Harnessing the GPS data explosion for interdisciplinary science. Eos, 99(2), e2020943118.

Bryant, M. L., & Garber, F. D. (1999, August). SVM classifier applied to the MSTAR public data set. In Algorithms for Synthetic Aperture Radar Imagery VI (Vol. 3721, pp. 355-360). SPIE.

Chaussard, E., Wdowinski, S., Cabral-Cano, E., & Amelung, F. (2014). Land subsidence in central Mexico detected by ALOS InSAR time-series. *Remote sensing of environment*, *140*, 94-106.

Chen, C. W., & Zebker, H. A. (2002). Phase unwrapping for large SAR interferograms: Statistical segmentation and generalized network models. IEEE Transactions on Geoscience and Remote Sensing, 40, 1709–1719.

Chen, S., & Wang, H. (2014, October). SAR target recognition based on deep learning. In 2014 International Conference on Data Science and Advanced Analytics (DSAA) (pp. 541-547). IEEE.

Covello, F., et al. (2010). COSMO-SkyMed an existing opportunity for observing the Earth. Journal of Geodynamics, 49(3), 171-180. De Waele, J. D., Plan, L., & Audra, P. (2009). Recent developments in surface and subsurface karst geomorphology: An introduction. Geomorphology, 106(1-2), 1–8.

Crosetto, M., Monserrat, O., Cuevas-González, M., Devanthéry, N., & Crippa, B. (2016). Persistent scatterer interferometry: A review. *ISPRS Journal of Photogrammetry and Remote Sensing*, *115*, 78-89.

Crosetto, M., Monserrat, O., Devanthéry, N., Cuevas González, M., Barra, A., Crippa, B., 2016. Persistent scatterer interferometry using Sentinel-1 data. Int. Arch. Photogramm. Remote Sens. Spatial Inf. Sci. 41, 835- 839.

Cruden, D. M., & Varnes, D. J. (1996). Landslide types and processes. In: Turner, A. K. & Schuster, R. L. (eds), Landslides: Investigation and Mitigation. Transportation Research Board, National Research Council, Special Report 247, pp. 36-75.

De Waele, J., Plan, L., & Audra, P. (2009). Recent developments in surface and subsurface karst geomorphology: An introduction. Geomorphology, 106(1-2), 1-8.

Deijns, A. A., Bevington, A. R., van Zadelhoff, F., de Jong, S. M., Geertsema, M., & McDougall, S. (2020). Semi-automated detection of landslide timing using harmonic modelling of satellite imagery, Buckinghorse River, Canada. International Journal of Applied Earth Observation and Geoinformation, 84, 101943.

Drouin, V., & Sigmundsson, F. (2019). Countrywide observations of plate spreading and glacial isostatic adjustment in Iceland inferred by sentinel-1 radar interferometry, 2015–2018. *Geophysical Research Letters*, *46*(14), 8046-8055.

Duncan, J. M., Wright, S. G., & Brandon, T. L. (2014). Soil strength and slope stability. John Wiley & Sons, Hoboken, New Jersey.

Ebel, P., Schmitt, M., & Zhu, X. (2020). Cloud removal in unpaired sentinel-2 imagery using cycle-consistent gan and sar-optical data fusion. IGARSS 2020 IEEE International Geoscience and Remote Sensing Symposium.

Mantovani, F., Soeters, R., and Van Westen, C.J. (1996). Remote sensing techniques for landslide studies and hazard zonation in Europe. Geomorphology, 15(3–4), 213–225.

Ebersole, S. M., Driskell, S., Tavis, A. M. Susceptibility to Landslides in Alabama. Geological Survey of Alabama, December 2011. *https://www.gsa.state.al.us/img/Geological/ Hazards/Landslides/Landslides_Poster_AdobeReduced.pdf*. Accessed June 25, 2018.

Ferretti, A., Prati, C., & Rocca, F. (2001). Permanent scatterers in SAR interferometry. IEEE Transactions on Geoscience and Remote Sensing, 39(1), 8–20.

Gao, B. C. (1996). NDWI—A normalized difference water index for remote sensing of vegetation liquid water from space. Remote Sensing of Environment, 58(3), 257-266.

Geological Survey of Alabama (GSA). 2024. *Sinkholes in Alabama*. Geological Survey of Alabama, Tuscaloosa, AL. *https://gsa.state.al.us/Scripts/GSAOGB/gsa/geologic/hazardsSinkholes.html*

Ghorbani, Z., Khosravi, A., Maghsoudi, Y., Mojtahedi, F. F., Javadnia, E., & Nazari, A. (2022). Use of InSAR data for measuring land subsidence induced by groundwater withdrawal and climate change in Ardabil Plain, Iran. Scientific Reports, 12(1), 13998.

Goldstein, R. M., & Werner, C. L. (1998). Radar interferogram filtering for geophysical applications. Geophysical Research Letters, 25, 4035–4038.

Grandoni, D., Battagliere, M. L., Daraio, M. G., Sacco, P., Coletta, A., Di Federico, A., & Mastracci, F. (2014). Space-based technology for emergency management: The COSMO-SkyMed constellation contribution. Procedia Technology, 16, 858-866.

Hartmann, W., Havlena, M., & Schindler, K. (2016). Towards complete, geo-referenced 3d models from crowd-sourced amateur images. ISPRS Annals of the Photogrammetry, Remote Sensing and Spatial Information Sciences, 3, 51-58.]

Hochreiter, S., & Schmidhuber, J. (1997). Long short-term memory. Neural Computation, 9(8), 1735- 1780. Hofmann-Wellenhof, B., Lichtenegger, H., & Collins, J. (1994). Global Positioning System: Theory and Practice. Springer-Verlag.

Hooper, A. (2008). A multi-temporal InSAR method for measuring ground deformation in the presence of atmospheric delay. Geophysical Research Letters, 35(22), L22301.

Hooper, A. (2008). A multi-temporal InSAR method incorporating both persistent scatterer and small baseline approaches. Geophysical research letters, 35(16).

Hooper, A., Segall, P., & Zebker, H. (2007). Persistent scatterer interferometric synthetic aperture radar for crustal deformation analysis, with application to Volcan Alcedo, Galapagos. Journal of Geophysical Research: Solid Earth, 112(B7), B07407.

Hrysiewicz, A., Wang, X., & Holohan, E. P. (2023). EZ-InSAR: An easy-to-use open-source toolbox for mapping ground surface deformation using satellite interferometric synthetic aperture radar. Earth Science Informatics, 16(2), 1929-1945.

Hughes, L., Schmitt, M., Mou, L., Wang, Y., & Zhu, X. X. (2018). Identifying corresponding patches in

Javid, A.H., Bulut, R., 2019. Equilibrium Suction Prediction Model for Subgrade Soils in Oklahoma. International Journal of Geomechanics 23(10), 04023165.

Kalia, A. C., Frei, M., & Lege, T. (2017). A Copernicus downstream-service for the nationwide monitoring of surface displacements in Germany. Remote Sensing of Environment, 202, 234-249.

Karamvasis, K., & Karathanassi, V. (2020). Performance analysis of open source time series InSAR methods for deformation monitoring over a broader mining region. Remote Sensing, 12(9), 1380.

Khan, J., Ren, X., Hussain, M. A., & Jan, M. Q. (2022). Monitoring land subsidence using PS-InSAR technique in Rawalpindi and Islamabad, Pakistan. Remote Sensing, 14(15), 3722.

Kingma, D. P., & Ba, J. (2014). Adam: A method for stochastic optimization. arXiv preprint arXiv:1412.6980.

Knights, M. J. (2018). Analysis of slope failures along Alabama highways (Master's thesis, Auburn University).

Knights, M. J., Montgomery, J., & Carcamo, P. S. (2020). Development of a slope failure database for Alabama highways. Bulletin of Engineering Geology and the Environment, 79(1), 423-438.

Krizhevsky, A., Sutskever, I., & Hinton, G. E. (2012). ImageNet classification with deep convolutional neural networks. Advances in Neural Information Processing Systems, 25, 1097-1105.

Kulkarni, S. C., & Rege, P. P. (2020). Pixel level fusion techniques for SAR and optical images: A review. Information Fusion, 59, 13-29.

Lanari, R., Lundgren, P., Manzo, M., Casu, F., 2004. Satellite radar interferometry time series analysis of surface deformation for Los Angeles, California. Geophys. Res. Lett. 31, L23613. Lazecký, M., Ou, Q., Shen, L., McGrath, J., Payne, J., Espín, P., Maghsoudi, Y., Spaans, K., González, P.J.,

Lattari, F., Leon, B. G., Asaro, F., Rucci, A., Prati, C., & Matteucci, M. (2019). Deep learning for SAR image despeckling. Remote Sensing, 11(13), 1532.

Maghsoudi, Y., Hooper, A.J., Wright, T.J., Lazecky, M., Ansari, H., 2022. Characterizing and correcting phase biases in short-term, multilooked interferograms. Remote Sens. Environ. 275, 113022.

Massonnet, D., & Feigl, K. L. (1998). Radar interferometry and its application to changes in the Earth's surface. Reviews of geophysics, 36(4), 441-500.

Mazza, A., Sica, F., Rizzoli, P., & Scarpa, G. (2019). TanDEM-X forest mapping using convolutional neural networks. Remote Sensing, 11(24), 2980.

Mei, S., Poncos, V., & Froese, C. (2008). Mapping millimetre-scale ground deformation over the underground coal mines in the Frank Slide area, Alberta, Canada, using spaceborne InSAR technology. Canadian Journal of Remote Sensing, 34(2), 113-134.

Mirmazloumi, S. M., Wassie, Y., Nava, L., Cuevas-González, M., Crosetto, M., & Monserrat, O. (2023). InSAR time series and LSTM model to support early warning detection tools of ground instabilities: mining site case studies. Bulletin of Engineering Geology and the Environment, 82(10), 374.

Montgomery, J., Jackson, D., Kiernan, M., & Anderson, J. B. (2020). Use of geophysical methods for sinkhole exploration (No. 930-945). Auburn University. Highway Research Center.

Montgomery, J., Knights, M., Xuan, M., & Carcamo, P. (2019). Evaluation of Landslides along Alabama Highways.

Montgomery, J., Xuan, M., Diekmann, A., Kiernan, M., Thompson, R., & Chancellor Davis, K. (2026). Characterization of the 2020 US-231 landslide near Lacey Springs, Alabama and the importance of nonlinear strength envelopes. Landslides, 1-12.

Morgan, D. A. (2015, May). Deep convolutional neural networks for ATR from SAR imagery. In Algorithms for Synthetic Aperture Radar Imagery XXII (Vol. 9475, pp. 116-128). SPIE.

Morishita, Y., Lazecky, M., Wright, T.J., Weiss, J.R., Elliott, J.R., Hooper, A., 2020. LiCSBAS: An open-source InSAR time series analysis package integrated with the LiCSAR automated Sentinel-1 InSAR processor. Remote Sens. 12, 424.

Özer, I.E., van Leijen, F., van Damme, M., Jonkman, S.N., Hanssen, R.F., 2017. Detection and Analysis of Weak Spots in Levees Based on Satellite Radar Interferometry. In: Fringe 10th International Workshop on: Advances in the Science and Applications of SAR Interferometry and Sentinel-1 InSAR. Özer, I.E., van Leijen, F.J., Jonkman, S.N., Hanssen, R.F., 2019a. Applicability of satellite radar imaging to monitor the conditions of levees. J. Flood Risk Manag. 12 (S2), e12509.

Özer, I.E., Rikkert, S.J., van Leijen, F.J., Jonkman, S.N., Hanssen, R.F., 2019b. Sub-seasonal levee deformation observed using satellite radar interferometry to enhance flood protection. Sci. Rep. 9, 2646.

Ndikumana, E., Ho Tong Minh, D., Baghdadi, N., Courault, D., & Hossard, L. (2018). Deep recurrent neural network for agricultural classification using multitemporal SAR Sentinel-1 for Camargue, France. Remote Sensing, 10(8), 1217.

Orange, B., & Smith, D. (2014). AL-21 Sinkhole remediation Talladega County. 57th Annual Transportation Conference, Auburn University.

Paradella, W. R., Mura, J. C., & Gama, F. F. (2021). Monitoramento DInSAR para mineração e geotecnia. Oficina de Textos.

Parikh, H., Patel, S., & Patel, V. (2020). Classification of SAR and PolSAR images using deep learning: A review. International Journal of Image and Data Fusion, 11(1), 1-32.

Pearlmutter. (1989, June). Learning state space trajectories in recurrent neural networks. In International 1989 Joint Conference on Neural Networks (pp. 365-372). IEEE.

Pechnikov, A. (2023). PyGMTSAR (Python InSAR): Sentinel-1 interferometry. GitHub Repository / Zenodo.

Pechnikov, A., 2024. PyGMTSAR: Sentinel-1 Python InSAR. An Introduction.

Piroton, V., Schlögel, R., Barbier, C., & Havenith, H. B. (2020). Monitoring the recent activity of landslides in the Mailuu-Suu Valley (Kyrgyzstan) using radar and optical remote sensing techniques. Geosciences, 10(5), 164.

Prats-Iraola, P., Scheiber, R., Marotti, L., Wollstadt, S., & Reigber, A. (2012). TOPS interferometry with TerraSAR-X. IEEE Transactions on Geoscience and Remote Sensing, 50(8), 3179-3188.

Rahimikhameneh, L., Montgomery, J., Knights, M., Alvarez_Reyna, A., O'Donnell, F., & Carcamo, P. (2025). Inventory of Landslides Along Alabama Highways.

Rahimikhameneh, L., Montgomery, J., Reyna, A. A., & O'Donnell, F. (2024). Monitoring and Assessment of Landslides Along Alabama Highways.

Reale, D., et al. (2011). Postseismic deformation monitoring with the COSMO/SKYMED constellation. IEEE Geoscience and Remote Sensing Letters, 8(4), 696-700.

Rosen, P. A., Gurrola, E., Sacco, G. F., & Zebker, H. (2012). The InSAR scientific computing environment. In: Proceedings of the 9th European Conference on Synthetic Aperture Radar (EUSAR 2012), pp. 730-733.

Rouse, W. (1973). Monitoring vegetation system in the great plain with ERTS. In 3rd ERTS symposium, NASA Washington DC, 1973 (Vol. 1, pp. 309-317).

Sandwell, D., Fialko, Y., Mellors, R., Wei, M., & Tong, X. (2011). CRUSTAL DYNAMICS RESEARCH WITH ALOS INTERFEROMETRY. 宇宙航空研究開発機構特別資料, PI114-1.

Scheiber, R., & Moreira, A. (2000). Coregistration of interferometric SAR images using spectral diversity. IEEE Transactions on Geoscience and Remote Sensing, 38(5), 2179-2191.

Scheip, C. M., & Wegmann, K. W. (2021). HazMapper: A global open-source natural hazard mapping application in Google Earth Engine. Natural Hazards and Earth System Sciences, 21, 1495-1511.

Schmidt, D. A., & Bürgmann, R. (2003). Time-dependent land uplift and subsidence in the Santa Clara valley, California, from a large interferometric synthetic aperture radar data set. Journal of Geophysical Research: Solid Earth, 108, 1–13.

Shi, Y., Tang, Y., Lu, Z., Kim, J. W., & Peng, J. (2019). Subsidence of sinkholes in Wink, Texas from 2007 to 2011 detected by time-series InSAR analysis. *Geomatics, Natural Hazards and Risk*.

Showstack, R. (2014). Sentinel satellites initiate new era in earth observation.

Simonyan, K., & Zisserman, A. (2014). Very deep convolutional networks for large-scale image recognition. arXiv:1409.1556.

Smith, R. G., Hashemi, H., Chen, J., & Knight, R. (2021). Apportioning deformation among depth intervals in an aquifer system using InSAR and head data.

Sun, Z., Dai, M., Leng, X., Lei, Y., Xiong, B., Ji, K., & Kuang, G. (2021). An anchor-free detection method for ship targets in high-resolution SAR images. IEEE Journal of Selected Topics in Applied Earth Observations and Remote Sensing, 14, 7799-7816.

Suzuki, S., Kankaku, Y., Imai, H., & Osawa, Y. (2012, November). Overview of ALOS-2 and ALOS-3. In Earth Observing Missions and Sensors: Development, Implementation, and Characterization II (Vol. 8528, pp. 175-182). SPIE.

Tiwari, A., Narayan, A. B., Dwivedi, R., Swadeshi, A., Pasari, S., & Dikshit, O. (2020). Geodetic investigation of landslides and land subsidence: Case study of the Bhurkunda coal mines and the Sirobagarh landslide. Survey review.

Torres, R., et al. (2012). GMES Sentinel-1 mission. Remote Sensing of Environment, 120, 9-24.

Ustin, S. L., & Middleton, E. M. (2021). Current and near-term advances in Earth observation for ecological applications. Ecological Processes, 10(1), 1. *https://doi.org/10.1186/s13717-020-00255-4*

Van der Kooij, M., Hughes, W., Sato, S., & Poncos, V. (2005). Coherent target monitoring at high spatial density: Examples of validation results. Proceedings of the Fringe 2005, ESA.

Varnes, D. J. (1978). Slope Movement Types and Processes. In: Schuster RL, Krizek RJ (eds) Landslides: Analysis and Control. Transportation Research Board Special Report 176, 11-33.

Vaswani, A., Shazeer, N., Parmar, N., Uszkoreit, J., Jones, L., Gomez, A. N., ... & Polosukhin, I. (2017). Attention is all you need. Advances in neural information processing systems, 30. Cruden, D. (1991). A simple definition of a landslide. *Bulletin of Engineering Geology & the Environment*, *43*(1).

Vecchiotti, F., Peduto, D., & Strozzi, T. (2017, May). Multi-sensor a priori PSI visibility map for nationwide landslide detection in Austria. In Workshop on world landslide forum (pp. 45-52). Cham: Springer International Publishing.

Wang, P., Zhang, H., & Patel, V. (2017). SAR image despeckling using a convolutional neural network. IEEE Signal Processing Letters, 24(12), 1763-1767.

Wang, Y., Zhang, Q., Zhao, C., Lu, Z., & Ding, X. (2011, October). Monitoring and inversion on land subsidence over mining area with InSAR technique. In *International Symposium on Lidar and Radar Mapping 2011: Technologies and Applications* (Vol. 8286, pp. 416-424). SPIE.

Wasowski, J., & Bovenga, F. (2014). Investigating landslides and unstable slopes with satellite Multi Temporal Interferometry: Current issues and future perspectives. *Engineering Geology*, *174*, 103-138.

Wegmüller, U., Werner, C., Strozzi, T., Wiesmann, A., Frey, O., & Santoro, M. (2016). Sentinel-1 Support in the GAMMA Software. Procedia Computer Science, 100, 1305-1312.

Wen, T. H., & Teo, T. A. (2022). Landslide inventory mapping from Landsat-8 NDVI time series using adaptive landslide interval detection. ISPRS Annals of the Photogrammetry, Remote Sensing and Spatial Information Sciences, 3, 557-562.

Werner, C., Wegmüller, U., Strozzi, T., & Wiesmann, A. (2000). GAMMA SAR and interferometric processing software. Proceedings of the ERS-Envisat Symposium, Gothenburg, Sweden.

Wurm, M., Stark, T., Zhu, X. X., Weigand, M., & Taubenboeck, H. (2019). Semantic segmentation of slums in satellite images using transfer learning on fully convolutional neural networks. ISPRS Journal of Photogrammetry and Remote Sensing, 150, 59-69.

Xiang, D., et al. (2022). Optical and SAR Image Registration Based on Feature Decoupling Network.

Xie, H., et al. (2017). Fast Factorized Backprojection Algorithm for One-Stationary Bistatic Spotlight Circular SAR Image Formation.

Xie, T., Perrie, W., Wei, C., & Zhao, L. (2020). Discrimination of open water from sea ice in the Labrador Sea using quad-polarized synthetic aperture radar. Remote Sensing of Environment, 247, 111948.

Yang, M., Jiao, L., Liu, F., Hou, B., & Yang, S. (2019). Transferred deep learning-based change detection in remote sensing images. IEEE Transactions on Geoscience and Remote Sensing, 57(9), 6960-6973.

Yunjun, Z., Fattahi, H., & Amelung, F. (2019). Small baseline InSAR time series analysis: Unwrapping error correction and noise reduction. Computers & Geosciences, 133, 104331.

Zhang, J., Liu, Z., Jiang, W., Liu, Y., Zhou, X., & Li, X. (2023). Application of deep generative networks for SAR/ISAR: A review. Artificial Intelligence Review, 56(10), 11905-11983.

Zhao, Q., & Principe, J. C. (2001). Support vector machines for SAR automatic target recognition. IEEE Transactions on Aerospace and Electronic Systems, 37(2), 643-654.

Zhou, C., Ye, M., Xia, Z., Wang, W., Luo, C., & Muller, J. P. (2025). An interpretable attention-based deep learning method for landslide prediction based on multi-temporal InSAR time series: A case study of Xinpu landslide in the TGRA. Remote Sensing of Environment, 318, 114580.

Zhu, X. X., et al. (2021). Deep learning meets SAR: Concepts, models, algorithms, and applications. IEEE Geoscience and Remote Sensing Magazine, 9(4), 143-172.

Zhu, X. X., Tuia, D., Mou, L., Xia, G., Zhang, L., Xu, F., & Fraundorfer, F. (2017). Deep learning in remote sensing: A comprehensive review and list of resources. IEEE Geoscience and Remote Sensing Magazine, 5(4), 8-36.

Zulfeqar, N., Khosravi, A., & Zou, S. (2025). Nano-Enhanced Electrokinetic Conditioning of Expansive Soils Using MgO Nanoparticles. Journal of Geotechnical and Geoenvironmental Engineering, 151(11), 04025120.